EFFECTS OF TRANSIENT LIQUID PHASE BONDING ON CORROSION PERFORMANCE OF A SINGLE CRYSTAL AEROSPACE SUPERALLOY

BY

OLANIYI JOSHUA ADEBAJO

A thesis submitted to the Faculty of Graduate studies in partial fulfilment of the requirements for the Degree of

MASTER OF SCIENCE

Department of Mechanical and Manufacturing Engineering

University of Manitoba

Winnipeg

ABSTRACT

Transient Liquid phase bonding (TLP) has evolved as a viable method of joining difficult-to-weld superalloys with potential of producing joints with comparable mechanical properties to the base material. Although the high temperature properties of aerospace superalloys have been studied extensively, there is little information on the corrosion behaviour of these special class of materials that had been subjected to TLP bonding. In this work, electrochemical assessment of the corrosion behaviour of TLP bonded nickel-based superalloy was performed. Microstructural evaluation of the TLP bonded joint revealed the presence of a centreline eutectic when isothermal solidification was not completed and the corrosion resistance increased with a decrease in this eutectic width. The use of a composite interlayer produces TLP joints with smaller eutectic size and results in complete isothermal solidification in shorter processing time. Complete isothermal solidification, achieved with the composite interlayer, results in a uniform chromium distribution in the joint centre and produced a corrosion performance similar to the as-received cast base metal. It was found that aside from the mere presence of chromium, which is widely recognised as necessary for corrosion resistance, its uniform distribution within the joint region is imperative for achieving adequate corrosion resistance in TLP joints.

Acknowledgments

Foremost, I would like to express my deepest gratitude to my supervisor Dr. Olanrewaju Ojo, for affording me the opportunity to work on this project and providing me with the necessary research facilities and materials. I am grateful for his patience, coaching, encouragement and immense knowledge which were a motivation towards the successful completion of this research work.

I am thankful to the University of Manitoba for the award of International Graduate Entrance Scholarship and NSERC, for the financial support. I want to say a big thank you to Trevor Smith, Mike Boswick and Dr. Abdul Khan for the technical support when using the research facilities at the material characterization laboratory of the University of Manitoba.

To my friends and colleagues Idris Adelakun, Emmanuel Ocran, Johnson Ania and Jinal Sanghvi, I am grateful for your help and support in getting me started with settling down and getting up to speed on my arrival. I specifically want to thank the Taiwo family for their enormous support, giving me a "home away from home" experience. An endless list of thanks goes to Wale Jegede, Adedayo Ogundipe, Akinwolemiwa Kolewole, Adetokunbo Adekanmbi, and Idowu Olanrewaju.

To my mum, Oladunni Adebajo and entire family, I say thank you for loving and supporting me in every way, being steadfast in the face of challenges and believing in my abilities. To Seun Adebanjo and family; and Quadri Sobowale, my thanks knows no bounds. You all have contributed in no small measure to getting me here.

Above all, I honor the source of life and fountain of wisdom, the Almighty God, for the enablement in wisdom, strength to preserve and sound mind to complete this research.

Dedication

This thesis is dedicated to the loving memories of my sisters Titilayo Adebajo and Oluwayemisi Adebajo. I miss you both dearly, your inspirations and support through the years were the motivation I held unto throughout the period of this program.

Table of Contents

List of Tables

List of Figures

Author's Declaration

I, *Olaniyi Joshua Adebajo*, hereby declare that the entire result presented in this thesis is the sole product of my work, under the supervision and approval from my supervisor and examiners.

I am aware that my thesis may be made electronically available to the public.

List of Symbols and Abbreviations

AEW	Average Eutectic Width
AJW	Average Joint Width
Al	Aluminum
AR BM	As-Received Base Metal
ASZ	Athermally Solidified Zone
C	Carbon
Co	Cobalt
Comp	Composite Interlayer
Comp NE	Composite TLP Bond with No Eutectic
Conv	Conventional Interlayer
Conv WE	Conventional TLP Bond with Eutectic
Cr	Chromium
CR	Corrosion Resistance
DAZ	Diffusion Affected Zone
DB	Diffusion Brazing
DS	Directionally Solidified
E_{coor}	Corrosion Potential
EDM	Electro Discharge Machining
EDS	Energy Dispersive Spectrometer
EFM	Electrochemical Frequency Modulation
EIS	Electrochemical Impedance Spectroscopy
EMF	Electromotive Force
EN	Electrochemical Noise
E_{pp}	Passivation Potential
ER	Electrical Resistance
FCC	Face Centred Cubic
Fe	Iron
FOD	Foreign Object Damage
H_2SO_4	Sulphuric Acid
HAZ	Heat Affected Zone
HCl	Hydrochloric Acid
HNO_3	Nitric Acid
i_{corr}	Corrosion Current Density
i_{crit}	Critical Current Density
IN	Inconel

i_{pass},	Passivation Current Density
ISZ	Isothermal Solidified Zone
Mo	Molybdenum
MPD	Melting Point Depressant
NB	NicroBraz
Nb	Niobium
Ni	Nickel
OCP	Open Circuit Potential
OIM	Orientation Imaging Microscopy
OM	Optical Microscope
P	Phosphorus
Re	Rhenium
Rh	Rhodium
R_p	Polarization Resistance
SCC	Stress Corrosion Cracking
SCE	Saturated Calomel Electrode
SEM	Scanning Electron Microscope
Si	Silicon
SiC	Silicon-carbide
SX	Single Crystal
Ta	Tantalum
TAP	Thermally Activated Process
TCP	Topologically Close Packed
t_f	Isothermal Solidification Completion Time
Ti	Titanium
TLIM	Transient Liquid Insert Metal
TLP	Transient Liquid Phase
Vf	Volume fraction
W	Tungsten
Zr	Zirconium
γ	Gamma
γ’	Gamma Prime
γ’’	Gamma double prime

CHAPTER 1. INTRODUCTION

1.1 Background Information

The development of advanced materials for specialized applications has brought about significant changes and improvements in the design, efficiency and reliability of various systems; however, this development is not devoid of rudimentary challenges either in the manufacturing process itself or production and/or applications of these advanced materials. Superalloys are a special class of advanced materials that have better performance due to their exceptional ability to retain both physical and mechanical properties at elevated temperatures beyond limits attainable by martensitic steels [1].

Nickel (Ni)-base superalloys, a subset in the superalloys class have an excellent combination of high temperature strength, toughness, and resistance to degradation in corrosive or oxidizing environments [2], and are used in a wide range of applications. IN 738 is a γ' precipitation hardened Ni-base superalloy, and extensively used to manufacture or produce components in the hot section of gas turbines that are used in commercial and military aircraft, power generation, and marine propulsion. They have also found applications in other challenging environments, including nuclear power and chemical processing plants and more recently in the oil and gas industry [3]. These applications demand higher reliability and efficiency, and thus the components of these engines operate under severe service conditions for extended periods or cycle time, which cause a much more rapid degradation or damage of the components through enhanced levels of creep, fatigue cracking, oxidation, and foreign object damage among others.

The outright replacement of damaged components in most cases is not economically justifiable in achieving a low life cycle cost, due to the associated cost of manufacturing, hence repair and/or refurbishment of in-service-damaged components is a much more feasible option.

Joining is a common procedure for manufacturing and repair of components or parts in all industries. In the selection of a joining method the cost of producing the joint and the structural integrity of the joint are of vital importance in ensuring optimal performance and durability. The use of conventional fusion welding, the most common form of joining in all industries, for Ni-base superalloys that contain significant amounts of titanium (Ti) and aluminum (Al) is somewhat limited as they are highly susceptible to weld-cracking during weld and post weld heat treatment [4,5]. Therefore, a metal joining process at temperatures lower than the melting point of Ni-base superalloy would be appropriate to prevent cracking in the fusion zone.

Transient liquid phase (TLP) bonding, which was developed by Duvall et al. [6], has evolved as a viable joining method for difficult to weld alloys. The process is also known as diffusion brazing (DB) [7-9], which utilizes an interlayer alloy that contains a melting point depressant (MPD) such as boron (B), phosphorus (P) or silicon (Si) and melts between the faying surfaces of the substrate materials to be joined. It has evolved into a popular joining method due to its technological and cost advantages, such as a lower pressure and temperature required during bonding [8] compared to solid state diffusion and fusion welding respectively. The resulting bond can also operate at the bonding or higher temperatures.

1.2 Research Problem and the Research Objective

1.2.1 Research Problem

Joining creates a microstructure that is although similar to, yet somewhat different from, the substrate material in the joint region and hence the fundamental relationship between the material and its microstructure is altered for the joint, since the characteristics of any material is a function of its microstructure. The mechanical properties of TLP bonded joints have been extensively studied [9-11], it has been found that the mechanical properties can be similar to

the properties of the base materials. Ni-base superalloys are known to have excellent corrosion resistance (CR) in the as cast condition (where the microstructure is homogeneous throughout). Therefore, the formation of a new microstructure in the TLP bonded region creates uncertainty with respect to the CR of such joints. A brazed joint with secondary intermetallic phases in the joint centre is synonymous to a complicated multielectrode system; the polarity of the electrode and the associated corrosion rate are influenced by several factors, hence predicting the CR is difficult [12].

Corrosion, the deterioration of a material due to chemical interactions with the environment [13-15], is a major threat to structural components, particularly those with metal. There is a knowledge gap on the CR of TLP bonded materials. To improve the commercial applicability of the TLP bonding process, it is important to know its impact not only on the mechanical properties of the joint produced but as well as the CR, particularly in Ni-base superalloys.

1.2.2 Research Objective

The objective of the current work is to evaluate the effect of TLP bonding on the corrosion performance of a single crystal Ni-base superalloy IN 738.

1.3 Major Findings

In achieving the objective of this work, bonding of a SX IN 738 superalloy is carried out at various temperatures, gap width and holding time by using AMDRY 790 (Ni-Si-B) and NB150 (Ni-Cr-B) as the interlayer alloys. The bonded joints are then examined by using both an optical microscope (OM) and scanning electron microscope (SEM) to characterize their microstructure. The experimental results obtained showed that conventional TLP bonding that uses 100% filler alloy produces a deleterious centreline eutectic due to extended isothermal

solidification completion time, for the NB150 interlayer, this eutectic comprises of Cr-rich and Ni-rich borides in the γ solid solution matrix.

Furthermore, the width of this eutectic relative to the joint width significantly depends on the key process parameters, such that 1) the width increases with increasing gap width, 2) the width decreases as the holding time is increased, 3) the width decreases with increasing bonding temperature up to a certain temperature beyond which the width drastically increases. A new method which uses a composite powder mixture of base material and interlayer alloy powders in a ratio of 3:7 during TLP bonding produces a joint with a much smaller eutectic width relative to the conventional TLP bonding of a corresponding gap width. This eutectic can be completely eliminated in a very short holding time thus resulting in complete isothermal solidification of the joint. Electrochemical potentiodynamic polarization in three different mineral acids, HNO_3, H_2SO_4 and HCl, showed that TLP bonded joint with a Cr-bearing interlayer alloy has better CR compared to a Cr-free interlayer alloy. The CR of bonded joints increases as the width of the centreline eutectic is reduced. TLP bonded joints that are bonded with the mixed composite powder method have better CR compared to those that use conventional TLP bonding. The bonded joint produced with the mixed composite powder mixture with no eutectic shows a comparable CR as the base material even at high temperatures in all three testing environments.

1.4 Thesis layout

This dissertation contains 5 chapters. The organization of the paper is as follows,

- Chapter 1 provides detailed background information, objectives of the research and major findings from the study,

- Chapter 2 provides a detailed review of the literature with focus on the microstructure of Ni-base superalloys, alloying elements and phases present, joining and repair

techniques for Ni-base superalloys, transient liquid phase bonding description and process parameters, and corrosion of Ni- base superalloys in aqueous media,

- Chapter 3 provides the experimental plan, materials used, preparation procedure, testing equipment and methods used to carry out the research work,

- Chapter 4 provides the results obtained from this study, and a detailed discussion of the results and how these results contribute to the current state of knowledge, and

- Chapter 5 summarizes the major findings, conclusions of the current work and suggestions for future work.

CHAPTER 2. Review of Literature

Ni-base superalloys are the dominant group in the category of high-temperature materials generally known as superalloys. They have emerged as the material of choice for high temperature applications where resistance to creep, fatigue, oxidation and environmental degradation is required. The development of superalloys parallels the evolution of gas turbine engines [1,2], where the need to increase the gas turbine inlet temperatures, in order to achieve higher thermal efficiency and overall system reliability, is of great concern in the aviation industry. Ni-base superalloys have a complex and sophisticated metallurgy. Irrespective of the elemental additions, they generally exhibit a reliable microstructure at elevated temperatures. This is due to the fact that Ni, the main alloying element, has an FCC crystal structure which is stable from room temperature to its melting point and hence there is no phase transformation that causes notable expansions and contractions which could inhibit its use in high temperature applications [2].

Depending on the microstructural changes or properties required, Ni-base superalloys could contain up to ten (sometimes even more) different alloying elements. Al, Ti and Cr reduce the density and improve the resistance of Ni-base superalloys to corrosion whereas tungsten, rhenium and tantalum increase the density and strength of the superalloy. The contribution of the alloying elements and main phases in Ni-base superalloy as well as classification will be discussed below.

2.1 Alloying Element Composition and Role in IN 738

A unique characteristic of Ni as a solid solvent is that its electronic configuration in the FCC lattice enables it to dissolve many other elements to achieve solid solution alloying. Each alloying element behaves differently and its influence on the phase stability to a large extent is

a function of its relative position in the periodic Table [2]. Cobalt (Co), Cr, iron (Fe), molybdenum (Mo), rhodium (Rh), rhenium (Re) and tungsten (W) are added for solid solution strengthening, which is achieved by lattice distortion [1]. They strengthen by partitioning the austenitic γ and in so doing, stabilises it [2]. When Al, niobium (Nb), tantalum (Ta) and titanium (Ti) are added, they promote the formation of ordered phases, such as Ni_3(Al, Ta, Ti) otherwise known as γ'. The increase in oxidation resistance is also achieved by the addition of Cr and Al (when sufficiently present) as they form impregnable passive layers of Cr_2O_3 and Al_2O_3 respectively during oxidation. Al, Cr, Mo and Ta also increase hardness. While Co increases the upper temperature limit to which an alloy can be used, it also increases the ability of the alloy to form the γ' phase, which is commonly obtained by the addition of Al and Ti [16]. In addition, Co also modifies the solubility of the γ' phase. Cr, Mo and Fe promotes the formation of topologically close-packed (TCP) phases in alloys. Boron (B), carbon (C) and zirconium (Zr) are added for improvements in creep properties and hot workability as they tend to segregate the grain boundaries of the γ phase and hence are known as grain boundary formers or boundary strengthening elements. Cr, Mo, Nb, Ta, Ti and W are strong carbide formers; and Cr and Mo promote boride formation within alloys [1,2]. In spite of the many benefits of Cr, Mo and W on the oxidation and creep strength of superalloys, their content must be limited in aerospace applications as they are precursors to the formation of deleterious intermetallic phases, namely the Laves phases μ and σ with an embrittling platelet like morphology [1,16]. Table 2-1 provides a list of the alloying elements in IN 738 while Table 2-2 gives a summary of the effects of each alloying element.

2.2 Phases in IN 738 Superalloy

The phases present in the microstructure with respect to the alloying element present and how this phase impacts the performance of IN 738 will be discussed next.

2.2.1 Gamma Phase γ

The Ni FCC lattice has very high stability over a wide range of temperatures and large solubility for many other metals, and thus the FCC phase is the continuous matrix phase for Ni-base superalloys. The addition of alloying elements into a substitutional solid solution of this matrix is known as the austenitic γ phase, which contains relatively large amounts of the elements Al, Co, Cr, Fe, Mo, Re, Ru, Ti, and W. Where these elements are present [2,17,18], they occupy substitutional atomic positions in the Ni crystal lattices since their atomic diameters differ from Ni by 1 – 18%, thereby producing a distorted lattice with a spherically symmetrical strain field. This strain field can interact with the strain field around a dislocation, thus producing an elastic dislocation-solute atom interaction and providing solid-solution strengthening. The γ matrix serves as a medium of dispersion for ordered intermetallic Ni_3(Al, Ti)-type γ' precipitates along with carbides and other phases present [1,18]. The addition of these elements to the γ matrix induces a gain in strength through solid solution strengthening as a result of the increase in resistance to the dislocation motion from the lattice distortion which is caused by the relative difference in atomic size between Ni and the alloying solute atoms, up to a maximum of 10% [1]. The strengthening of the γ phase becomes diffusion controlled at temperatures greater than 60% T_m (T_m is the melting temperature of the alloy with the use of the Kelvin scale) and the slow diffusing Mo and W produce greater hardening by reducing high temperature creep [1].

The ability of the γ matrix to withstand severely high temperatures is due to the high tolerance of Ni for alloying without phase instability owing that it has a nearly filled third electron shell [17,19]. Cr in the γ matrix, depending on the relative amount present, forms Cr_2O_3-rich protective scales with low cation vacancy content, thereby restricting the diffusion rate of the metallic elements outward, and that of oxygen, nitrogen, sulphur and other aggressive atmospheric elements inward. There is also the additional tendency to form Al_2O_3-rich scales with exceptional resistance to oxidation [19].

Table 2-1: Nominal composition on IN-738LC [2,16,20]

Elements	Nominal Composition of IN 738LC wt%
Carbon	0.110
Chromium	16.000
Cobalt	8.500
Molybdenum	1.750
Tantalum	1.750
Titanium	3.400
Aluminum	3.400
Tungsten	2.600
Silicon	0.040
Niobium	0.900
Iron	0.070
Boron	0.010
Manganese	0.010
Sulphur	0.001
Zirconium	0.000
Nickel	Bal

Table 2-2: Effect of major alloying elements in IN 738 [1]

Element	Matrix Strengthening	Increase γ' volume fraction	Grain boundaries	Other effects
Cr	moderate	moderate	$M_{23}C_6$ and MC	improves corrosion resistance promotes TCP phases
Mo	moderate	moderate	M_6C and MC	increases density
W	moderate	moderate		promotes TCP phases σ and μ (Mo,W)
Ta	high	large		
Nb	high	large	NbC	promotes γ' and δ phases
Ti	moderate	very large	TiC	
Al	moderate	very large		improves oxidation resistance
Fe		γ'→β, η, γ'' or δ		decreases oxidation resistance promotes TCP phases σ, Laves
Co	slight	moderate in some alloys		raises solidus; may raise or lower solvus
Re	moderate			retards coarsening increases misfit
C	moderate		carbides	
B, Zr	moderate			inhibits carbide coarsening improve grain boundary strength improve creep strength and ductility

Table 2-3: Mechanical and physical properties of IN-738 [16,20]

Temperature (˚C)	Yield strength (Mpa)	Ultimate Tensile strength (Mpa)	Elongation (%)
21	951	1096	5.5
649	910	1055	7
760	793	965	6.5
871	552	772	11
982	345	455	13
Density		$8.11 g/cm^3$	
Melting Range		1232 - 1315 ˚C	
Young Modulus		200.2 Gpa	
Shear Modulus		78 Gpa	
Poisson's Ration		0.29	
Coefficient of Thermal Expansion		15.36×10^{-6} @ 1093˚C	

2.2.2 Gamma prime (γ'), Gamma double prime (γ'') and Delta (δ) Phases

The γ' phase is the principal high temperature strengthening phase in many precipitate-hardened Ni-base superalloys. It is an FCC ($L1_2$) ordered intermetallic phase with a basic composition of Ni_3(Al, Ti) with Al (or Ti) atoms at the cube corners and Ni atoms at the centre of the faces (see Figure 2-1) formed in Ni-base superalloys that contain Al or Ti in an amount that exceeds their solubility in Ni. The γ' can homogenously precipitate and remain stable at high temperatures in the γ matrix, and due to the proximity of the lattice parameter of the γ matrix and γ' precipitate, there is a distinct cube-cube orientation [1,2]. The γ' precipitate contributes to strength and creep by restricting the amount of dislocation movement and thus a larger volume fraction of γ' is desirable as considerable energy is required for a dislocation to penetrate γ' particles [1], and the volume fraction of the γ' phase formed is a function of the hardening element content. The morphology of γ' is a function of the γ/ γ' lattice mismatch, and with increasing mismatch, the shape changes in the following order: spherical, globular, blocky, and cuboidal [16].

For Ni-base superalloys that contain a significant amount of Fe and Nb, the principal strengthening phase is not the γ' but a body centered tetragonal ordered phase called γ'', which exhibits a disc-shaped morphology on the {100} planes with an approximate thickness of 10 nm and diameter of 50 nm, and generally found to be coherent with the matrix [2,16]. The γ'' phase provides very high strength at low to intermediate temperatures; however, it becomes very unstable at temperatures beyond 1200˚C. Precipitate strengthening with both γ' and γ'' is possible in Ni-base superalloys that contain Al, Nb and Ti in significant proportions. The formation of the undesired orthorhombic δ phase which is incoherent with the matrix and does not confer strength occurs when the γ/γ' lattice mismatch is high at increased exposure to temperatures above 700˚C [16] and in over aging of Ni-base alloys that contain γ'' precipitates [17].

2.2.3 Carbides and Borides

Carbides MC, M_6C, $M_{23}C_6$ and M_7C_3, where M stands for a metal, are formed in Ni-base superalloys between refractory metals like Mo, Nb, Ta, Ti and W when the carbon content is greater than 0.05% [21]. M_3B_2 borides with a tetragonal structure are common in superalloys when the boron content is 50 to 500 ppm, and often segregating at the γ-grain boundaries [16]. M_5B_3 borides have been reported to occur during certain heat treatment conditions [22]. MC is the most common carbide found in Ni-base superalloys, precipitating from a liquid phase during solidification [2,21]. These carbides are unstable; hence under the influence of service temperature and time, they may experience transformations that change their size, morphology and type, which inherently influences the behaviour of the alloy at elevated temperatures [2,16]. They are often found in the interdendritic regions (either intragranular or intergranular positions) with no distinct orientation relationship with the γ matrix with blocky or script morphologies [2]. $M_{23}C_6$ are formed during the transformation of MC carbides upon prolonged exposure at service temperature (around 750˚C) via reaction of the following type:

$$MC + \gamma \rightarrow M_{23}C_6 + \gamma' \quad \ldots\ldots\ldots\ldots\ldots\ldots \quad (2.1)$$

$$MC + \gamma \rightarrow M_6C + \gamma' \quad \ldots\ldots\ldots\ldots\ldots\ldots\ldots \quad (2.2)$$

The $M_{23}C_6$ are found to preferentially precipitate on the γ-grain boundaries [2], which leads to a temporary increase in the creep resistance and improvement of the plasticity of Ni-base superalloys by hindering grain boundary sliding at elevated temperatures [2,16]. The preferential precipitation of borides and carbides at the γ-grain boundary and their resultant effect on the rupture strength via the inhibition of grain boundary sliding is the reason that they are known as grain boundary strengtheners.

2.2.4 Topologically Close-packed Phases

Intermetallic phases, including Laves phases μ and σ which exhibit a plate-like morphology with complex crystal structure that has a high uniform packing density of atoms, and are generally referred to as topologically close-packed phases for this reason [2], are precipitated when there is an excess of alloying elements such as Cr, Mo, Re and W [1,2,16,23]. Topologically close-packed phases tend to hold down essential γ and γ' strengtheners and have also been found to be detrimental in damaging the mechanical properties of superalloys as crack initiators, owing to their brittle nature [17]. They can be formed in IN 738 under certain conditions either during heat treatment or more commonly during service conditions.

2.2.5 Classification of Nickel-based Superalloys

The technique used in the manufacture of any material has a key influence on the microstructure, phases present and actual properties. Hence, for Ni-base superalloys irrespective of the relative alloying compositions, a wide variety of properties could be obtained by adopting a specific manufacturing technique and controlling various aspects, such as the heating rate and the solidification process. When the grain formation is controlled, the result is three different class of microstructures, which are 1) polycrystalline 2) directionally solidified (DS) polycrystalline, and 3) SX. Polycrystalline microstructures could also be equiaxed or columnar grains, which also applies to the case of DS polycrystalline microstructures. In the application of superalloys for the production of jet engine components, it was found that the grain boundaries are the point of weakness, owing to the high stress concentration in these areas, and therefore, performance could be significantly improved by reducing the volume of grain boundaries [1,2,16], particularly that of γ/γ' to produce columnar structures through directional solidification with the grain boundaries aligned parallel to the axis. Advancement in material

process techniques have led to further progress with the development of a new generation of superalloys that have fewer grain boundaries or elimination of grain boundaries, with each consisting of single crystals along different orientations with a higher stability and larger volume fraction of γ'. Although superalloys with all three classes of microstructures are being used for various components in current modern jet engines based on the severity and hostility levels of the environment in which the components are used, a lower grain boundary density is favourable for elevated temperatures where oxidation is most likely to occur. The elimination of grain boundary strengthening elements such as B, C and Si have ensured that the single crystals would have an even better performance, including, increased melting temperature as the rebalanced chemistries of the alloying elements increase the solidus temperature obtained beyond the γ', lower elastic modulus along the <100> directions, increase in creep resistance which increases thermomechanical fatigue in areas of constrained thermal expansions, and better creep resistance, since the grain boundaries are susceptible to intragranular corrosion [2]. Investment casting is used to produce SX components, such as turbine blades, although some other techniques use the principle of directional solidification, as the high cost of the casting technique necessitates that the SX superalloys are predominantly used in vanes and blades located in the hot sections of turbines engine where the turbomachinery is pushed to extremes of the material properties [2,24]. The demand for higher operating efficiencies viz-a-viz operating temperature in jet engines has led to the extensive use of SX superalloys in the aerospace industry in the last two decades.

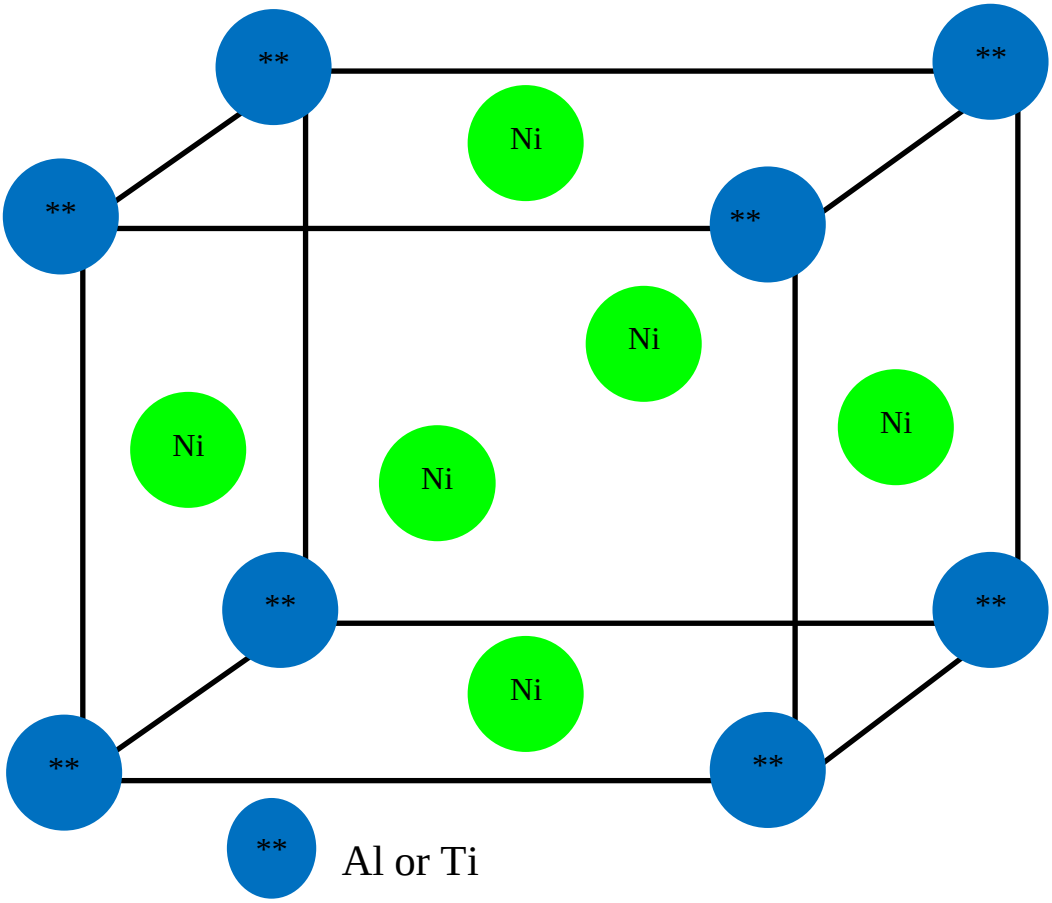

Figure 2-1: L12 FCC structure of $Ni_3(Al, Ti)$

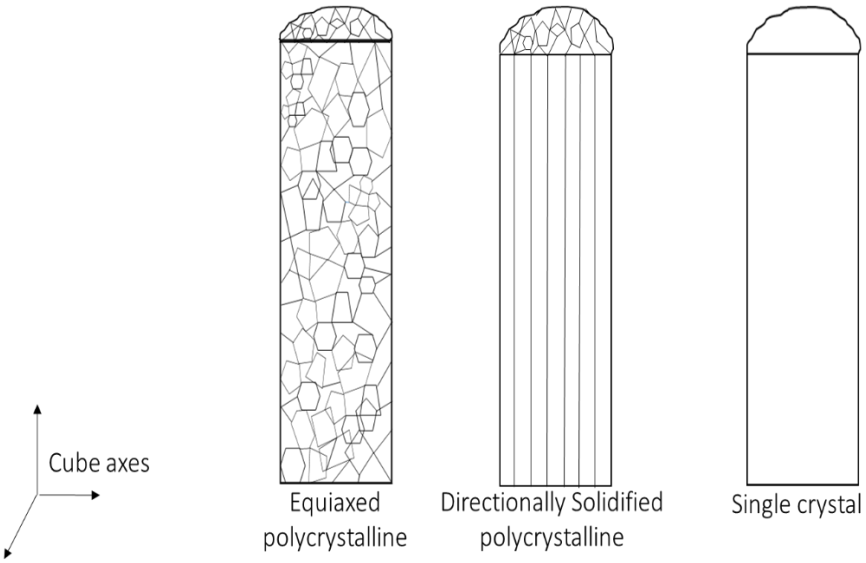

Figure 2-2: Classification of Ni-base superalloys based on grain formation

2.3 Joining and Repair Techniques for Ni-base Superalloys

A fundamental feature of technological advancement in the aerospace industry is the creation of single, large and continuous structures, which takes advantage of the unique characteristics of Ni-base superalloys. Consequently, joining techniques that preserve the basic microstructure of these superalloys, as this is the origin of their excellent performance, are required. There are three basic techniques used in engineering for joining materials and these are [25]:

- mechanical,
- chemical, and
- physical methods

Mechanical methods, including the use of fasteners and similar components, are typically used in situations where frequent disassembling is required, while chemical methods involve the use of certain adhesives or chemicals with hydrating effects to join materials. Both of these joining methods are typically used for temporary joints and therefore not suitable for the Ni-base superalloys which are expensive to manufacture.

Physical joining, however, includes all processes based on the phase transition from the liquid to the solid state, examples of which are fusion welding, brazing and soldering and solid-state joining processes or diffusion bonding [25,26]. They are typically used for permanent joints and advantageous in that the process can be controlled such that the microstructure at the joint region and the base substrate are similar, and for this reason they tend to be favoured in the joining of most metallic materials. Ni-base superalloys are used in component such as turbine blades, which operate for protracted length of time in severe service conditions that then causes the rapid degradation of the blades either through creep, fatigue or foreign object damage (FOD). Outright replacement of these parts may not be economical due to part complexity and the specialized methods used to manufacture them, which are quite capital intensive, hence

repair is becoming a more viable option in lieu of replacement. However, this option has meant that much research is being carried out towards finding a joining and repair technique that not only produces an effective joint from a structural point of view but incorporates both mechanical and physical properties of the Ni-base alloy at the joint region. Generally, welding and brazing are the two common joining methods used for the repair of Ni-base superalloys. A review of these physical methods for joining Ni-base superalloys, examination of the process, and their limitations, advantages and disadvantages will be discussed.

2.3.1 Fusion welding

Fusion welding is a generic term used to describe all welding processes that involve localized heating of the materials that will be joined thereby creating a liquid which is subsequently cooled. This type of welding creates a temperature gradient along the material, mostly between the weld pool and the far end of the base materials, as the base material is at or near room temperature during the welding process [27]. Due to this high heat transition, a heat affected zone (HAZ) is created [28] as shown in Figure 2-3. In some cases, the high temperature at which the fusion takes place means that atmospheric oxidation is prevented by use of either a shielding gas or flux that melts to produce a viscous slag on the weld metal that eventually solidifies and can be removed. Also some types of fusion welding could involve the use of a filler material such as a wire or consumable electrode that has a lower melting point than the components that are being joined, then fed into the weld pool in situations where there is a wide gap between the faying surfaces.

There are three broad categories of fusion welding as follows.

1. Gas welding
    - Oxyacetylene welding

2. Arc welding
    - Electro-slag welding
    - Flux cored welding
    - Gas-metal welding
    - Gas-tungsten welding
    - Plasma arc welding
    - Shielding metal arc welding
    - Submerged arc welding
3. High-energy beam welding
    - Electron beam welding
    - Laser beam welding

The heat sources for the three categories of welding are easily determined by their name, which are gas, electric arc and high energy beams respectively. Gas welding is the most common and widely used fusion welding process as it is relatively simpler and cheaper, and the welding equipment is portable; however, it produces the highest amount of heat input into the work piece and lowest power density compared to arc and high energy beam welding. A consequence of using low power input in gas welding is that the welding process occurs at much lower speeds thereby producing more heat input which results in a HAZ and severe distortion of the joint area. High energy beams which have the lowest heat input provide deep penetration and generally produces quality welds in a short amount of time; hence, joints that require multiple-pass welds during gas welding can be welded in a single pass by electron beam welding at high speeds, which results in a very narrow HAZ and little distortion [27]. However, the equipment required for electron beam welding is very expensive and the associated high vacuum and x-ray shielding are inconvenient and time consuming.

2.3.1.1 Limitations of Fusion Welding

Fusion welding is generally used to join various superalloy materials, but its application to Ni-base superalloys that contain substantial amounts of Al and Ti has been restricted due to their high susceptibility to HAZ cracking during welding and post welding heat treatments [4,5], and associated distortion of components that could exist in the HAZ due to the thermal gradient. This has been linked to the large shrinkage stress that develops in Ni-base superalloys due to the rapid precipitation of the γ' particles during cooling down from the welding [29], and cracking probability is normally related to the volume fraction (V_f) of γ' particles present in the alloy. Also localized melting occurs at the grain boundaries thus causing thermally induced welding strains and very low ductility in the alloy, which may induce cracking in the HAZ [30]. Some mechanical properties, like fatigue resistance of the welded joint are usually inferior to those of the base alloy [5,27]. This has been attributed to the stress concentration generated by the high thermal gradients produced during welding which result in the distortion of the welded component in the HAZ area [5].

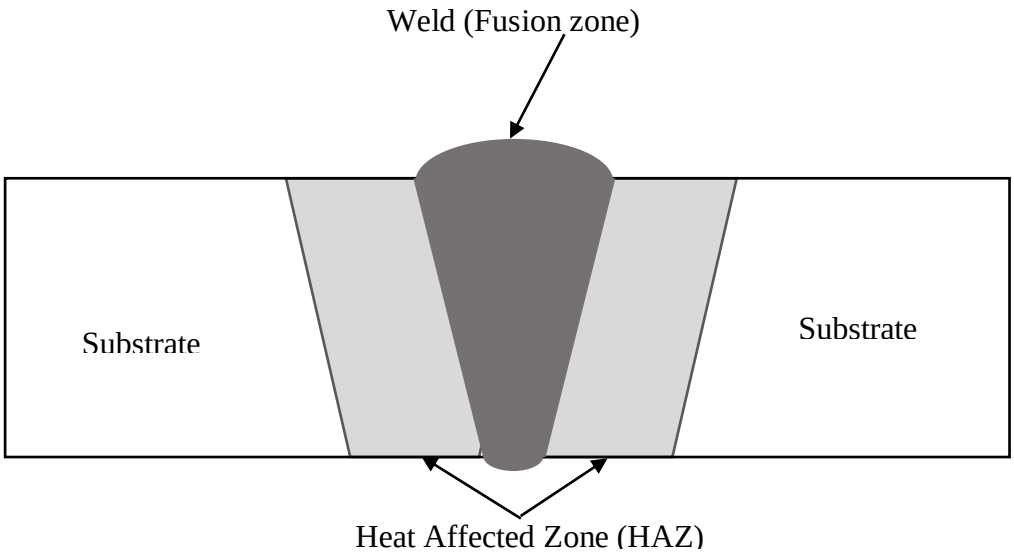

Figure 2-3: Cross-section of a fusion zone joint

2.3.2 Brazing

Brazing is a liquid-solid phase bonding process, where a liquid phase (filler metal is melted) is joined to a solid phase (base material which is not melted). Conventional brazing is a joining technique that involves the joining of two metal surfaces by use of a filler metal and heating to a temperature above 425˚C, which is usually above the melting point of the filler metal thus causing the filler to melt but is lower than the solidus temperature of the base material [31]. The resultant liquid is drawn into the gap between the mating surfaces by capillary action. Metallurgical reactions take place between the liquid and the base material, thus causing erosion (melt-back) around the joint region, which results in cooling. Due to the short holding time, the rate of the solid state diffusion of the solute elements in both the filler metal and base material is limited [27].

During brazing, effective capillary action that is necessary to achieve a high quality joint is to a large extent dependent on the efficient transfer of heat from the heat source to the joint which is invariably a function of the assembly size, number of joints required and the rate of production. Other significant factors that should be considered for the selection of the heat source includes: the rate of heating, thermal gradients and cooling rates, all of which can significantly vary with different heating methods. Brazing techniques are commonly classified by the heat source of heating and the different techniques are [31,32]:

- torch brazing,
- furnace brazing,
- induction brazing,
- dip brazing,
- resistance brazing,
- infrared brazing,

- blanket brazing,
- electron beam and laser brazing, and
- Braze welding.

Other process variables or parameters that affect the quality of the joint obtained during brazing outside of the heat source are:

- the nature of the base material,
- surface preparation,
- the nature of filler alloy,
- gap size,
- brazing temperature, and
- time.

The need for an alternative repair technique that is suitable for the difficult to weld Ni-base superalloys has led to the optimization of the brazing process to what is known as DB. It is called DB as it allows for longer brazing times and a much higher temperature than conventional brazing (albeit lower than the fusion temperature of the base alloy) such that significant elemental diffusion takes place. DB offers the possibility of overcoming the shortcomings of welding processes, with respect to part geometry, excessive thermal gradient cracking and distortion.

Advanced DB techniques are currently being used at a large scale in the aerospace industry for joining most superalloys (Ni-, Ti-, and Co-base alloys). The versatility of the process is such that it can be used for various forms of alloys: cast, wrought or powder, and for joining metals to non-metals, ceramics or fibre composites. It can be well adapted to join single crystal alloy parts without destroying their crystalline form. However, due to the high affinity of superalloys and brazes for oxygen, brazing can only be effectively done in vacuum by using a pressure of

the order 10^{-4}- 10^{-6} torr [33]. Vacuum brazing produces clean and superior joints with high strength, ductility and uniformity.

2.3.2.1 Wide Gap Brazing

In many instances of the brazing of superalloys, wide joint gaps (a gap width of 100 µm or more) are expected partly due to the nature of the damage that occurs in the components to be repaired and allowance that must be made for thermal expansion in the case of dissimilar metals. Wide gap brazing is mostly employed to fill large defects and wide gap cracks, rebuild large worn surface areas of airfoils and components that have been subjected to hot corrosion and/or FOD. The technique is performed by using a mixture of a braze alloy (filler metal that melts) and a high temperature-melting powder (superalloy powder that does not melt, usually referred to as a gap filler). The gap filler particles remain largely un-melted and provide the necessary capillary forces to retain the molten filler metal within the joint in achieving wettability, thus preventing excessive fluidity within the gap of the faying surfaces and acting as a sink for the melting point depressant (MPD) in wide gap brazing. The mixture thus behaves like slurry with sufficient bridging power to fill the gap [31].

2.3.2.2 Advantages of Brazing

Brazing has many distinct advantages. It is an economical means to join simple, complex and multi-component assemblies, and has excellent stress distribution and heat transfer properties. It can also be used to join metals to non-metals as well as metals with thickness that vary widely in size [31]. Strong, uniform and leak proof joints can be rapidly and simultaneously made and close tolerances (dimension precision) can be made via brazing as opposed to fusion welding due to the much lower amount of base-metal melting [34]. The use of an oxygen (and similar

oxidizing substances) free atmosphere such as in a vacuum during brazing produces clean superior brazes. Unlike fusion welding, there is no thermal gradient and hence no HAZ since the whole assembly is brought to the brazing temperature, thus incorporating subsequent heat treatment or ageing process into the brazing cycle can further reduce the overall processing time and cost.

2.3.2.3 Limitations of Brazing

For superalloys that contain significant amounts of Ti and Al, particularly Ni-base superalloys, brazing has proven to be a better joining technique compared to fusion welding. However, some challenges still remain, as follows.

1) Melt-Back: During the metallurgical reaction of the liquid filler metal with the faying surfaces, the diffusion of MPD elements into the base alloy reaches a maximum concentration at the liquid-solid interface which causes melting of this base alloy, known as melt back or base-metal erosion. This causes a reduction in the effective thickness of ductile base alloy and could have serious consequences when thin materials are brazed or the joint is to be used in impact or vibration load conditions.
2) Grain Size: Grain formation within the joint area usually occurs with an optimum grain size that runs through the entire joint width. This is detrimental for high temperature materials as this creates an easy path for crack propagation which is known preferentially occur along the grain boundaries.
3) Porosity: Ni-base superalloys are known to oxidize upon exposure to air, hence, the presence of oxide residues or contaminants (such as organic binders which burn during brazing thereby forming a carbonaceous residue)) promotes the formation of pores and partially filled cracks that weaken the joint.

4) Formation of intermetallic phases: The short thermal cycle during brazing limits the diffusion of the MPDs into the base alloy, which triggers the formation of second phase precipitates or the so called intermetallic precipitates (such as borides, phosphides and silicides). The presence of intermetallic precipitates in Ni-base braze alloys used for high temperature applications is detrimental as they reduce the ductility. These phases are brittle in nature and when formed in a continuous manner, could form a path for crack propagation thereby reducing the toughness of the joint.

Overcoming these limitations of brazing in the joining of Ni-base superalloys, Scot et al. [35] optimized the brazing process and patented a process that they called "transient liquid phase (TLP) bonding". The process has received wide acceptance since it was first used by Scot et al. to join heat resistant alloys, as it holds high promise especially for alloys susceptible to hot cracking during fusion welding. A review of this process is discussed in the following.

2.4 Transient Liquid Phase (TLP) Bonding

TLP bonding is a fluxless process that employs an interlayer alloy (with MPD elements) that has a low melting point with the base alloy to be joined. Heating to the bonding temperature causes melting of the interlayer alloy, which reacts with the base alloy to form a liquid. Isothermal diffusion of the MPD in the interlayer causes transient growth of this liquid phase and subsequently solidification occurs. The process integrates the beneficial features of solid-state diffusion bonding with conventional brazing; hence, it is commonly referred to as diffusion DB. However, the process differs from DB as it incorporates a much lower pressure than that applied in DB to ensure that the mating surfaces are in proximity [8,31] and formation of the liquid interlayer therefore eliminates the need for high a clamping force [36].

Unlike conventional brazing, TLP bonding is more suited for joining components intended for elevated temperatures. The thermal exposure used in the TLP bonding cycle has to be sufficient to induce isothermal solidification at the bonding temperature. During TLP bonding, complete isothermal solidification is possible given a protracted holding time at the bonding temperature while combining isothermal solidification with a subsequent solid state homogenization which offers the possibility of producing joints with a similar microstructure and composition as that of the base alloy [10]. As brazing formation of second phase precipitates (eutectic or peritectic [37]) is possible from the cooling of the liquid that remains in the bonding region if isothermal solidification is not completed, this could greatly impair the mechanical properties of the joint.

In understanding the mechanisms and kinetics of the TLP bonding process, several models that are both analytical and numerical have been developed [37-46] in describing the process, some of which are based on binary alloy system with a liquid interlayer, with the premise that the isothermal solidification process is completed without the precipitation of second phases during holding at the bonding temperature, and the dilution of the remaining MPDs by the base alloy occurs during prolonged homogenization, which produces a joint free of second phase precipitates [11]. However, commercial applications of the TLP bonding use ternary interlayer alloys like Ni-Si-B and Ni-Cr-B, which refute these models and suggest that there is the likelihood of precipitation of second phases at the early stages of the bonding. Indeed, the first use of TLP bonding process was based on an isomorphous azeotropic system, whereas modern theories have been developed on the basis of binary eutectic systems. The application of the TLP bonding process is not solely limited to binary eutectic, but can also be applied to any system in as far as the base-metal or alloy forms a relatively low melting temperature phase and has solubility for the MPD elements [36].

2.5 Process Description and TLP Bonding Process

The term, TLP bonding process, has been interchangeably used in the literature with similar joining processes, such as DB and transient liquid insert metal (TLIM) diffusion bonding, and as such, the description of the process has also been reviewed in various steps or stages. Duvall et al. [6] described the mechanism of bond formation through isothermal solidification in 5 steps. Step 1 involves heating to the bonding temperature and subsequent melting of the interlayer. Step 2 is the dissolution of the base alloy by the liquid interlayer. Step 3 is the isothermal solidification which is completed in Step 4 while Step 5 is the homogenization of the excessive solute at the bond line. These 5 steps were then shortened into 3 discrete stages: base-metal dissolution, isothermal solidification and the homogenization of joints. Tuah-Poku et al. [41] defined four stages during the TLP bonding of silver with then use of copper as the interlayer by expanding the first stage of base-metal dissolution into two stages: dissolution of the interlayer and homogenization of the liquid (by additional dissolution of the base alloy). Insufficient diffusion of solute into the base-metal during the initial heating time from room temperature reported by Niemann and Garrett [47] led Macdonald and Edgar [36] to incorporate an initial stage (Stage 0) to account for this effect. Zhou et al. [37] further classified the TLP bonding process in to four different stages as follows.

Stage I: Heating stage (stage 0 per Macdonald and Edgar [36])

Stage II: Dissolution and widening

- II-1: Heating from melting point to bonding temperature
- II-2: Isothermal dissolution at the bonding temperature

Stage III: Isothermal solidification

Stage IV: Homogenization

From the foregoing, it can be said that a fitting description of the critical stages in the classification of the TLP bonding process can be achieved by using a binary eutectic equilibrium phase diagram in conjunction with the time–temperature relationship as shown in Figures 2-4 and 2-5 respectively.

2.5.1 TLP Bonding Process Parameters/Variables

The process variables or parameters in brazing processes are well applicable to the TLP bonding process. An additional variable of utmost importance is the joining atmosphere during TLP bonding as process occurs at a much higher temperature than brazing. Therefore, there is greater potential for oxidation. The effect of this variable in producing a defect free joint will be discussed in the following section.

2.5.1.1 Joining Atmosphere

The joining atmosphere is very critical for achieving joints of high quality; therefore, by conducting the TLP bonding under a protective atmosphere with a shielding gas (chemically inert or active gas) or in vacuumed environments prevents joint contamination from volatile substances and formation of oxides. The TLP bonding of Ni-base superalloys takes place at temperatures above 1000˚C, and at this high temperature, there is a significant tendency for the base alloy to oxidize, and as such, complete shielding of the atmosphere is required. In the selection of an appropriate shielding gas, due consideration must be given to the combination of the shield gas with the base alloy. Chemically inert gases like argon, helium and nitrogen function by preventing oxygen and other gaseous elements that might react with the braze assembly to form surface films and restrain flowing and wettability of the liquated interlayer alloy [34]. Chemically active gases like ammonia, carbon monoxide and hydrogen which have

the ability to dissociate at high temperatures react with any surface oxide present or formed during the bonding. However, in certain alloys that contain Al and Ti, such as Ni-base alloys, it was found that the effectiveness of a hydrogen shield is reduced [34]. Also a hydrogen atmosphere can lead to hydrogen embrittlement in alloys that contain Ta, Ti and Zr while nitrogen is not compatible with alloys that contain Mo, Ti and Zr due to the nitriding effects. The use of a vacuum furnace for brazing eliminates the various challenges with shielding gases, gives a better heat distribution within the brazing chamber, and lower operation costs can be realized. Hence the TLP bonding of most Ni-bases alloys are done inside a vacuum furnace, with a vacuum from $10^{-4}$to 10^{-6} which is maintained throughout the bonding cycle.

2.5.1.2 Surface Cleaning and Preparation

The main physical phenomenon that keeps the liquid interlayer within the faying surface is capillary flow which is a function of the surface tension (high), wettability (high) and viscosity (low) of the liquid interlayer. A contaminated surface reduces the surface tension, and increases the contact angle (reduces wettability) and viscosity of the liquid interlayer. Ni-base superalloys are known to oxidize when exposed to air, thus forming a protective oxide layer. The oxide layer can affect the diffusion of elements across the solid-liquid interface; therefore, a clean surface is vital to producing a good quality joint. Surface oxide on the interlayer material has two possible effects. One the oxide layer could act as a container that restrains the liquid interlayer from spreading and its presence could modify interfacial energy and/or interfacial reactions. The presence of surface oxide on the interlayer can be of great significance especially if the oxide layer of the interlayer becomes entrapped between the liquid/solid interface. In that case, the oxide layer can act as a diffusion barrier [10]. For repair of in-service components, surface integrity can be compromised by the presence of combustion products, debris build up and oxidation, as well as coatings that might have been applied for corrosion prevention.

Removal of contaminants like grease, oil or any residual films or oxide is important and this can be done by any of the following methods or their combinations as required:

- mechanical cleaning (grinding and grit blasting),
- chemical cleaning (fluoride ion and hydrogen gas cleaning), and
- physical cleaning (vacuum cleaning).

Once surface cleaning and preparation have been carried out, the components should be immediately assembled and bonded.

2.5.1.3 Nature of Base Material

The chemical and physical characteristics of the base alloys influence the interlayer alloy used, and bonding temperature and time required to achieve quality joints during TLP bonding. The main factors of consideration are the effects of change on the concentration of MPD elements in the base alloys [34], since it must be able to adequately accommodate the MPD elements regardless whether there is some initial quantity. At the chosen bonding temperature, the base alloy must possess sufficient strength as well as both chemical and thermodynamic stability such that the formation of second phase precipitates at the bonding temperature does not occur. The microstructure of the base alloys also influences the TLP bonding process as shown by Saida et al. [48], in that the grain size increases the isothermal solidification completion time in the order of SX, coarse-grained and fine-grained Ni-base alloys. Also, the formation of second phase precipitates in the base alloy region adjacent to the base alloy-joint interface which is a common occurrence in polycrystalline superalloys influences the holding time and these precipitates have been found to profoundly affect the mechanical properties negatively when present [49]. The presence or absence of the grain boundary in the base alloy can significantly affect the rate of isothermal solidification, as grain boundary diffusion is faster than bulk

diffusion over a certain temperature range (depending on the melting point of the base alloy) and increases with decreasing grain size [8].

2.5.1.4 Filler or Interlayer Alloys

For a high quality joint, the filler alloy and base material must be highly compatible in terms of both the composition and physical characteristics. A critical physical characteristic is that the melting temperature of the filler alloy must be lower than that of the base material to be joined, and this difference in temperature is the autogenesis of isothermal solidification. Furthermore, the composition and amount of the filler alloy must be such that the microstructural and chemical homogeneities of the bond region with the base material can be achieved with realistic processing times. The filler alloy must also have proper fluidity at the bonding temperature to ensure adequate wetting and capillary flow [10]. Fillers with eutectic compositions have the best spreading characteristic compared to hypo- or hyper-eutectic compositions. Typical fillers used in the brazing of superalloys are those that are Ni and Co-base which contain one or more MPD element(s), such as B, Si and P, added in specific amounts to produce the required melting temperature. A peculiar requirement of MPD elements is high solubility and /or infusibility in the base alloy, hence B is present in most fillers due to its small atomic radius and the resultant high interstitial diffusion in Ni-base alloys. Other elements, such as Al, C and Ti, are reduced to as low as possible or intentionally not used in filler alloys since they have the tendency to form stable interfacial phases in the bond [5]. Cr is often added to the filler in amounts up to 20% to enhance the oxidation and CR and to improve the mechanical properties of the joint [34]. Filler alloys are available in various forms, such as amorphous foil, tape, powder or paste and rapidly solidified sheets. Foils which are produced by rapid solidification during melt spinning operations are available in thicknesses of 0.0025-0.6 mm and widths up to 50 mm while powders are produced by gas atomization and available in specific particle sizes [50].

Often, powders are mixed with organic binders or plasticizers to enhance positioning on the faying surfaces. Foils and tape fillers are suitable for applications that require joints with a large bond area, good fit-up or in situations where flow and wettability are a challenge [51]. The type of solute MPD and amount (or thickness) of the filler alloy have significant impacts on the kinetics of TLP bonding with respect to the time required for the completion of isothermal solidification. MPDs with high solubility and diffusivity in the base alloy are favourable. Combinations such as Ni-Bi-Si, B with high diffusivity and Si with high solubility in Ni, are widely used; however, for high temperature applications like Ni-base superalloys which require oxidation and corrosion resistant joints, Ni-Cr-B commercial filler alloys are used. The degree of base-metal dissolution increases as the amount of interlayer material increases, which in turn, leads to longer processing times for the completion of isothermal solidification. There is a critical interlayer thickness below which shrinkage of the base-metal and pore formation in the joint occur, and above which formation of secondary intermetallic precipitation phases occur and hence longer processing times [52].

2.5.1.5 Gap Size

The gap size influences both the quality and microstructure of the joint. For effective capillary flow, the gap size should be narrow (<100 μm) for the liquid interlayer to flow through, an overly narrow gap causes "sluggishness" of the liquid interlayer at the bonding temperature, while an overly large gap lacks adequate capillary forces to hold the liquid between the faying surfaces which causes the liquid interlayer to flow out of the joint. Both scenarios cause the formation of voids due to shrinkage effects which leads to poor joint quality. Their influence on the joint microstructure is driven by the amount of interlayer alloy (that contain MPD elements) required to produce the joint. An overly narrow gap causes significant diffusion of the MPDs into the base alloy while a wide gap requires a long processing time for the diffusion

of MPDs into the base alloy. Both conditions cause deviations in the chemical and microstructural homogeneities of the joint region to the base alloy. A wider gap results in a longer the processing time required to obtain a joint that is free of deleterious second phase precipitates since it will take a longer time for the MPDs to be fully diffused away from the joint.

2.5.1.6 Bonding Temperature and Time

The bonding temperature is the ultimate parameter that determines the final quality of the joint as it controls critical kinetic processes (like wetting, braze flow and diffusion) [33,53-57] that are involved in the development of the microstructure during joining. For thermally activated processes (TAPs) such as TLP bonding, significant changes in temperature cause the greatest amount of changes in the process kinetics compared to other process variables. The minimum bonding temperature must be higher than the melting temperature of the interlayer alloy but lower than that of the base alloy [31,58]. Excessively high temperatures may initiate other TAPs, like annealing, grain growth or warpage and the dissolution of precipitates in the base alloy. The lowest bonding temperature tends to be favoured due to: 1) the heating effects on the base-metal, 2) minimization in the heating energy cost, and 3) minimization of interlayer alloy-base alloy interactions (i.e. less base-metal dissolution) [10,33,57]. Higher temperatures could be suitable under certain circumstances, such as by: 1) combining post weld heat treatment with a brazing cycle, 2) removing oxides and surface impurities by vacuum brazing, 3) enabling the use of higher melting temperatures but more efficient interlayer alloys and 4) promoting base-metal-interlayer interactions in order to modify the composition and microstructure of the brazed joint [33]. The significance of time is intricately linked with the rate of diffusion of the MPDs (which diffuse into the base alloy) and base alloy strengthening elements (diffuse into the joint) which increases with increases in temperature. Higher diffusion rates allow for the

completion of isothermal solidification in a shorter period of time, which in effect, results in a joint that is both chemically and microstructurally similar to the base alloy. While lower diffusion rates lead to incomplete isothermal solidification, the outcome is the presence of second phase precipitate or eutectic within the joint. Thus, holding time plays a crucial role in the TLP bonding and a combination of optimal bonding temperature and time is paramount [54,59-61]. This can be achieved by gaining a thorough understanding of both the physical metallurgy of the base alloy and the interaction of the base-metal with the filler alloy [33].

2.5.2 Wide Gap TLP Bonding

Similar to wide gap brazing, wide gap TLP bonding is typically used to join large gaps in which the isothermal solidification completion time exceeds that which is theoretically feasible. Wide gap TLP bonding incorporates the use of multiple interlayers (or composite interlayers) that consist of a nominally non-melting phase (with a melting temperature higher than the bonding temperature) and a liquid forming phase within the joint to shorten the processing time [10,62-66]. This higher temperature constituent does indeed partially melt and partakes in the dissolution process [10,66], and therefore, should have a similar composition as the base alloy. In addition to filling large gaps, wide gap TLP bonding performs two other functions: acts as a sink for the solute (Si or B) in the brazed joint by increasing the interfacial area (effective diffusion path) between the liquid and solid phases and also provides a capillary path for the liquid interlayer, thereby reducing the relative amounts of solute within the brazed joint or volume of melting interlayer material required to achieve complete isothermal solidification [10,62,65,66]. In the application of wide-gap TLP bonding, the interlayer material combination has varied from a mixture of foil and power coatings [39,67,68] to powder compact mixture which has been extensively applied in conventional TLP bonding to accelerate the isothermal solidification and homogenization process [69,70]. A critical requirement in wide-gap TLP

bonding is further optimization of the process parameters that influence the joint quality during conventional TLP bonding [49,65]. Among these parameters, bonding temperature is one of the most important because it could cause the formation of porous joints if it is not high enough. The chemical composition of the non-melting interlayer or composite mixture ratio which influences the number and type of phase stabilized in the brazement [10,65] is also important. The application of wide-gap TLP bonding to join SX Ni-base superalloys has generated different views owing to the above mentioned issues that could occur along with the possibility of stray-grain formation during the isothermal solidification process, which compromises the high temperature properties of the bonded joint. This has been associated with the fact that the majority of the studies on the wide-gap TLP bonding process has been limited to metallurgical aspects and not the process kinetics (such as the dissolution of the interlayer material at the bonding temperature) [10].

2.5.3 Initial Conditions during TLP Bonding

2.5.3.1 Stage I – Heating stage

The first stage which begins the TLP bonding process is the heating stage, since sample preparation and assembly are standard for all joining processes. The heating process is accomplished by simply heating the sandwiched sample from room temperature to the melting point of the interlayer alloy, T_m, and subsequently, the interlayer alloy liquefies. During the rise in temperature to the melting point of the interlayer alloys, some solid state diffusion between the base-metal and the interlayer alloy occurs; consequently, the solute concentration at the base-metal-interlayer alloy interface changes. The degree of solid state diffusion and solute concentration change at this interface during the heating stage is largely dependent on the rate of heating and the heating method used as well as the diffusivity of the MPD elements. Very low rates of heating may cause high volume diffusion of the MPDs from the joint region into

the base-metal before reaching the melting point, which results in low liquid volume or no liquid formation upon reaching the bonding temperature. Also, the initial gap size (in the case of powder interlayer alloy) or interlayer thickness (in the case of foil) must be such that the amount of interlayer alloys within the gap exceeds that which is consumed through solid state diffusion; otherwise no liquid is formed at the bonding temperature, T_B [10,52].

2.5.3.2 Stage II-1: Heating from melting point to bonding temperature

The heating is then continued until the bonding temperature, T_B, is reached, which is usually some temperature above the melting point of the interlayer alloy so as to ensure the complete melting of the interlayer alloy i.e. a liquid interlayer alloy is obtained, which flows throughout the joint. Heating beyond the melting point T_m to the bonding temperature, T_B, also causes an increase in the diffusivity of the MPD solute into the base-metal. Consequently, upon reaching the bonding temperature T_B, interdiffusion between the MPD solute elements and the base-metal takes place, such that the concentration of the MPD solute at the base-metal mating surface increases beyond $C_{\alpha L}$.

2.5.3.3 Stage II-2: Isothermal dissolution at the bonding temperature

Immediately, liquidification of the interlayer alloys takes place upon heating beyond the interlayer alloy melting point to the bonding temperature T_B, and partial liquation of the base-metal begins, i.e. the interlayer alloy and base-metal undergo diffusion to form a liquid phase and the composition moves from $C_{\beta L}$ to $C_{L\beta}$, where C is the concentration of the MPD solute. Such dissolutioning (also known as base-metal erosion) results in an increase in the total liquid volume within the joint and hence an increase in the joint width as well as a moving solid-liquid interface until the bonding temperature T_B, is reached; after which, isothermal dissolutioning of

the base-metal takes place, due to the established equilibrium condition at the solid-liquid interface which is defined by a constant diffusion of the MPD solute concentration into the base-metal. The liquid reaches its maximum width at the end of the isothermal dissolution stage.

It is critical to note that the extent of base-metal dissolutioning depends on a number of factors which includes: the initial concentration of the MPD solute in the interlayer alloy composition, initial interlayer thickness or joint gap, rate of heating from the melting point to bonding temperature and the applied bonding temperature. However, dissolution does not require long range diffusion in the solid state. Previous studies have shown that higher applied bonding temperatures results in higher dissolution rates of the base-metal and also more MPD solute in the filler alloy means more dissolutioning. It should be noted that excessive melt back or erosion of the base-metal can have detrimental effects on the final bond as well as result in a longer processing time to achieve complete isothermal solidification. The dissolutioning of the base-metal is intricately unavoidable in the TLP bonding process and has the main beneficial effect of enhancing the alloying process due to the migration of the elements from the base-metal into the joint and thereby improving the mechanical properties of the bonded joint [71]

2.5.3.4 Stage III: Isothermal Solidification

Stage III is the most critical stage in the TLP bonding process. Once local equilibrium is established and maintained at the solid-liquid interface, the base-metal dissolution stops. Continuous diffusion of the MPD solute into the base-metal at the bonding temperature, $T_{B,}$ owing to the difference in the chemical potentials of the MPD solute in the interlayer liquid and the base-metal, results in contraction of the liquid region by conservation of mass as the solidus and liquidus concentrations are now fixed at $C_{\alpha L}$ and $C_{L\alpha}$ respectively. Consequently,

isothermal solidification of the joint proceeds inwards towards the joint centre from the mating of the solid-liquid interface by the interface growing into the liquid.

This stage is critical since the completion time for the entire TLP bonding process is largely dependent on the time required to achieve complete isothermal solidification. The isothermal solidification is very slow compared to the dissolution stage as it is controlled by solid state diffusion of the MPD into the base-metal. Therefore, the time necessary to achieve complete isothermal solidification depends on the diffusion flux of the MPD solute in the base-metal as well as the amount of solute that needs to be diffused. As such, isothermal solidification controls or limits the time to produce a successful TLP bond [10]. Several factors can influence these two variables. Among them are the initial interlayer thickness or joint gap, solubility of the MPD solute and its concentration gradient in the base-metal and the bonding temperature.

Ideally, a single solid solution phase is obtained along the brazement when the holding time is sufficient for complete isothermal solidification. Non-equilibrium solidification of the liquid insert which result from insufficient holding time required to complete isothermal solidification induces a secondary (hard but brittle eutectic microstructure) phase along the joint.

2.5.3.5 Stage IV: Homogenization

This stage proceeds after the completion of isothermal solidification and can take place either at the bonding temperature, or above or below the bonding temperature. During homogenization, solid state solute redistribution occurs to allow parity between the chemical composition of the bonded joint and the base-metal or when the maximum solute concentration at the joint centre reaches a predetermined value in order to attain appropriate levels of mechanical and physical properties in the joint (such as hardness, CR, strength, etc.) or similar to those of the base-metal.

The above stages are well documented in the literature as the primary stages involved in the TLP bonding process and have been studied in detail to understand how each of these stages influences both the process kinetics and the final microstructure, and hence the mechanical properties of the joint.

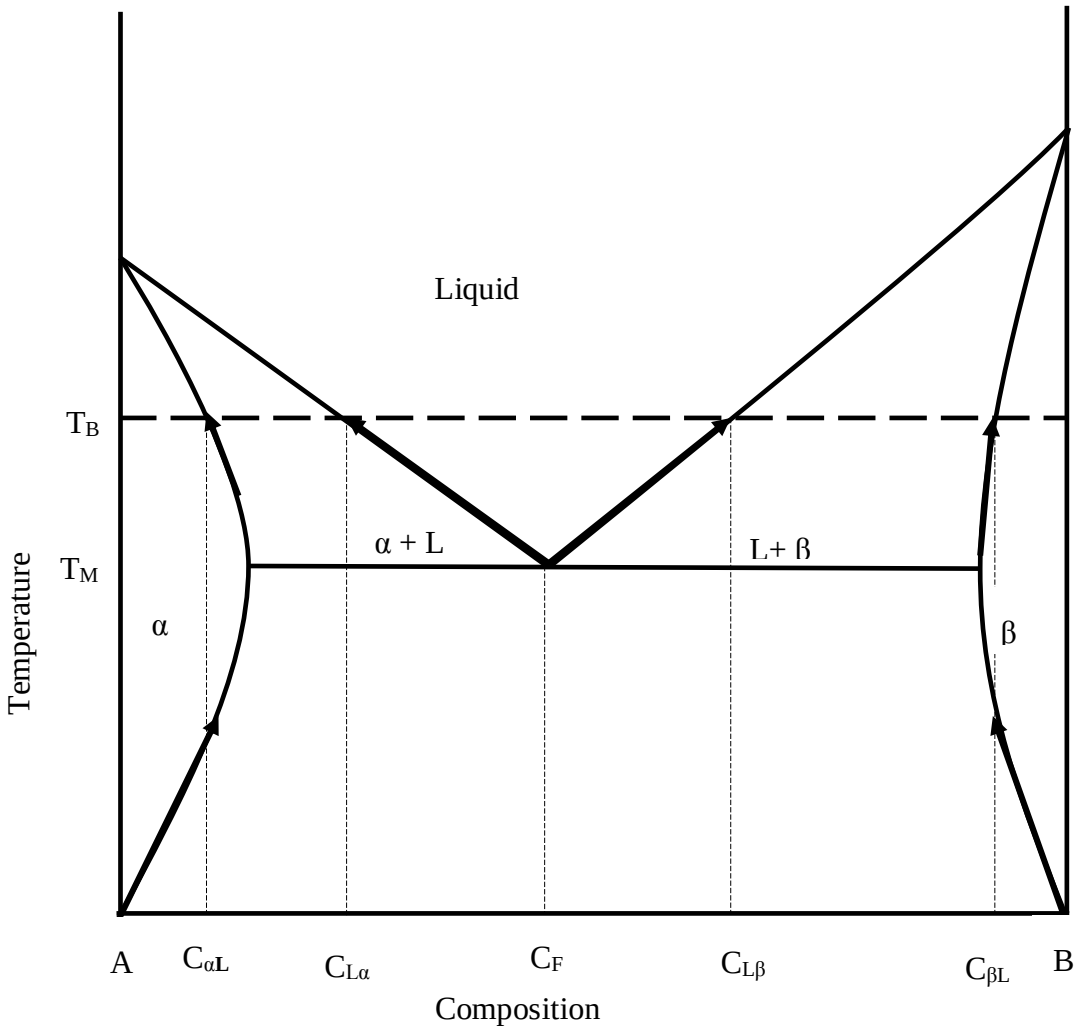

Figure 2-4: Schematic showing hypothetical binary eutectic phase diagram [36]

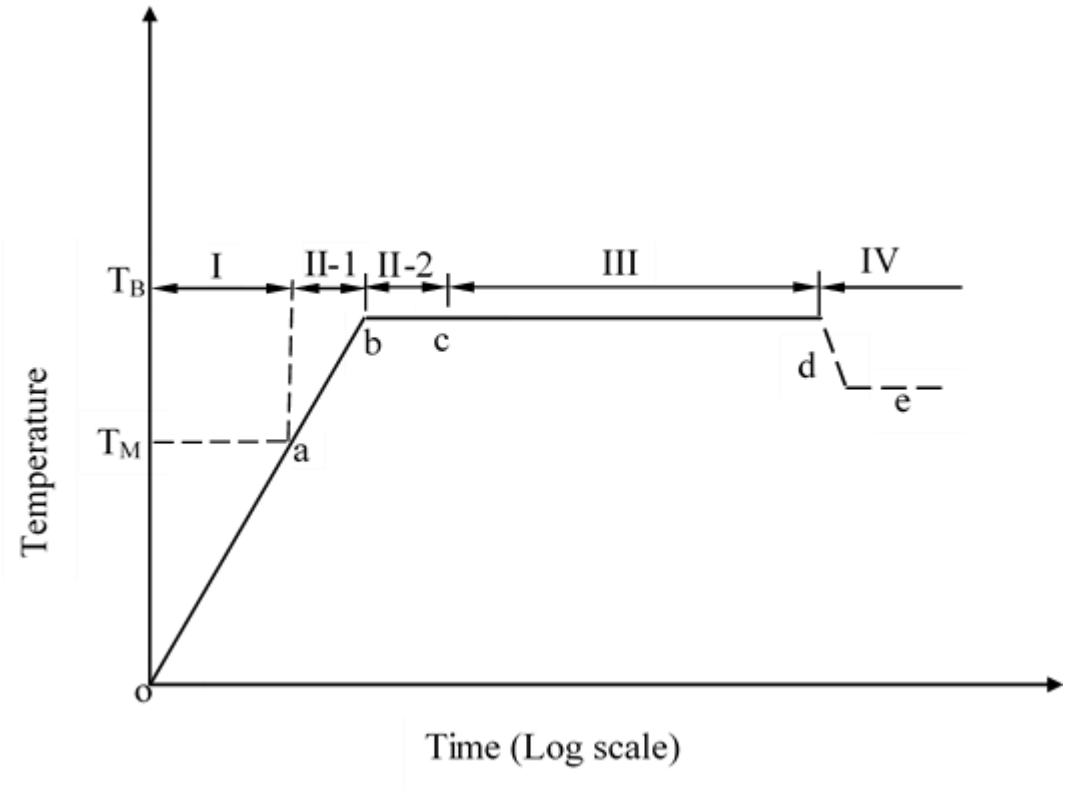

Figure 2-5: Schematic of heating cycle during TLP bonding stages [37]

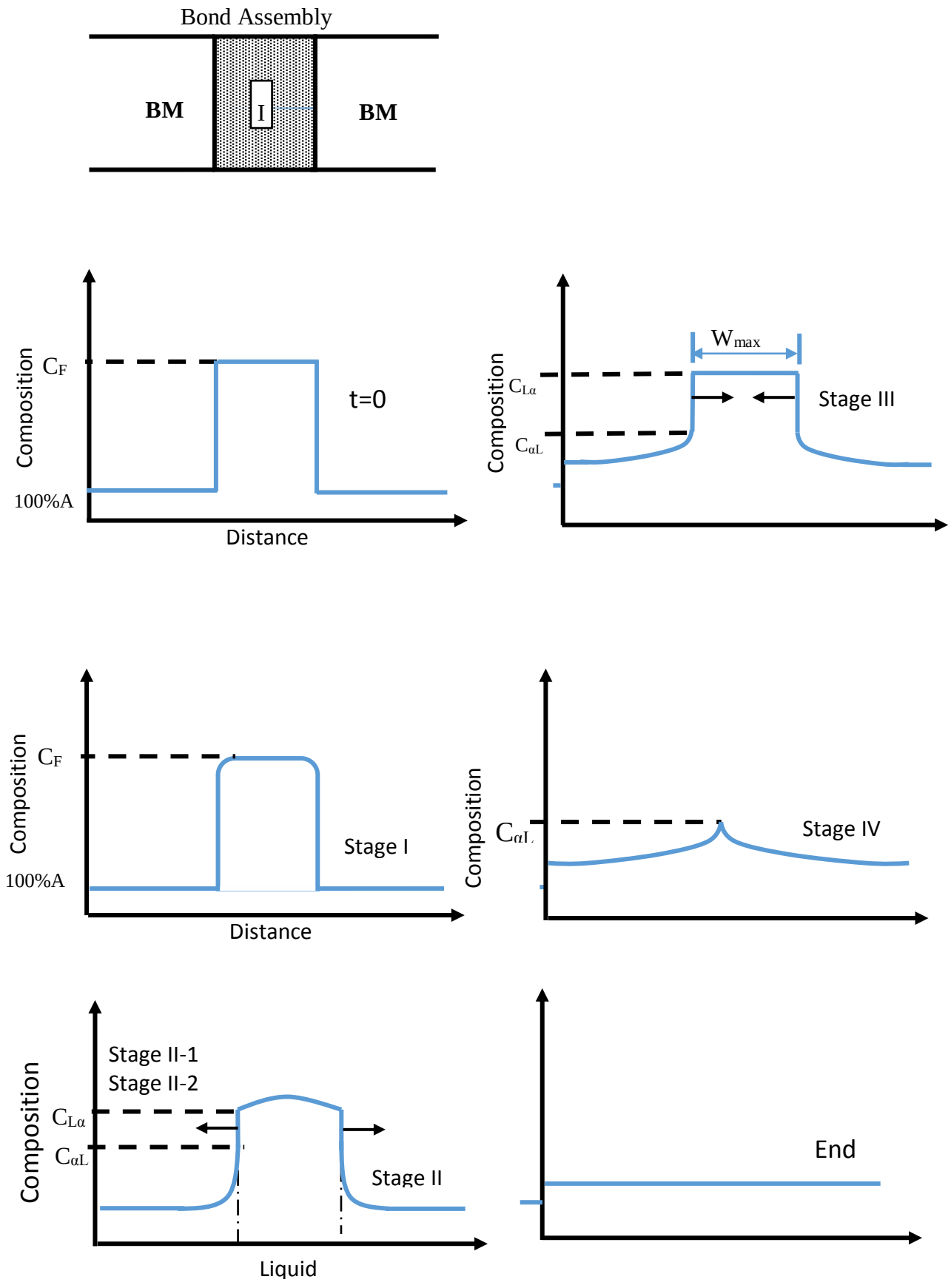

Figure 2-6 Schematic of the controlling stages of TLP bonding process in a binary alloy when using an interlayer alloy with a near eutectic composition [37]

2.6 Prolonged Isothermal Solidification Completion Time in IN 738 SX with Increase in Temperature

The application of TLP bonding to joining of SX Ni-base superalloys has generated different views owing to complications that have been encountered during TLP bonding using SX materials with both binary and/or ternary interlayer alloys with more than one MPD during the bonding process. An important parameter in the application of TLP bonding for commercial purposes is the holding time, $t_{f,}$ that is required to achieve complete isothermal solidification in preventing the formation of deleterious centreline eutectic microconstituents. In an attempt to overcome a prolonged isothermal solidification completion time, t_f, in SX Ni-base superalloys, high bonding temperatures have been proposed with the premise that the higher diffusion rates that are associated with increases in bonding temperature would result in an increase in isothermal solidification rates as predicted by analytical TLP models. Furthermore, most interlayer materials suitable for the bonding of Ni-base superalloys are highly alloyed and have high melting temperatures. Therefore, to achieve complete melting of the interlayer, higher bonding temperatures are required for quality joints.

The TLP bonding of SX Ni-base superalloys at high bonding temperatures have resulted in even longer isothermal solidification completion times, $t_{f,}$ which has further reduced the commercial appeal of the TLP bonding process in the industry. A number of factors contribute to the longer isothermal solidification completion time t_f, as reported by previous works [40,41,54,72] carried out on TLP bonding and these are due to:

1) the absence of grain boundaries in SX alloys, which results in a longer isothermal solidification completion time since intragranular diffusion is faster than bulk lattice diffusion and thus the isothermal solidification rate increases with increases in the grain size of the base-metal [41,48,72,73],

2) deviation from the parabolic law at higher temperatures due to the presence of a second MPD solute element in the interlayer, which degenerates the isothermal solidification kinetics into two regimes that are controlled by the slower diffusing solute [10,40,74],
3) the formation of second phase particles at the substrate-joint interface, DAZ, which slows down the diffusion of solute elements from the joint into the base-metal [10,54,75],
4) an increase in the volume of the interlayer liquid at the joint centre due to increasing base-metal melt back or erosion with increases in the bonding temperature [37,72],
5) a decrease in the solubility of the MPD solute in the base-metal with increasing bonding temperature [41,76].

In the analytical TLP models for which the above factors were derived, some fundamental assumptions have been made in attempts to fit in the theory of TLP to a diffusion mathematical model. Standard analytical models are based on solutions for the Fick's second law of diffusion equation:

$$\frac{\partial C}{\partial t} = D\frac{\partial^2 C}{\partial x^2} \qquad 2.3$$

where $\frac{\partial C}{\partial t}$ is the change in the solute concentration with time at a given point in the base-metal, D is the diffusion coefficient of the MPD solute in the base-metal and $\frac{\partial^2 C}{\partial x^2}$ is the rate of change of the solute concentration gradient $(\frac{\partial C}{\partial x})$ with respect to distance, *x*, [38,41,71]. One of the assumptions in this model is that during the isothermal solidification stage, the unidirectional diffusion induced migration of the solid-liquid interface, *h*, assuming local equilibrium, follows a parabolic law

$$h = 2\varphi(t^{1/2}) \qquad 2.4$$

where, t, is the holding time and φ is the parameter that denotes the rate of the interface migration. Equation 2.4 implies that a direct linear relationship exists between the square root of the holding time and the thickness of the residual interlayer, which could transform into centreline eutectic phase. An explicit assumption in these models is that the base-metal has infinite or semi-infinite thickness, and hence permits the use of an error function solution of Fick's diffusion equation in representing the solute distribution in the solid substrate. The outcome of this assumption is that the migration of the solid-liquid interface maintains a parabolic relationship with time during the continuous diffusion of the MPD solute into the substrate despite that the concentration gradient in the substrate is consistently reduced. Although the assumption of a local equilibrium does hold true for solidification in usual processes such as casting, the solute distribution at the solid-liquid interface will deviate from the equilibrium state during rapid solidification and rapid dissolution processes [45]. Therefore, at such high bonding temperatures diffusion-induced isothermal solidification is not only diffusion dependent but solubility controlled. Therefore, discrepancies arise between theoretical assumptions and experimental reality.

More recent research works on TLP bonding [10,76-82] have dispelled some of these causes for prolonged isothermal solidification completion time, t_f. According to Gale and Butts [10], the bonding temperatures employed during TLP bonding are generally a high enough fraction of the absolute melting temperature of the substrates, hence there is no significant difference between grain boundary and bulk diffusions. Adam [77] who used a 2-D numerical simulation to study the grain boundary diffusion during isothermal solidification, showed that there is no significant difference between the polycrystalline solid of various grain sizes and single crystal solid and hence the presence or absence of grain boundaries has very marginal or no influence on the rate of diffusion during isothermal solidification.

In TLP bonding that uses a single MPD solute element in the interlayer, anomalies have been reported [10,78], hence the deviation from the parabolic law in the presence of a fast diffusing MPD solute and the presence of a second slower solute does not justify the reduction in the isothermal solidification rate. Rather, a fundamental activity related to the diffusion process may be responsible.

Ramirez and Liu [78] observed during an experimental investigation that with an increase in the bonding temperature, the precipitation of second phase particles is considerably reduced and hence the presence of second phase particles is not intricately linked to the extended isothermal solidification completion time. Similar diffusional anomalies have been observed in systems that do not form interfacial precipitates.

Increases in the bonding temperature increase the dissolution width [56] and therefore the volume of liquid insert in the joint centre increases. However, there is a corresponding increase in the rate of diffusion associated with an increase in temperature [36], and also diffusion is faster in liquid and thus more MPD solute quickly reaches the liquid-solid interface. This increase in the rate of diffusion which counters the effect of the increased liquid volume and thus the solubility of the MPD solute at a particular bonding temperature, then becomes the sole determining factor [83].

Abdelfattah [84] carried out theoretical (analytical and numerical) and experimental works, and Adam [77] used both numerical and experimental techniques to investigate the effect of a decrease in the MPD solute solubility with increasing bonding temperature on the isothermal solidification rate during the TLP bonding of Ni-base superalloys and determine whether this is responsible for the deviation from the parabolic relationship. The analytical TLP model approach by Abdelfattah incorporated a constant interlayer liquid width, similar to Nakao et al. [39], and the result showed that a critical temperature exists, and beyond which, a decrease in the solubility of the MPD solute causes a deviation from the parabolic relationship and

invariably an increase in the isothermal completion time, t_f. This result is in line with the results reported by Tuah-Poku et al. [41], which highlighted that there is a temperature at which a minimum in the solidification time occurs but this time far exceeds observations and findings from experimental investigations on the effect of bonding temperature on isothermal solidification [85-88].

Numerical simulations were carried out by both Abdelfattah [84] and Adam [77] in addressing the assumption of an infinite or semi-infinite base-metal thickness. This would lead to the premise of continuous diffusion of the MPD solute into the base-metal, by considering a substrate of a finite thickness and thus reduction in the rate of change of the solute concentration gradient, $(\frac{\partial C}{\partial x})$ with respect to distance. The results showed that there is a critical value of $(\frac{\partial C}{\partial x})_c$ at any location in the substrate beyond which significant deviation from the parabolic relationship between the migration of the solid-liquid interface and holding time occurs. However, this gradient is influenced by the solubility of the diffusing MPD solute in the solid substrate at a particular bonding temperature. It is therefore suggested that the φ parameter, which represents the migration of the solid-liquid interference, becomes invalid in representing the isothermal solidification rate since the rate continuously reduces in within the deviation zone [83,89,90].

2.7 Reduction in Isothermal Solidification Completion Time by Composite Powder Mixture

As discussed above, the basic factor that leads to an extended isothermal solidification completion time, t_f, with increasing bonding temperature during TLP bonding is the aberration of the diffusion controlled solid-liquid interface migrating during isothermal solidification from the parabolic relationship with the holding time. This aberration has been linked to the reduction

in the solute concentration gradient $(\frac{\partial C}{\partial x})$ below a critical level $(\frac{\partial C}{\partial x})_c$, owing to the continuous diffusion of the MPD solute into the base-metal. This therefore suggests that controlling MPD solute diffusion into the base-metal such that the critical gradient concentration level, $(\frac{\partial C}{\partial x})_c$, is not attained or exceeded would result in a reduced isothermal solidification completion time, t_f. According to Ojo [91], an effective way to limit the reduction in $(\frac{\partial C}{\partial x})$ is done so by reducing the amount of MPD solute that is required to diffuse into the base-metal to achieve complete isothermal solidification. This can be accomplished by using a composite mixture interlayer. The composite interlayer mixture is commonly used in wide-gap TLP bonding of polycrystals, which consists of a powder mixture of a commercial melting filler alloy that contains the MPD and a non-melting gap filler powder [62,65,66,69]. The gap filler increases the interfacial area between the liquid and solid phases. As such, a more efficient path for the solute diffusing from the liquid to the solid is created, which also reduces the volume of liquid needed to fill the gap so that less solute is required to diffuse in order to achieve complete isothermal solidification, effectively reduces the base-metal melt back or erosion, and when a base-metal-like powder is used as the gap filler, enriches the joint with base-metal alloying elements [9,63-65,69,70]. The application of a wide-gap in TLP bonding of SX materials has been limited owing to the formation of stray grains by the non-melting gap filler in the composite mixture and porosity in the joint centre [9,64], thus leading to the compromise of the single crystallinity of the substrates and subsequent degradation of the properties of the SX material.

A recent numerical simulation and experimental study by Adam [77,79] indicated that numerical modelling, with use of cellular automata to investigate the dissolution kinetics of the gap filler alloy powder by the molten filler alloy, showed the complete melting of the gap filler alloy powder and use of the composite mixture in the TLP bonding of SX materials. This would therefore avoid stray grain formation in the joint centre, by consciously selecting a combination

of certain parameters that affects the dissolution of the gap filler by the molten interlayer alloy. The parameters that should be controlled include:

i. the type of MPD solute,
ii. the concentration of the MPD solute in the filler alloy,
iii. the size of the base alloy powder particles,
iv. the ratio of the volume of filler alloy to base alloy powder $R_{F:B-A}$, and
v. the bonding temperature.

The experimental study involved the TLP bonding of IN 738 SX as the base-metal and a commercial Ni-Cr-B filler alloy powder and IN 738 powder as the gap filler alloy. The compositions of the base-metal and filler alloy are similar to those provided in Tables 3-1 and 3-2 respectively. Composite powder mixtures with ratios $R_{F:B-A,}$ of 7:3 and 1: 1 were used in the TLP bonding at various temperatures. It was observed that at temperatures below 1150˚C, partial melting of the gap filler alloy particles occurred in both mixture ratios. However, upon reaching a bonding temperature of 1150˚C, the molten filler produced a complete melting of the gap filler alloy particles with only the 7:3 mixture ratio but incomplete melting with the 1:1 mixture ratio. An orientation imaging microscopy (OIM) analysis of an initial gap size of 200 µm for the SX IN 738 bonded for 1 hr by using both composite mixture ratios revealed remnants of partially melted gap filler particles in the 1:1 mixture ratio but not in the 7:3 in which the liquid transformed into eutectic solidification products. A complete agreement between the numerical simulation and experimental results was obtained with the outcome that complete melting of the gap filler powder particles by the molten interlayer alloy can be obtained with no formation of stray grains during solidification by using a composite mixture powder. In the present work, a composite mixture ratio of $R_{7:3}$ was explored for the TLP bonding of SX IN 738 at 1150˚C.

2.8 Corrosion of Ni-Base Superalloys in Aqueous Environments

Corrosion is defined as the deterioration of materials due to reactions with their environments, where materials comprise all substances (metals, polymers and ceramics) used in the construction of components, process equipment, machines or any other manufactured product and the environments are mainly liquid and/or gas. Corrosion mainly involves the transport of mass across an interface to the environment (electrode-electrolyte) and this can occur in one of three ways: electrochemically, chemically and physically. Electrochemical corrosion involves the movement of ions from the material to the environment. A prerequisite for electrochemical corrosion is that the material must be conductive. Hence, corrosion in metals or metallic corrosion is generally classified as electrochemical in nature. Ni-based superalloys are metallic in nature; therefore, their corrosion mechanism or behaviour can be understood by using electrochemical studies.

2.8.1 Corrosion Process

The corrosion of metals is as a result of an irreversible oxidation-reduction reaction wherein an oxidizing or reducing agent in the environment attacks the metal. It is simply an electrochemical process whereby metals atoms are oxidized and released into a solution as described by Equation 2.5 below.

$$M \rightarrow M^{n+} + ne^{-} \qquad 2.5$$

The above reaction occurs at a site known as the anode; therefore, the reaction is typically referred to as an anodic reaction. The electrons produced from the oxidation or anodic reaction must be consumed in a cathodic reaction such as the reduction of oxygen or water. The nature of the corrosive environment determines to a large extent the type of cathodic reaction that can

occur. The most common cathodic reactions that are possible if the metal is not immune to a given aqueous are as follows:

Oxygen reduction in an acidic environment: $O_2 + 4H^+ + 4e^- \rightarrow 2H_2O$ 2.6

Oxygen reduction in a neutral/alkaline environment: $O_2 + 2H_2O + 4e^- \rightarrow 4OH^-$ 2.7

Water reduction (neutral/alkaline environment): $O_2 + 2H_2O + 4e^- \rightarrow 4OH^-$ 2.8

Proton/hydrogen reduction (acidic environment): $2H^+ + 2e^- \rightarrow H_2$ 2.9

The above reactions can occur at any position on the metal surface, and it is common to observe preferential sites for either anodic or cathodic reactions on the same metal surface. More importantly, more than one type of reduction and cathodic reaction can occur depending on the nature of the environment and type of electrolyte [13,14]. In the case of an isolated piece of metal, the total rate of oxidation must equal the total rate of reduction for corrosion to take place, and the potential at which the two rates of reactions are equal is known as the free corrosion potential (E_{corr}) or the open circuit potential (OCP). It is the potential that defines where all half-cell reactions balance out to a net zero current [14,92,93]. The relative magnitude of the OCP and equilibrium potential give insight into the direction of the redox reaction. Specifically, if the OCP is above a particular half-cell equilibrium potential, then that half-cell reaction will be an oxidation reaction, whereas if the OCP is below the half-cell potential, then the reaction will be a reduction reaction. The rate of the specific reaction will be governed by the magnitude of the voltage difference between the OCP and the equilibrium potential, availability of the species, and voltage–current characteristic behaviour that governs the kinetics of the reaction.

2.8.2 Aqueous Corrosion of Ni-base Superalloys

In addition to high temperature oxidation in air, it is also important to investigate the corrosion behaviour of Ni-base superalloys at ambient temperatures in aggressive aqueous environments,

such as in sulphate or chloride containing solutions or solutions of different pH values. Sulphates are typical products of the combustion process and saline marine air leads to the presence of chlorides on the alloy surface. Since Ni-base superalloys may also suffer from corrosion prior to or after an operation at high temperatures, additional examination of the corrosion properties under the mentioned conditions (ambient temperature, aqueous solution) is indispensable. Given the potential applications of Ni-base superalloys, and due to the aggressive nature of the environments where they are used, the demand is not only on their mechanical properties but also high CR. Thus a study of the CR of Ni-base superalloys in corrosive aqueous environments is important, particularly the general corrosion attacks in acid media. Depending on the chemical composition, thickness, porosity, and adhesion, the oxide layers may have very different protective properties. Electrochemical measurements are typical tools for investigating the corrosion behaviour of materials, and examinations are typically carried out in an aqueous corrosive medium at an ambient temperature in an accelerated manner.

Corrosion reactions in aqueous solutions are characterized by the following features [94].

- The electrified interface between the metal and the electrolyte solution (the metal surface may be film-free or partially or completely covered with films or corrosion products).
- Transfer of positive charge from the metal to the solution with subsequent oxidation of the metal to a higher valency state.
- Transfer of positive charges from the solution to the metal with consequent reduction of a species in the solution (an electron acceptor) to a lower valency state.
- Transfer of charges through the solution and corroding metal.
- The stability of corrosion can be influenced by thermodynamics and kinetics.

2.8.3 Thermodynamic Stability of Corrosion Process

A metal, when exposed to a corrosive aqueous medium, would behave in a particular manner depending on the nature of the aqueous medium (oxidizing or reducing), ambient temperature and pressure as well as hydrogen ion concentration (pH) of the aqueous medium. This behavior was extensively studied by Marcel Pourbaix [95] who examined the thermodynamic stability of the products or ions formed during the corrosion process by varying the electrode potential of the metal over a range of pH of the corrosive medium, and demonstrated that the material will show immunity, corrosion and passivity when exposed to an aqueous corrosive medium. The plotting of these thermodynamic activities for the respective equilibrium potential favored over a range of pH resulted in a chart known as the Pourbaix diagram. A typical Pourbaix diagram for Ni, as the principal element of Ni-base superalloys, is shown in Figure 2-7.

While the basic trend of the Pourbaix diagram is the same for all metals, each is specific to the particular metal-aqueous system. For Ni, the three possible behaviors of immunity, corrosion and passivity are provided in Figure 2-7, and broadly identified by mapping as shown in Figure 2-8. Metals that are thermodynamically stable in a variety of corrosive media are known as noble metals, since their potential is lower than the reduction potential of the surrounding species. In contrast, less noble metals with higher oxidation potential may corrode due to the difference in the redox potential of the two phases in contact. The driving force of oxidation can lead to either active corrosion (dissolution) of the metal or formation of a stable oxide layer (passivation) on the metal surface. Depending on the pH value of the aqueous solution, the possible reduction reactions are provided in Equations 2.6 to 2.9 and can drive the oxidation of Ni as well as any of the alloying elements in Ni-base superalloys.

However, it is noteworthy to state that in all Ni-base superalloys, a primary alloying element is Cr, which is added since it a nobler (more passive) metal than Ni and readily passivates at much lower potentials than Ni by forming a much more stable oxide layer, since Ni in acidic solutions

is only capable of passivation to a considerable extent. For Ni alloys that contain a significant Cr content, passivity at negative potentials is determined by the properties of Cr and thus active Ni dissolution is subdued due to formation of Cr_2O_3 films [97]. It is therefore more common to use the Pourbaix diagram for Cr in analyzing the corrosion behavior of Ni-base superalloys in an aqueous medium, which is shown in Figure 2-9. For Ni-base superalloys exposed to an aqueous medium, the expected oxidation reactions are:

$$2Ni \rightarrow Ni^{2+} + 4e^{-} \qquad 2.10$$

$$2Cr + 3H_2O \rightarrow \ Cr_2O_3 + 6H+ 6e^{-} \qquad 2.11$$

Cr is a prime promoter of CR in some aqueous media at low temperatures but other alloying elements are also quite significant in the enhancement of CR

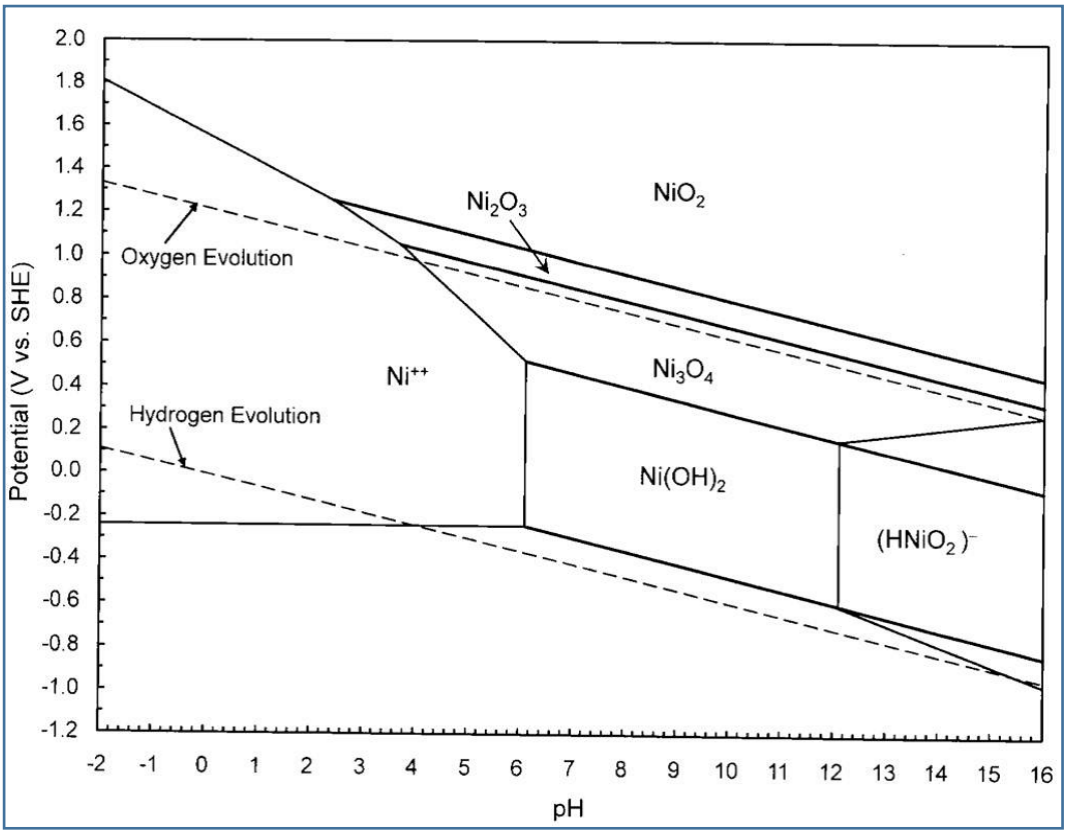

Figure 2-7: Pourbaix diagram for Ni at 25ºC showing products or ions formed [96]

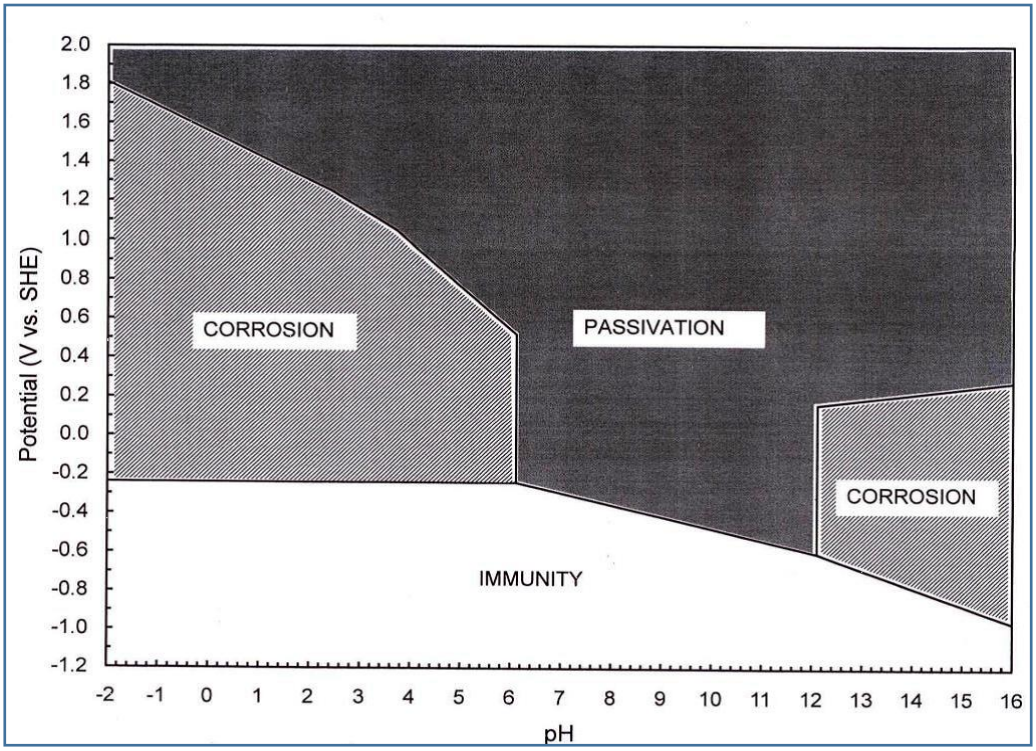

Figure 2-8: Pourbaix diagram for Ni which shows 3 possible behaviours in aqueous medium [95]

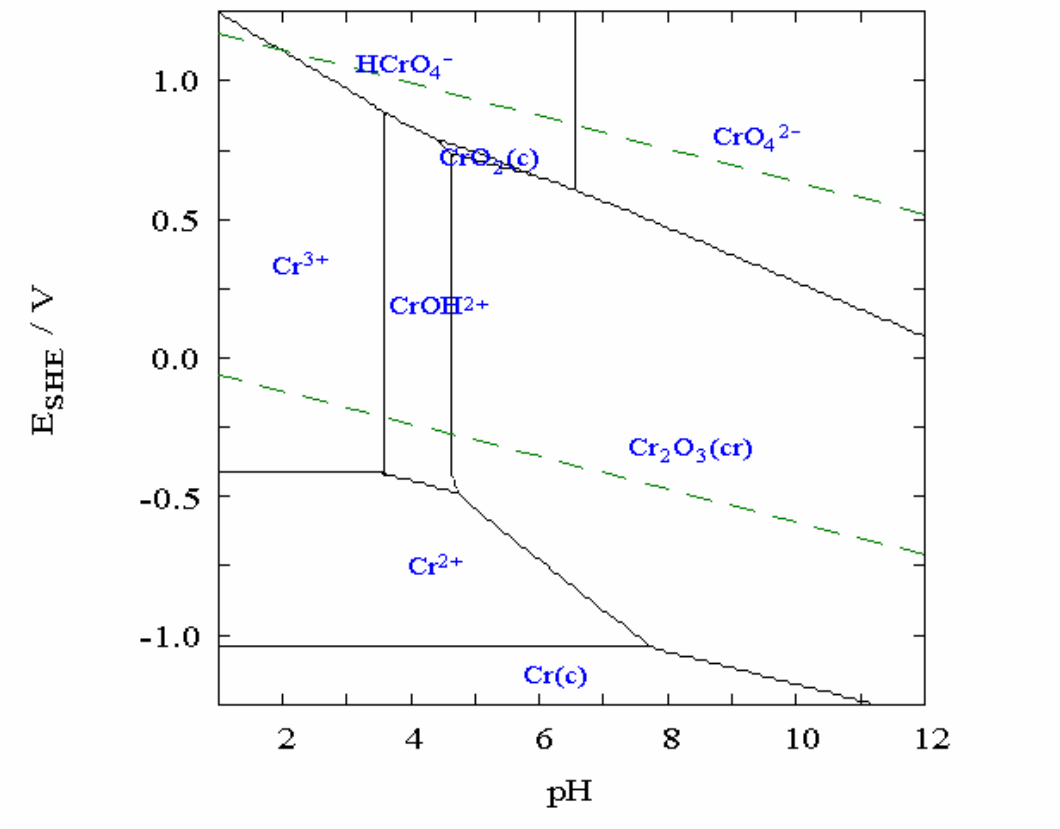

Figure 2-9 Pourbaix diagram for aqueous chromium at 25˚C [98]

2.8.4 Forms of Corrosion.

General corrosion: a uniform corrosion attack and it is the most common type of corrosion. General corrosion is chemical or electrochemical in nature and occurs uniformly over the entire exposed surface thus leading to the gradual thinning of the metal. This accounts for the greatest destruction of the metal [14] and is the most common form of corrosion experienced by Ni-base superalloys.

Galvanic corrosion: results from the electrical coupling of two dissimilar metals in a corrosive medium or when the same metal is exposed to an electrolyte in different concentrations, thus creating what is known as a galvanic couple and results in the attack of the less noble (more active) metal. The metallic differences may be due to the metal structure as well as the composition. Less noble material becomes anodic while more noble metals become cathodic. The anodic material actually protects the cathodic, which leads to its own accelerated decay. The ranking of materials is done so according to the redox potential in what is known as an electromotive force (EMF) or galvanic series in a specific media will help to predict the propensity of this type of corrosion. The further apart the materials are in the series, the greater the likelihood of attack on the less noble material.

Pitting corrosion: a form of extreme localized attack on a metal that results in the formation of holes in the metal. While the holes formed are typically small, they can propagate very quickly and deep into the material, thus leading to material perforation and eventual failure in a very short time. The micro-environment within the pits themselves can be autocatalytic in nature, making this form of attack very dangerous. Ni-base superalloys are alloyed with certain alloying elements, such as Mo and W, which resist pitting attacks but in some situations where

a passive film cracks or breaks, pitting can be experienced to a greater extent. In general, metals that passivate or form passive layers are highly susceptible to pitting corrosion which is usually initiated from passive film breakdown. Pitting can occur in a homogeneous alloy depending on the presence of certain species in the environment e.g. chlorides [14,93,94]

Crevice corrosion: usually takes place in confined or very tight spaces (crevices) between two surfaces, where access to the working fluid from the environment is very limited. As with pitting, the micro-environment within the crevice can greatly differ from the general medium. This type of corrosion can be very rapid in the presence of concentration cells and is often influenced by the crevice geometry, and metallurgical and environmental factors.

Although other forms of corrosion, such as stress corrosion cracking (SCC), intragranular corrosion, and corrosion fatigue and dealloying have been reported to occur in Ni-base superalloys, their occurrence is application or material dependent.

2.8.5 Passivity of Ni-base Superalloys in Aqueous Environment

In the application of metals for construction, a main limiting factor has been corrosion and various methods such as cathodic protection, and the use of organic coatings, corrosion inhibitors and additives to control pH, etc. have been applied in attempts to control corrosion. The most effective means of corrosion protection is the use of metals or alloys which have inherently low corrosion rates in solutions due to a passive oxide film. The excellent CR of Ni-base alloys is largely because their surface is protected in an aqueous medium or moist air by ultrathin dense oxide/hydroxide films. Pure Ni has good chemical properties and good CR to various environments, as Ni-oxides are thermodynamically stable in neutral and moderately alkaline solutions, although not in acidic or strong alkaline solutions [99]. The alloying of Ni

in Ni-base alloys with elements such as Cr, Al, etc., further enhances its CR [1,100]. The CR of these alloys is either due to passivity or their noble behaviour which means they are noble enough to not displace hydrogen from acidic solutions. Therefore, they can be successfully used in various types of media, acids, salts and alkalis (both oxidizing and non-oxidizing in character), sea and natural waters and the atmosphere [94]. Depending on the pH of the solution, the passivity of Ni-base superalloys is likely to break down in the presence of chlorides in the environment since either pits are formed on the surface or the metal uniformly corrodes in a more acidic medium [96,97]. In contrast to active corrosion (dissolution) of a metal, the formation of a second phase film (usually an insoluble three dimensional surface oxide layer) is favoured. This passive film can form at the equilibrium, i.e. at E_{corr}, but also as a result of the application an external anodic potential.

In the corresponding potentiodynamic polarisation curve, see Figure 2-10, anodic passivation can be observed as an abrupt decrease of the corrosion current density (several orders of magnitude possible) at a specific onset potential, known as passivation potential E_{pp}. Here, the metal changes from an active to a passive state). In terms of an electrochemical treatment, passivation of a metal surface represents a significant deviation from ideal electrode behaviour [14,92,93]. Generally, the reaction scheme for passivation can be divided into the active and passive ranges followed by transpassivity at higher potentials.

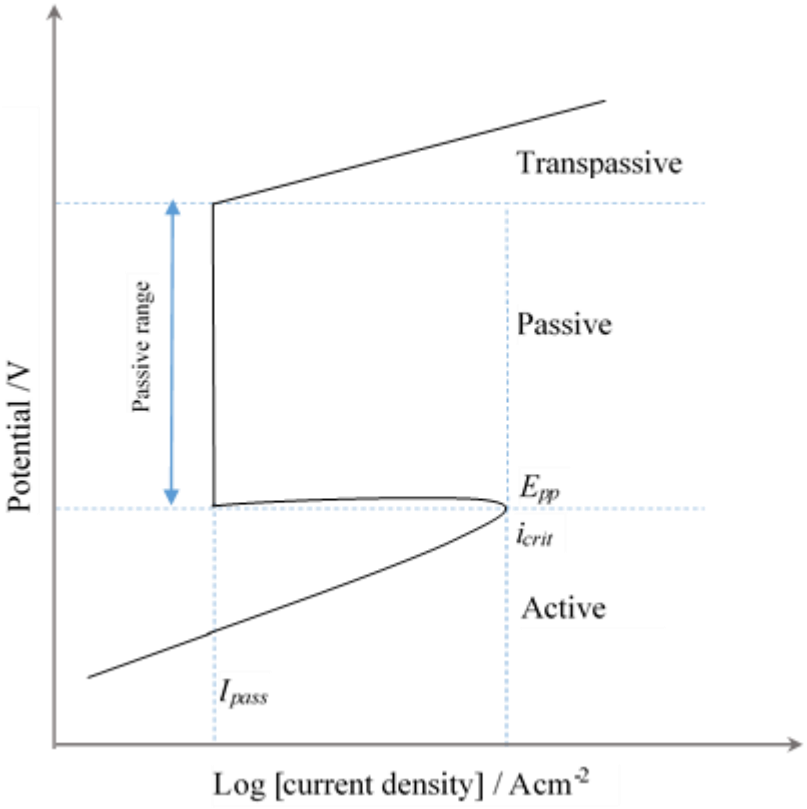

Figure 2-10: Potentiodynamic anodic polarization curve for a passivating metal

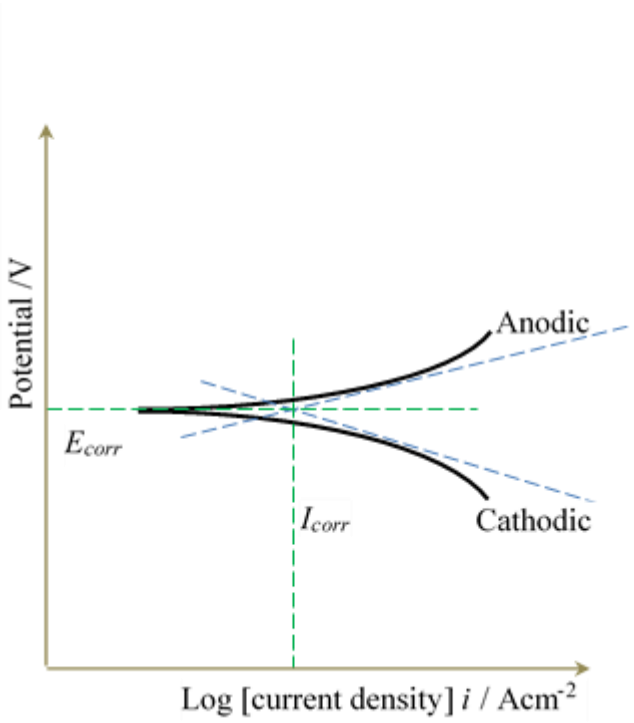

Figure 2-11: Schematic of the potential vs. log current density for anodic and cathodic potentiodynamic polarization curves

2.8.6 Corrosion Testing and Corrosion Rate Measurement

Corrosion is an insidious process and often difficult to identity until it is well advanced, hence testing of metallic materials before use is critical in assessing their corrosion behaviours in different environment and service conditions. In assessing this behaviour, certain indicators, metrics or parameters are used in either quantifying or qualifying the metallic interactions with the environment. The rate of corrosion in materials can be measured and quantified by using different techniques. These are largely divided into two methods: electrochemical and non-electrochemical measurements.

The non-electrochemical measurements are:

i. rate of weight-loss (mass loss),

ii. solution analysis, and

iii. changes in electrical resistance (ER) of a probe sample.

The electrochemical measurements are:

i. potentiodynamic polarization,

ii. galvanostatic polarization,

iii. polarization resistance (R_p) by using the Stern-Geary equation,

iv. electrochemical impedance spectroscopy (EIS),

v. electrochemical noise (EN), and

vi. electrochemical frequency modulation (EFM).

Most corrosion processes during the service life are gradual and time dependent, hence most corrosion testing is done on a small scale, e.g. in the laboratory, to simulate the actual service environment and conditions. However, these service conditions are never ideal nor constant and thus small scale testing is only approximate and valid for predicting what is expected of the material in certain environments. For materials such as Ni-base alloys, which have low

corrosion rates, slow measurement methods are well suitable, since the electrodes will slowly change through corrosion and the low currents involved will be more easily perturbed in the short term by factors such as double layer charging and currents associated with the thickening of the passive oxide films [101]. Potentiodynamic polarization measurement techniques have been extensively used to study metallic corrosion, especially in passivating metals.

2.8.6.1 Potentiodynamic Polarization Measurement

The potentiodynamic polarization measurements are the most common electrochemical method used in corrosion research and testing. They are developed on the basis of the mixed potential theory, and use data obtained from the relationship between the current and potential, usually over a relatively wide range of potentials. Linear and Tafel polarization are the two primarily used methods for obtaining corrosion rate measurements.

Polarization curves are obtained by applying voltages that range from ±50 mV from OCP in small uniformly spaced increments; the applied voltage increment should be small, and a recommended rate of applying the potential is 0.006 to 0.012 V/min [101,102], recording the steady-state current over a period of time, and plotting the potential of the electrode against the logarithm of the applied current. Then, a potentiodynamic polarization plot is obtained. A schematic of the potentiodynamic polarization plot is presented in Figure 2.11. The curve obtained is nonlinear at low currents, but at higher currents, the curve can be linear on the semi-logarithmic plot, usually at approximately 50 mV more active than the corrosion potential [92,102]. The straight-line portion of the curve is the Tafel slope. The linear portion of the curve can be extrapolated and will intersect at E_{corr}. Further extrapolation of these lines brings them to the potentials for the reversible anodic and cathodic reactions. These reactions determine the polarity of the corrosion cell, with the anode being negative and the cathode positive. The extension of the anodic line to the reverse potentials brings it to a potential at which the metal is in equilibrium with its ions, and the extension of the cathodic line

brings it to the reversible potentials for the cathodic reaction. Potentiodynamic anodic polarization curves can be used to judge the CR of alloys and the corrosivity of solutions. They are easily reproducible and can be obtained in a few hours to a few days. A typical potentiodynamic anodic polarization curve is shown in Figure 2-10. The following information is obtained from the anodic potentiodynamic anodic polarization [93].

1. Irrespective of the thermodynamic stability of the alloys, or whether the alloy is the active-passive type, the corrosion rate is proportional to the anodic current density in the active region.
2. The current density (rate) of reduction must exceed the critical current density for passivation to ensure low a corrosion rate in the passive state
3. Borderline passivity should be avoided in which either the active or passive state may be stable.
4. Breakdown of the passive film in oxidizing conditions due to transpassivity or initiation of localized corrosion should be avoided
5. The passive state in oxidizing conditions is essential for CR, but reasonably small variations in the passive current density may not be significant.

2.9 Scope of Current Work

The use of SX Ni-base superalloys for the construction of the hottest section of aero-engines - land-based turbine engine components, has been a tremendous endeavour in achieving higher operating temperatures and hence efficiency in the engines. However, the inherent flaws in these materials, which are their high susceptibility to cracking in the HAZ during conventional welding and formation of stray grains in the weld region, present a challenge in joining multiple single components or even constructing more complex ones.

TLP bonding is fast evolving as a primary joining technique for the joining and repair of these difficult to weld alloys. Despite its tremendous advantage of the ability to operate at temperatures close to the bonding temperature and relative ease of joining, three critical factors have so far limited the commercial applicability of this process particularly in SX Ni-base superalloys:

1) the presence of deleterious second phase particles at the joint centre,
2) the lengthy processing time required to achieve complete isothermal solidification in the joint, t_f, and
3) the formation of stray grains in the microstructure of the joint.

These factors can be controlled by consciously selecting the variables or parameters in the TLP bonding process. Various studies and research have been carried out to understand the effect of each of the process parameters, such as interlayer alloy type, composition and thickness, bonding temperature, etc. on the rate of isothermal solidification of the liquated interlayer that determines the t_f in relation to the final microstructure of the joint and invariably the mechanical properties of the TLP bonded joint. Ni-base superalloys are not only used for their excellent elevated mechanical properties but also their CR in many corrosive environments.

Hence, the ultimate objective of this research is to understand the effect of the process conditions of the TLP bonding viz-a-viz the final microstructure on the CR of SX superalloy for aerospace component, IN 738. As Ni-base superalloys are mostly utilized at high temperatures, their electrochemical behaviour at room temperature has been less studied; therefore, the aim of the present work to analyse the aqueous corrosion of a TLP bonded SX superalloy, IN 738, and compare to the as-received cast base-metal alloy. To achieve this objective, IN 738 specimens were bonded via conventional TLP bonding and a variant TLP bonding process, which is an extension of the TLP bonding by using a composite interlayer in

the conventional bonding process and the corrosion behaviour of the bonded specimens are tested in both oxidizing and reducing corrosive media.

CHAPTER 3. EXPERIMENTAL RESEARCH

3.1 Experimental plan

The experimental investigation in this work is carried out in two phases.

1) TLP bonding and microstructural analysis of the brazed joints
2) Electrochemical corrosion study of brazed joints by using potentiodynamic polarization with man focus on general corrosion, although general and localized corrosion are usually examined together.

The following ASTM standards are adopted for this study where applicable:

- G1-03: Standard Practice for Preparing, Cleaning, and Evaluation Corrosion Test Specimens
- G3-14: Standard Practice for Conventions Applicable to Electrochemical Measurements in Corrosion Testing
- G5-14: Standard Reference Test Method for Making Potentiodynamic Anodic Polarization Measurements
- E200-08: Standard Practice for Preparation, Standardization, and Storage of Standard and Reagent Solutions for Chemical Analysis

3.2 Materials

3.2.1 Base Material

The Ni-base superalloy used in the experimental investigation of this work is a SX superalloy, IN 738, which was supplied by PCC Air foils, LLC, in the form of 180 mm × 51 mm × 11 mm cast plates. The alloy was used in the as cast condition and its chemical composition is shown in Table 3-1.

3.2.2 Filler Alloys

Commercially available interlayer powders, AMDRY 790 (Ni-Si-B), Nicrobraz 150 (Ni-Cr-B) and an additive gap filler, IN 738 powder, were used as the filler alloys. Their respective compositions and melting temperatures are shown in Table 3-2.

3.3 TLP Bonding and Microstructural Analysis of Brazed Joints

3.3.1 Sample Preparation and TLP Bonding

The as-received base material was sectioned into test coupons with dimensions of 15 mm × 10 mm × 15 mm by using numerically controlled Hansvedt model DS-2 travelling wire electro-discharge machining (EDM). A BUEHLER® Isomet® 1000 precision sectioning saw was used to create the slot for gap sizes less than 500 µm at the midspan of the test coupons, see Figure 3-1. This provided an oxide free surface and also ensured that the crystallographic orientation of the grains was preserved to prevent the formation of stray grains during bonding. The EDM was used for gap sizes greater than 500 µm, and the machined surfaces were subsequently polished by using 600 grade silicon-carbide (SiC) papers to remove the oxide layers, and afterward, ultrasonically cleaned in acetone for 15 minutes.

A ceramic coating, Nicrobraz Green Stop-Off, was then applied to the non-mating surfaces of the specimens to prevent spillage and escape of the liquated filler out of the joint area during bonding.

The filler alloy powder was placed between the mating surfaces to fill in the gap without a reservoir, compacted with just enough volume to fill the gap, and the assembly was placed in a vacuum furnace, LABVAC II, which operated at a vacuum of 10^4 to 10^5 Torr at different temperatures and holding times. The TLP bonding process was achieved by using a temperature-time cycle as schematically shown in Figure 3-2.

Table 3-1: Chemical composition of IN 738

Elements	wt%
Carbon	0.16
Chromium	16.09
Cobalt	8.44
Molybdenum	1.74
Tantalum	1.82
Titanium	3.36
Aluminum	3.5
Tungsten	2.64
Silicon	0.04
Niobium	0.79
Iron	0.07
Boron	0.01
Manganese	0.01
Sulphur	0.001
Zirconium	0.055
Nickel	Bal

Table 3-2: Actual compositions and melting temperatures of interlayers

Name	Ni	Cr	B	Si	Solidus ^{o}C	liquidus ^{o}C
AMDRY 790	94.5	-	3.5	2.0	1093	1093
Nicrobraz,NB150	81.5	15	3.5	-	1055	1055

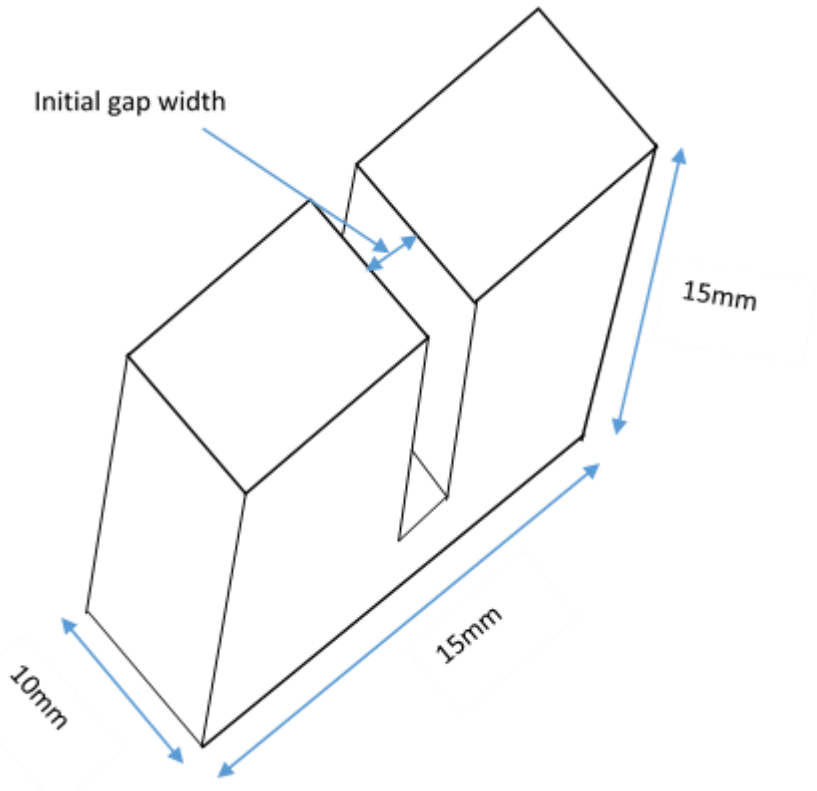

Figure 3-1: Configuration of specimens

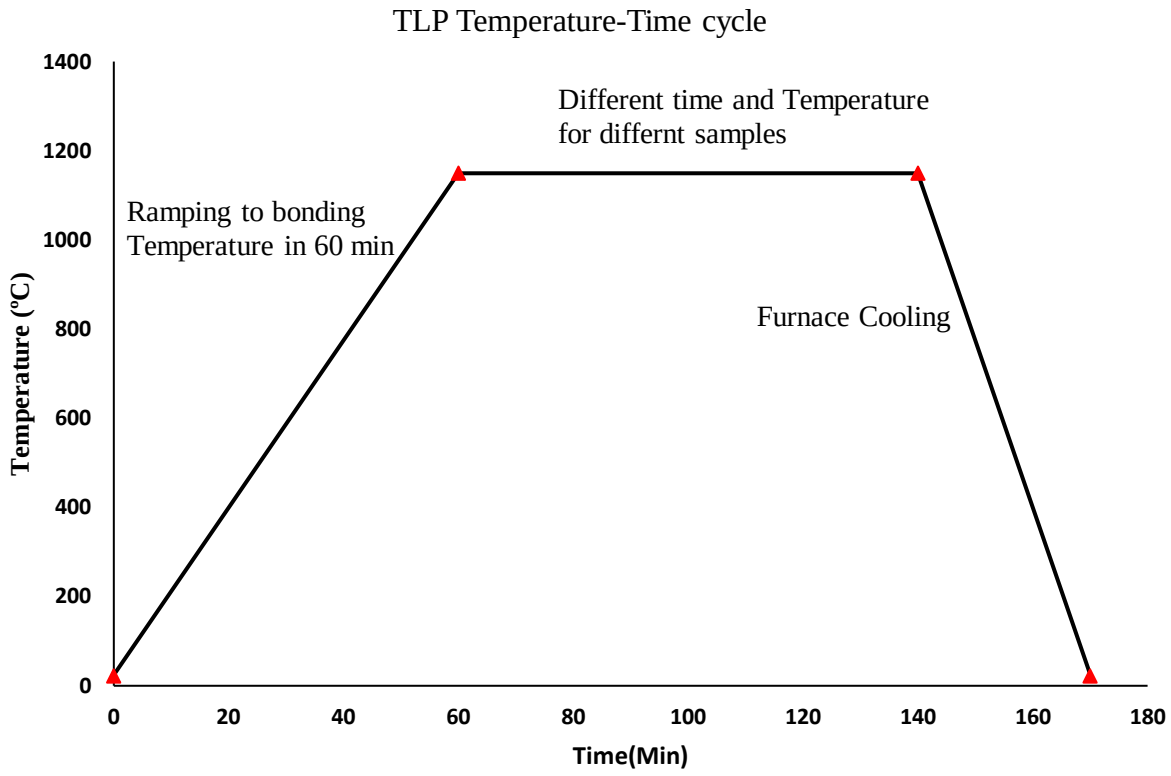

Figure 3-2: Schematic of heating cycle used for TLP bonding

3.3.2 Examination and Analysis of Brazed Microstructure

The examination and analysis of the microstructure involved the use of light, scanning electron, and energy dispersive spectroscopies to assess the characteristics of the TLP bonded specimens. After TLP bonding, the bonded specimen were transversely sectioned to the bonding surface by using the travelling wire EDM and mounted onto a hot press with bakelite powder by using the BUEHLER® SimpliMet® 3000 mounting press as shown in Figure 3-3. The bonded samples were prepared for examination of their microstructure via a standard metallographic procedure through grinding with SiC paper of 180 grit to 1200 grit, and subsequently polished by using 6 µm silica paste and finally, 1 µm diamond paste. A preliminary assessment of the joint microstructure was performed by using a ZEISS Axiovert25 inverted reflected light OM which was equipped with a CLEMEX vision 3.0 image analyzer (Clemex Technologies Inc., Longueuil, Canada). A secondary assessment of the joint microstructure was performed by electrolytic etching of the bond of the samples in 12 mL H_3PO_4 + 40 mL HNO_3 + 48 mL H_2SO_4 solutions at 6 volts for 7 seconds. A SEM (JEOL JSM 5900LV) was used to examine the microstructures of the brazement which is capable of operating in both the secondary and backscatter emission modes, and equipped with an ultrathin window energy-dispersive spectrometer (EDS; Oxford Instruments, Oxford, United Kingdom) with INCA software for the compositional analysis. The EDS spectrum consisted of a series of peaks which represents the type and amount of each element.

3.4 Electrochemical Corrosion Study

Electrochemical polarization studies provide a quick means to predict the corrosion behaviour of metals and alloys in various corrosive aqueous solutions given that the actual corrosion process is an electrochemical time dependent activity. Hence, such studies can be applied to

successfully predict the long term corrosion rate and behaviours (occurrence and tendency towards localized corrosion) in any particular aqueous environment.

3.4.1 Reagent Preparation

Three types of test solutions, HNO_3, H_2SO_4 and HCl, were used as the electrolytes in the corrosion testing and prepared in accordance with ASTM E200 − 08.

3.4.2 Test Specimen Preparation

All of the brazed samples were cut into dimensions of 10 mm × 7 mm × 10 mm, with the edges trimmed to avoid any physical crevices, and then mounted with bakelite powder by using a BUEHLER® SimpliMet® 3000 mounting press with an embedded thickness of 10 mm so that the total surface area of the specimen that was directly exposed to the electrolyte was only 0.7 cm^2. Ideally, the testing conditions of the test specimen should in all aspects be similar to the actual state in service; however, this is difficult to achieve because the surface of commercial metals and alloys varies as produced or fabricated. Also, to ensure the basis for comparison of the results from one specimen to another, the surface of the specimens was prepared in accordance with ASTM G1-03. Hence, the test specimen surface was grinded down to 1200/1400 grit with SiC paper and polished up to 1 µm diamond paste to achieve a highly polished surface prior to electrochemical potentiodynamic polarization experiment. Ni-base alloys are primarily designed to resist corrosion, hence, for such materials wherein the corrosion rates are extremely low, a smoother surface finished is required [14]. The samples were ultrasonically cleaned in an ethanol bath for 10 minutes after grinding and polishing prior to the experiment. All of the polished samples were immediately assembled and transferred into the corrosion test cell that had been filled with electrolyte.

Table 3-3: Experimental Matrix used

Bonding Temperature	1110 °C		
Initial Gap width	300µm	500µm	1000µm
Holding time	35h	35h	35h

Bonding Temperature	1150 °C						
Initial Gap width	70µm	170	300µm	400µm	500µm	800µm	1000µm
Holding time	1h	1h	1h	1h	1h	1h	1h
		5h	5h		5h		5h
		10h	10h		10h		10h
		20h	20h		20h		20h
		30h	30h		30h		30h
		35h	35h		35h		35h

Bonding Temperature	1190 °C		
Initial Gap width	300µm	500µm	1000µm
Holding time	35h	35h	35h

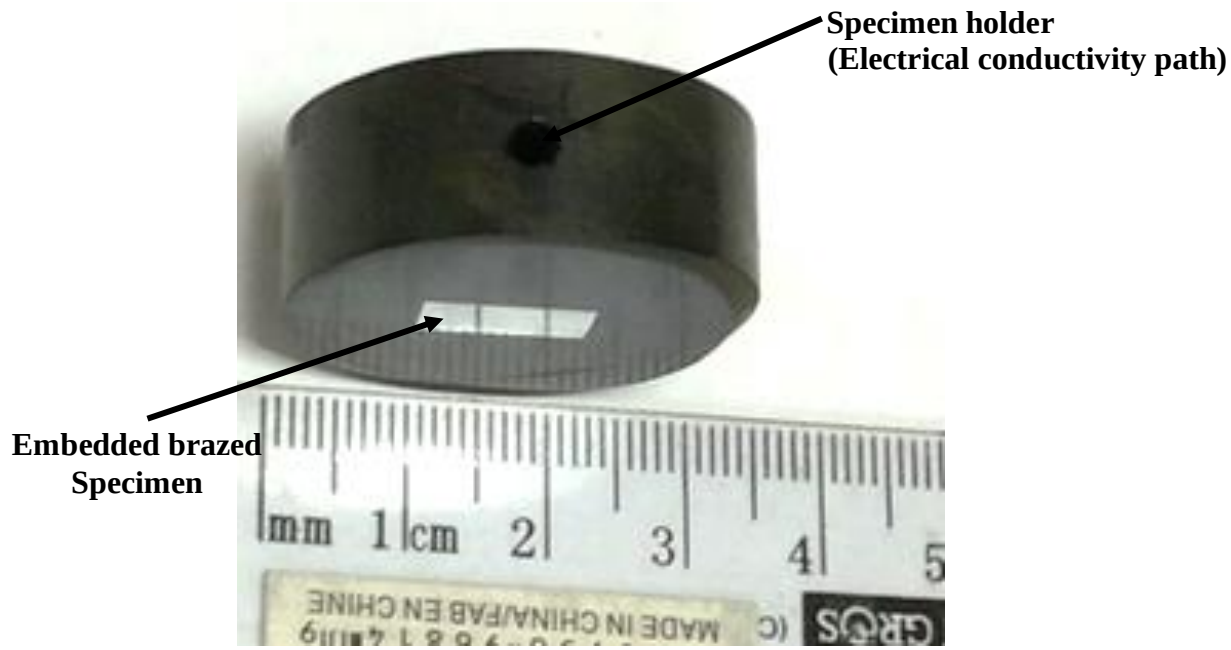

Figure 3-3: Potentiodynamic polarization test specimen

3.4.3 Testing Method and Equipment

Electrochemical corrosion measurement techniques, such as potentiodynamic polarization scans, can be used to acquire real time electrochemical information, such as the corrosion rate, susceptibility to pitting, passivity behaviour as well as anodic and cathodic behaviours of an electrochemical system, even at very low activity rates. The experimental set up was such that the ionic conduction path was provided by using a solution of known molarity (electrolyte) that connected the counter and working electrodes, while the electrical conduction path was made by using potentiostat equipment. The driving force for the electrochemical reaction that occurs at the working electrode surface was controlled by the potentiostat.

A Princeton Applied Research Corrosion Cell Kit and a Versa STAT 3 single channel potentiostat equipped with Versastudio software were used to perform the potentiodynamic polarization for all the samples. The electrochemical set up incorporated a three-electrode system, saturated calomel electrode (SCE) (Sat'd KCl) as the reference electrode, a pair of graphite rods as the counter electrodes and the embedded brazed specimen as the working electrode in a 1.5 L glass cell. Prior to taking the potential measurements with potentiodynamic polarization, all of the samples were degreased and washed in alcohol and distilled deionized water respectively, and then immersed into the electrolyte for a duration of 60 minutes to ensure the stabilization of the OCP and all potential measurements were made with reference to the SCE. A potentiodynamic scan rate of 0.1666 mV/s was used and scanning was performed from a cathodic potential of -0.3 V to an anodic potential of 1.6 V in an aerated environment. All of the experiments were repeated a minimum of three times with the results averaged to ensure consistency and reproducibility. Real time data were captured by using the Versastudio software, which plotted a semi-log graph of the potential (E mV) vs the log of current density (A/cm^2). The current density (i_{corr}) and corrosion potential (E_{corr}) were then read off from the polarization plots through Tafel slope extrapolation with the use of the Versastudio software.

The potentiodynamic polarization plots were used to access the corrosion performance of the TLP bonded samples.

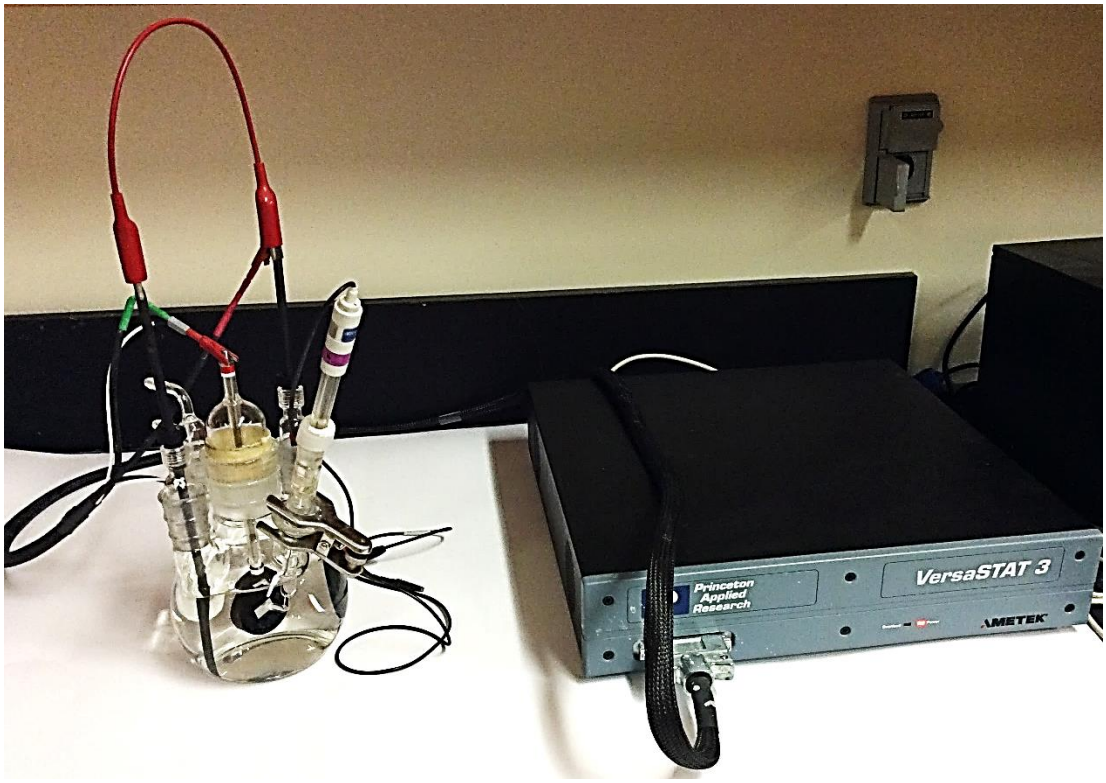

Figure 3-4: Experimental set up for corrosion measurement

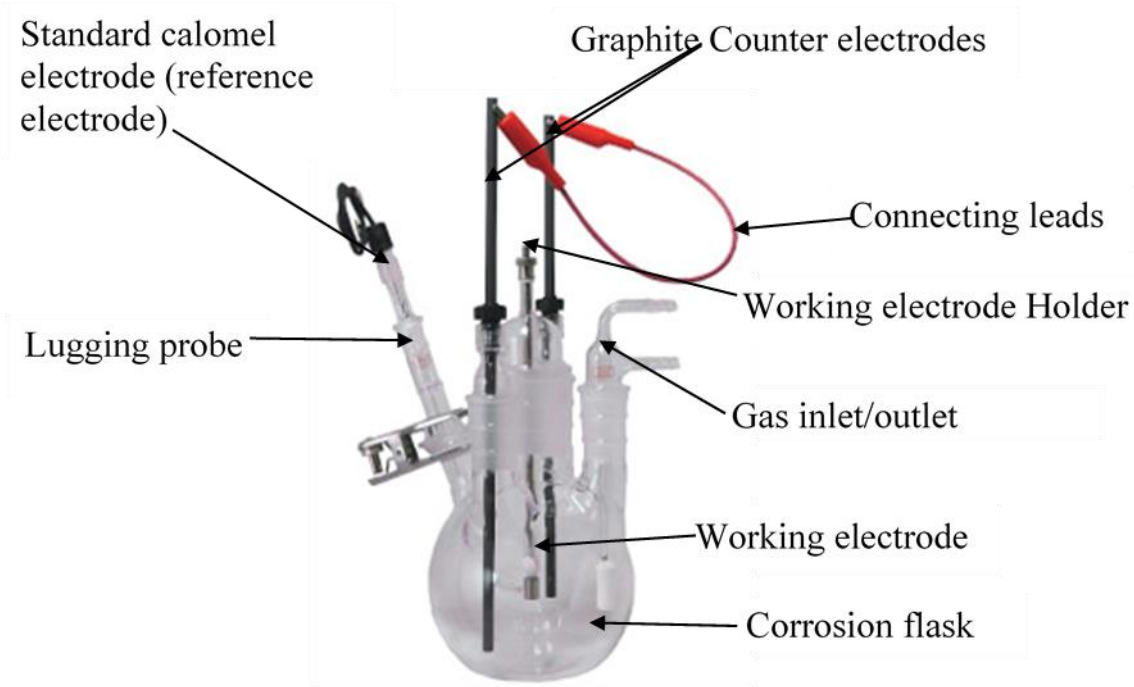

Figure 3-5: Princeton Applied Research Corrosion Cell Kit

CHAPTER 4. RESULTS AND DISCUSSION

In this chapter, the results of the investigation on the effects of TLP bonding, with respect to the microstructure of a bonded region, on the CR of SX superalloy for aerospace, IN 738, are presented and discussed. This chapter is divided into 3 major sections, which includes: microstructural evaluation of TLP bonded joint using both conventional and composite interlayer, effect of process parameters on joint microstructure, and potentiodynamic polarization of TLP bonded joint.

4.1 Microstructure of As-received cast IN 738 SX

An optical micrograph of a polished as-received cast IN 738 SX specimen is shown in Figure 4.1, which shows the presence of carbides, that are randomly distributed, and a very small volume fraction of micropores, which is a well-known casting defect. The optimization of the casting process along with the elimination of the grain boundaries in the SX superalloy has contributed to this very low volume fraction of micropores. Optical and scanning electron microscopes were used to produce the micrographs of the electro-etched as-received cast IN 738 SX as shown in Figures 4.2 and 4.3 respectively. The micrograph from the OM reveals a solidification structure with a dendritic core, which is nominally associated with cast alloys. The SEM micrograph shows that the microstructure both in the dendritic and interdendritic areas consists of unimodal γ’ phase particles along with several second phase particles, MC carbides and γ- γ’ eutectic which are randomly distributed within the fcc γ matrix.

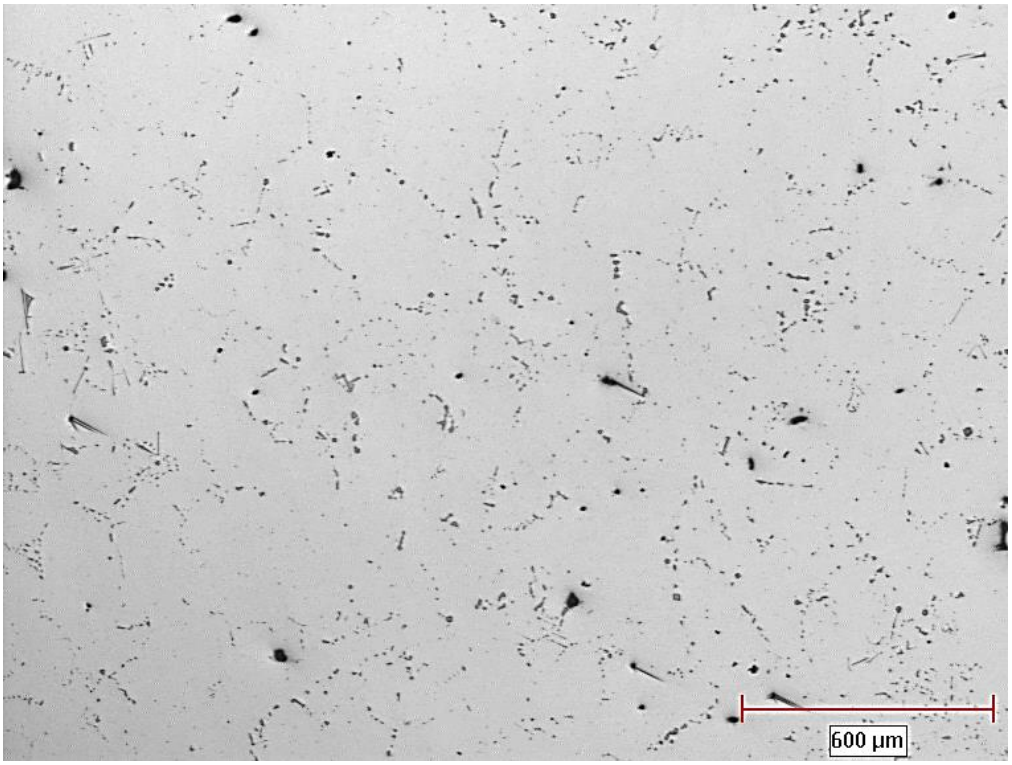

Figure 4-1: Optical micrograph of polished cast as-received IN 738 SX, showing carbides and micropores.

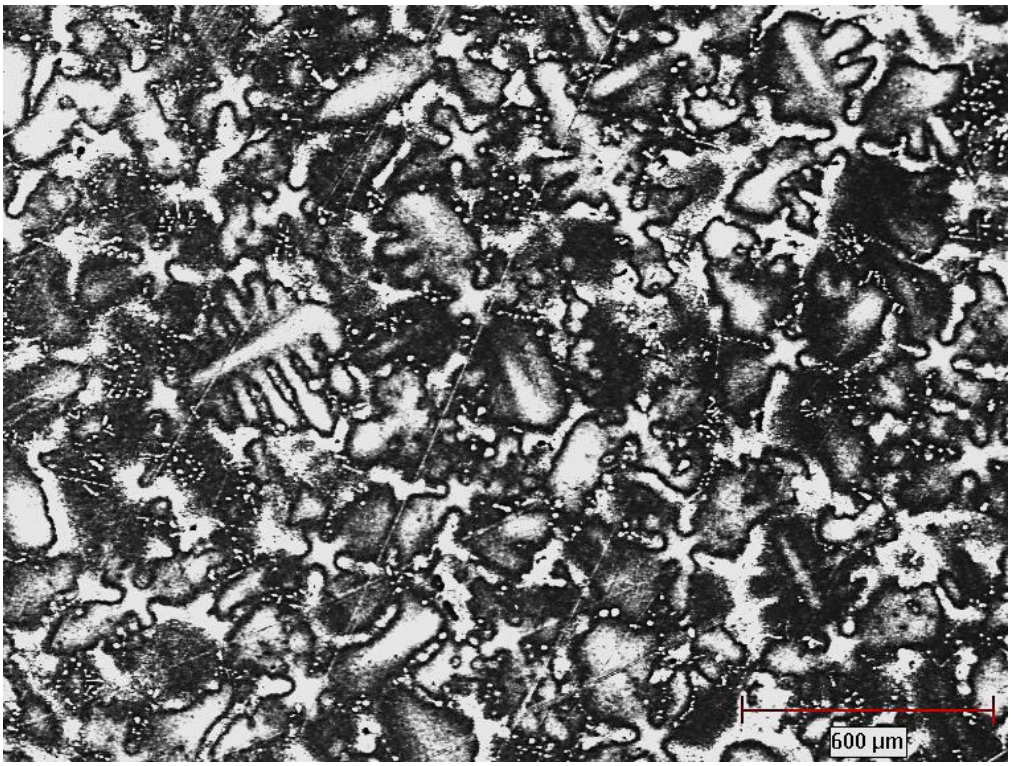

Figure 4-2: Optical micrograph of etched as-received cast base-metal IN-738 showing dendritic structure.

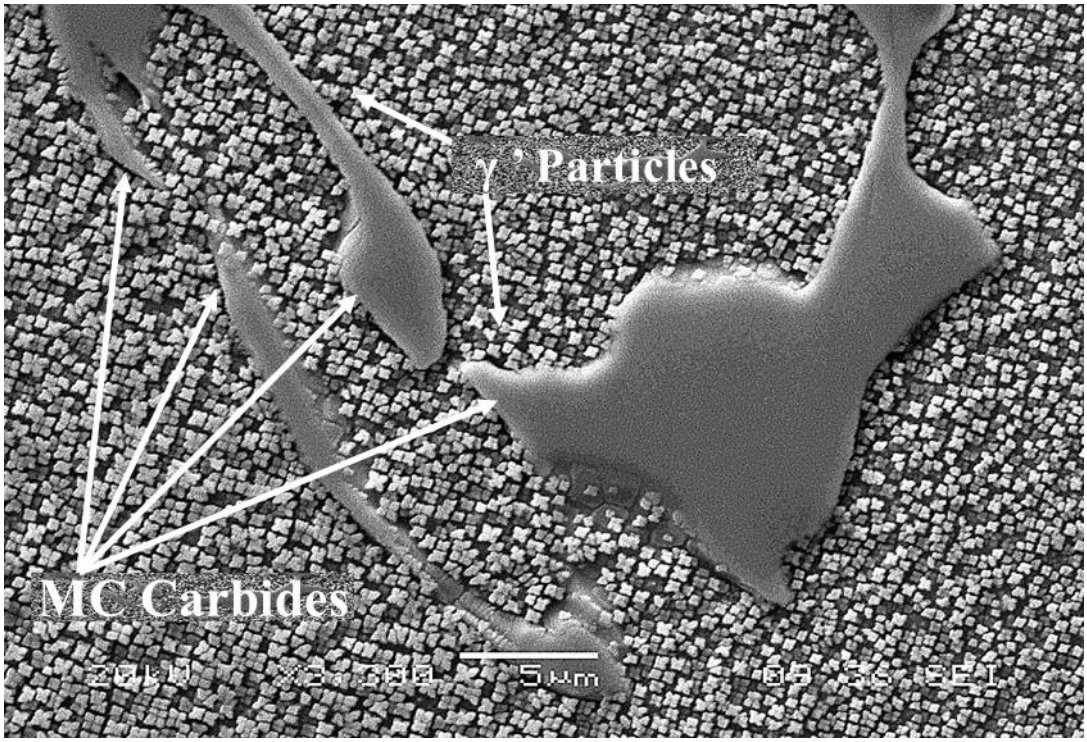

Figure 4-3: SEM micrograph of cast as received IN-738 SX showing uniformly dispersed cuboidal shaped γ' particles within the γ matrix and MC carbide

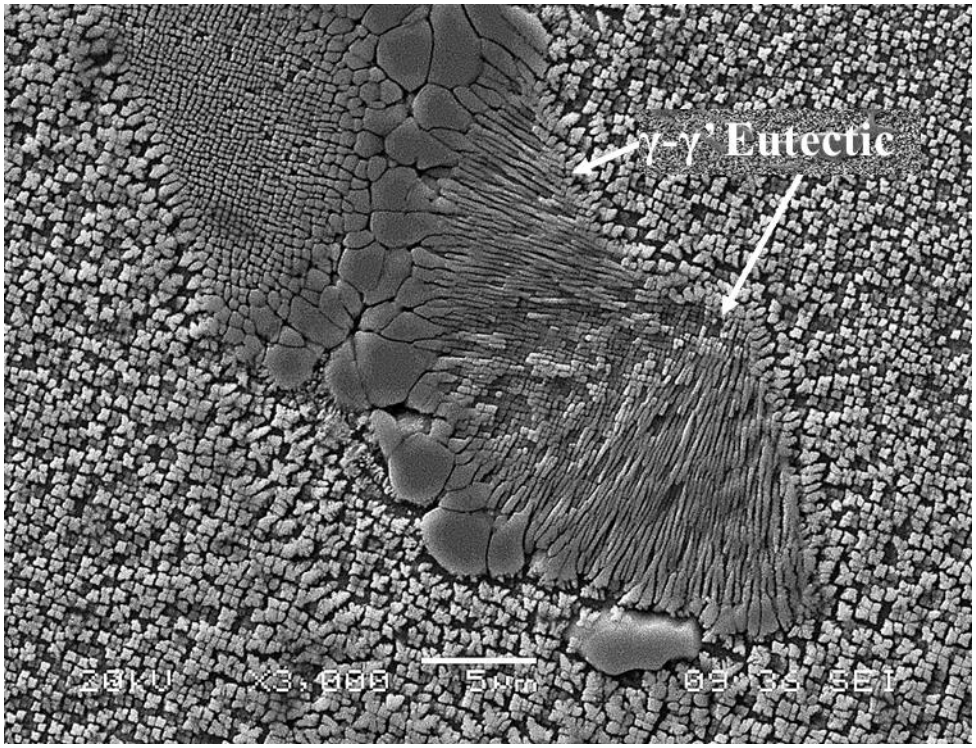

Figure 4-4: γ-γ' eutectic in cast As-received IN 738

4.2 Microstructure of Brazed Joints

To study the effect of the interlayer alloy type on the joint microstructure, IN 738 SX coupons with dimensions of 15 mm × 10 mm × 15 mm and a gap width of 300 μm were TLP bonded in a vacuum furnace with both AMDRY 790, which contains Si and B as the MPD elements, and NB150, which contains B as the only MPD element and Cr, a solid solution strengthening element. The evolution of the joint microstructure was studied for a bonding temperature range from 1100^{o}C to 1190^{o}C and holding time from 1to 35 hrs, and this is presented in the discussion that follows.

4.2.1 Microstructure of AMDRY 790 Brazement

The microstructure of a section of the AMDRY 790 brazement carried out at 1150 ^{o}C for 60 minutes is shown in Figures 4-5 and 4-6. The microstructure across the joint consists of three main regions, an athermally solidified zone (ASZ) sandwiched between the layers of the isothermal solidified zone (ISZ) and diffusion affected zone (DAZ) on both sides of the substrate. The DAZ, shown in Figure 4.8, mainly contains particles with acicular (or blocky) shape and particles of a needle-like morphology (mainly borides) due to the B diffusion into the base-metal. The EDS analysis reveals the presence of both B and C in these precipitates, although their concentration could not be accurately determined due to the difficulty of quantifying light elements. The EDS compositional analysis of the other elements indicates that both precipitates are likely Cr-rich carbo-borides. The microstructure of the ISZ consists of a pro-eutectic Ni-rich γ-solid solution phase. The microstructure of the ASZ consists of three distinct phases: a Ni–rich solid solution phase, a boron-bearing phase and a silicon-bearing phase. EDS compositional analysis of the other elements shown in Table 4.1 suggests that these boron and silicon bearing phases are likely Ni-rich boride and Ni-rich silicide respectively.

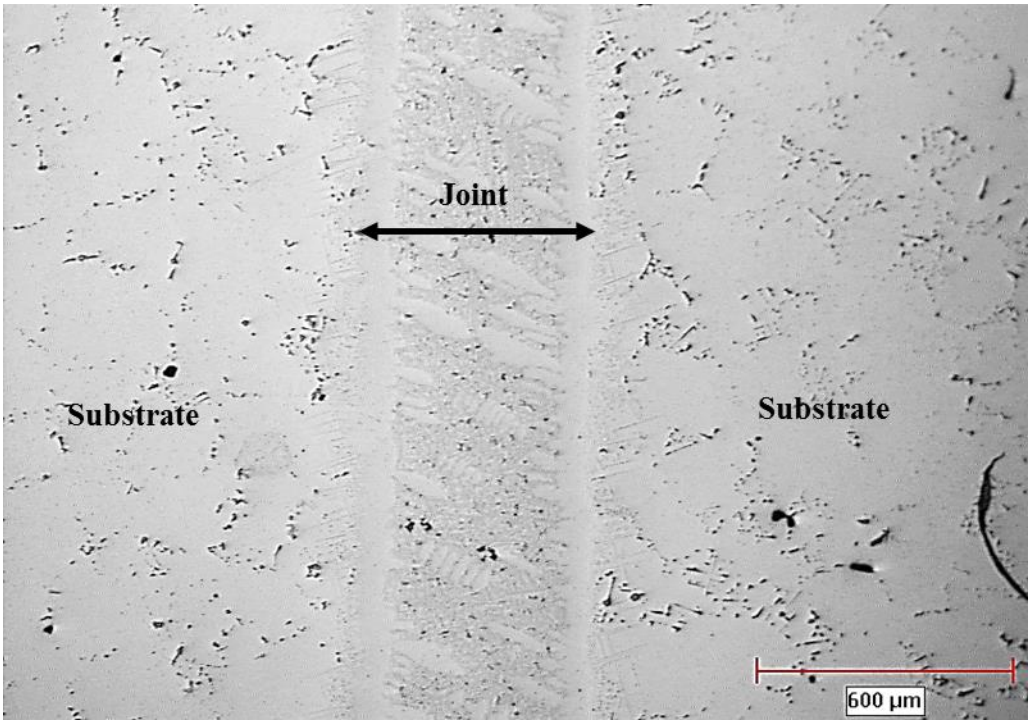

Figure 4-5: Optical micrograph of AMDRY 790 Brazement.

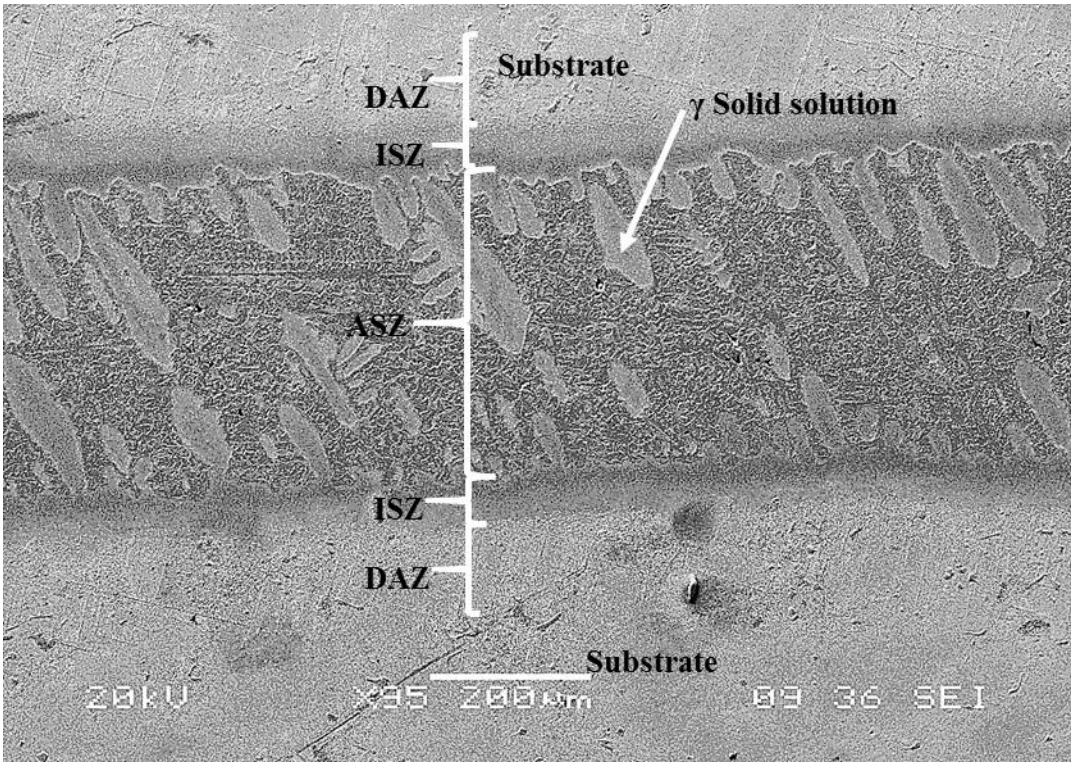

Figure 4-6: SEM micrograph of AMDRY 790 Brazement

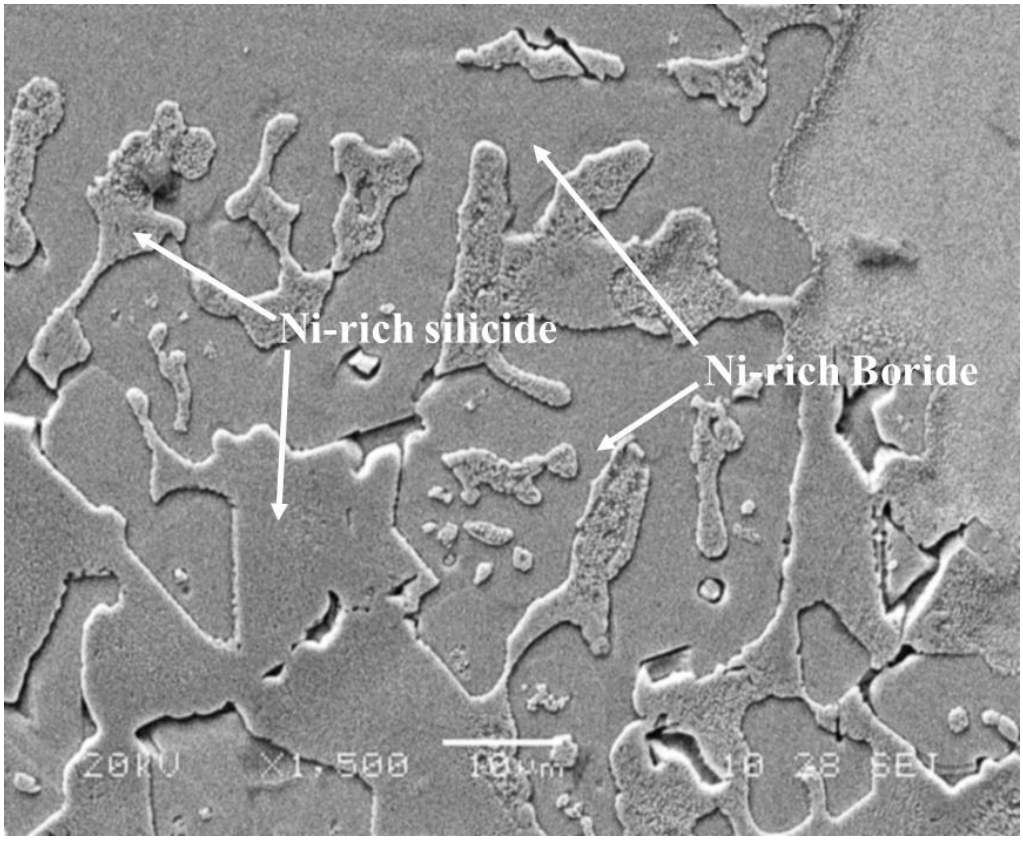

Figure 4-7: SEM micrograph showing eutectic microconstituents in the AMDRY 790 brazement

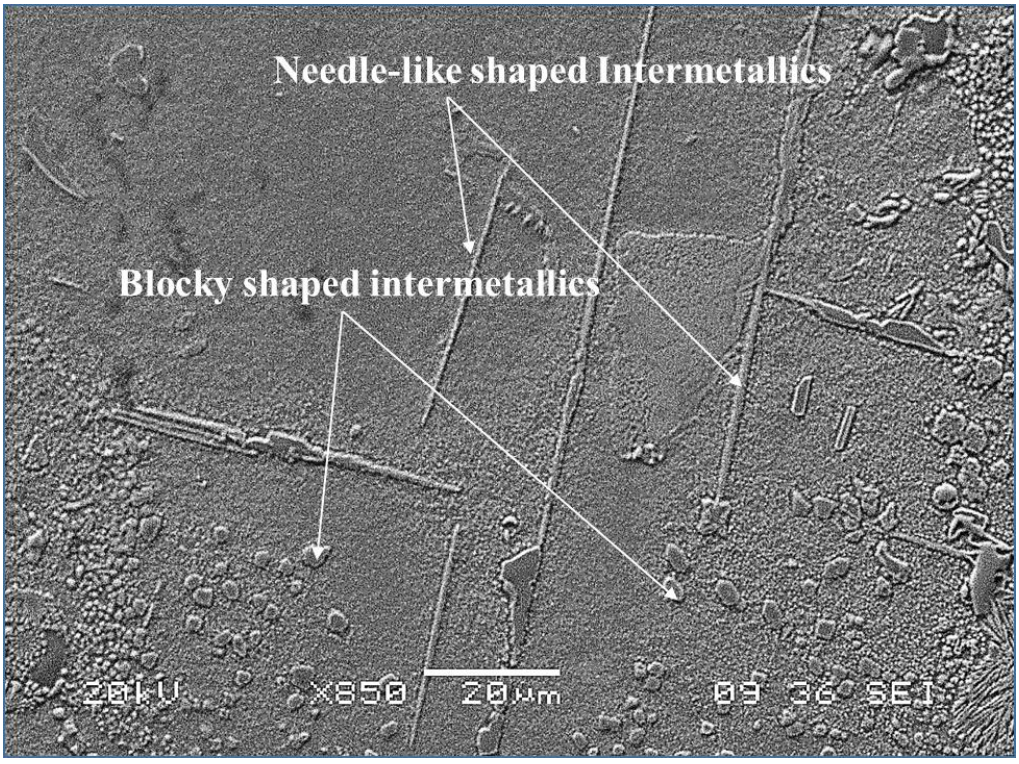

Figure 4-8: SEM micrograph of DAZ in AMDRY 790 brazement

Table 4-1 : Chemical composition (at.%) of different phases observed in AMDRY 790 bonds made at 1150˚C for 60 min

Region	ISZ	ASZ			DAZ	
Element	Proeutectic γ-solid solution	Ni-rich boride phase	Ni-rich silicide phase	Eutectic γ-solid solution	Blocky Shape Cr-rich phase	Needle-Like Cr- rich phase
Ni	74.2	75.7	69.7	74.1	3.5	2.5
Cr	8.8	8.9	3.2	8.3	72.2	76.3
W	0.9	0.5	-	0.8	11.4	11.0
Co	3.7	2.1	1.8	3.5	1.6	1.5
Ti	1.2	2.0	0.3	1.7	0.7	0.7
Al	4.2	1.2	3.3	4.5	0.3	-
Mo	0.5	0.2	-	-	8.7	6.6
Si	5.6	8.8	21.7	6.9	1.6	1.4
Ta	0.9	0.6	-	0.2	-	-

4.2.2 Microstructure of NB150 Brazement

The microstructure of NB150 brazement that was carried out at 1150^{o}C for 60 minutes is shown in Figures 4-9 and 4-10. As with the AMDRY 790 brazement, the joint microstructure consists of the three regions of DAZ, ISZ and ASZ. The ASZ is formed as a result of the insufficient time required for the completion of isothermal solidification, and the microstructure in this case consists of microconstituents with an eutectic-like morphology. The EDS spectra analysis indicates that it is made up of three distinct phases with two boride phases, unlike the single boride phase in the AMDRY 790 brazement. The EDS compositional analysis of each of the phases, presented in Table 4-2, identified the two boride phases to consist of Cr-rich and Ni-rich boride phases and the third phase is a Ni–rich solid solution. The ISZ region is formed due to interdiffusion–induced compositional changes, and consists of a pro-eutectic Ni-rich γ solid solution phase. This zone contains a certain amount of Al, Co, Ta, Ti, Mo, and W which were not present in the initial composition of the interlayer alloy. The DAZ consists of second phase particles with two different morphologies: particles with a blocky morphology and particles with a needle like morphology similar to those in the AMDRY 790 brazement. Idowu et al. [85] studied the precipitation behaviour of the DAZ with the TLP bonding of IN 738LC using a Ni-B-Cr interlayer and found that a significant volume fraction of complex face-centred cubic structure of Cr-Co-Mo-W rich carbon borides could be observed at the joint-base-metal interface.

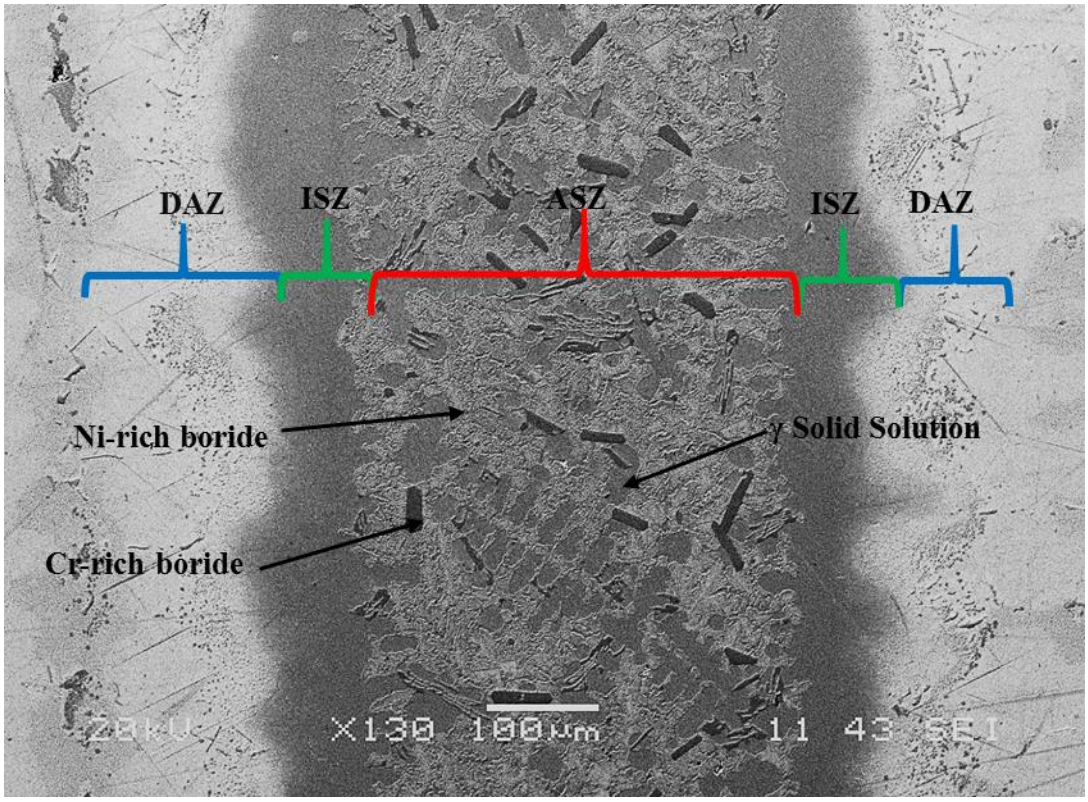

Figure 4-9: SEM micrograph of NB150 brazement

Table 4-2: Chemical composition (at.%) of different intermetallic constituents of phases observed in NB150 bonds made at 1150˚C for 60 min

Element	Proeutectic γ-solid solution	Ni-rich boride phase	Cr-rich boride phase	Eutectic γ-solid solution
Ni	72.0	80.2	5.9	72.8
Cr	16.8	11.1	86.9	16.0
W	0.7	0.3	2.4	0.7
Co	3.9	2.1	1.6	3.9
Ti	1.4	3.2	0.2	1.4
Al	4.5	2.1	-	4.5
Mo	0.4	0.3	3.0	0.4
Ta	0.3	0.7	-	0.3

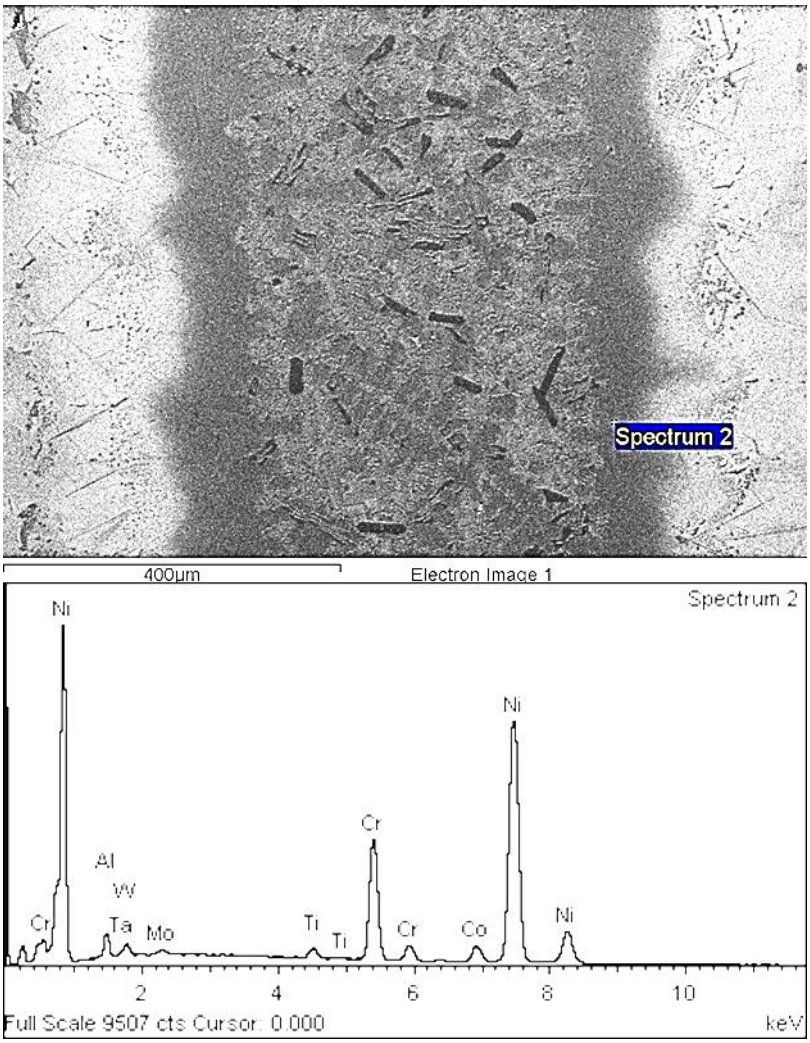

Figure 4-10: EDS spectra analysis of pro-eutectic Ni-rich γ solid solution in NB150 brazement.

4.2.3 Microstructural Evolution during TLP Bonding

At the commencement of the TLP bonding process, MPD solute in the interlayer alloy (powder AMDRY 790 and NB150) diffused into the base-metal through solid state diffusion. The extent of this solid state diffusion is dependent on the rate of heating. In this work, the rate of heating was kept constant at 4.8K/sec. Upon heating beyond the melting temperatures of 1055˚C and 1093˚C for NB150 and AMDRY 790 respectively, the interlayer became a liquid, flowed and filled the joint, thereby wetting the faying surface of the base-metal in the process. This initiated the base-metal dissolution process and the joint width began to increase. Upon reaching the bonding temperature, the joint attained its maximum width, the MPD elements continued to diffuse into the solid substrate, until local equilibrium was achieved at the solid-liquid interface, thus marking the onset of isothermal solidification. For the isothermal solidification process to continue, local equilibrium must be maintained and therefore, the MPDs continue to diffuse while the liquid narrowed during the holding time. The cooling of the TLP bonded samples before isothermal solidification was complete, resulted in the formation of a continuous centreline eutectic in the bond centre.

The ISZ, which is a pro-eutectic region, therefore represents the movement of the solid-liquid interface, i.e. isothermal solidification by interdiffusion, induced due to compositional changes, towards the joint centre until the cooling began. The EDS compositional analysis revealed that this region has a composition similar to that of the Ni-base γ-solid solution present in the centreline eutectic as seen in Table 4-1. A continuous centreline eutectic in the ASZ was formed along the joint centreline since cooling to room temperature began before isothermal solidification was completed due to reduced solubility of the MPDs at lower temperatures.

Similar eutectic microstructures in the centreline of TLP bonded Ni-base alloys have been observed and reported by various researchers. For instance Ohsasa et al. [44] used Scheil

simulation to study and model the solidification behaviour of the residual liquid during the cooling stage when the TLP bonding of pure Ni was done by using a Ni-B-Cr ternary filler alloy. They reported the formation of a ternary centreline eutectic that comprises of Ni-rich solid solution phase (γ), Ni-rich borides (Ni_3B) and Cr-rich borides (CB) at 997˚C. Their simulation results showed that for samples initially held at 1110˚C, an Ni-rich γ phase formed as the primary phase during solidification of the residual liquid, followed by the eutectic reaction $L \rightarrow \gamma + Ni_3B$ at 1042˚C. Complete solidification was reported to occur with a ternary eutectic reaction $L \rightarrow \gamma + Ni_3B + CrB$ at 997˚C.

In a similar work done by Gale et al. [11], the TLP bonding of pure Ni with the use of Ni-Si-B as the filler alloy and high temperature X-ray diffraction resulted in the formation of a deposit of Ni +Ni_3B eutectic mixture in the sample joint at 1150˚C for 5 mins. The centreline eutectic observed in the TLP bonded specimens at 1150˚C for 1 hr to 35 hrs in this work is believed to have been formed by eutectic transformation (solidification reaction) during cooling due to insufficient diffusion time for complete isothermal solidification during holding at the bonding temperature.

4.3 Effects of TLP Bonding Parameters

The TLP bonding process has a number of process variables or parameters that determine the final characteristics of the joint from the microstructure to mechanical properties. Three critical process parameters which have been identified to have more significant influences were varied, while keeping all of the other parameters constant in this research work to evaluate their influence on the bond microstructure. These are:

1) initial gap size/ interlayer thickness,
2) holding/diffusion time, and
3) bonding temperature

4.3.1 Effect of Initial Gap Size

To study the effect of the gap size on the microstructure of IN 738 SX bonded with a NB150 filler alloy, brazing was done at a bonding temperature of 1150˚C for initial gap sizes of 70, 300, 400, 500, 800 and 1000µm for holding times of 1hr and 5hrs with NB150 as the interlayer alloy. All of the joint microstructures consist of a continuous centreline eutectic constituent bounded by small regions of ISZ and DAZ. Analytical observations of these microstructures, showed a consistent and progressive increase in the width of the centreline eutectic from 24 µm for gap size of 70 µm to 1.4 mm for a gap size of 1000 µm. During the isothermal solidification stage in the TLP bonding process, migration of the solid-liquid interface occurs by diffusion of the solute away from the liquid into the solid base alloy. Hence, at a constant bonding temperature and holding time, the level of MPD solute (B in this case) diffusion and thus the degree of isothermal solidification would be independent of the initial gap size. The rationale is that B has a certain value of diffusivity (7.2×10^{-13} cm^2/sec) at a bonding temperature of 1150˚C and thus for the same holding time, the distance travelled away from the solid-liquid

interface would be constant. The degree of the dissolution of the base-metal increases with increase in the initial gap size, since the amount of MPD solute within the joint increases, and thus more liquid is formed within the joint. Therefore, the width of the residual liquid, which transformed during cooling into a centreline eutectic, is expected to increase with an increase in the initial gap size. This in fact, is the trend observed for all specimens brazed for both 1 hr and 5 hrs of holding time, and a plot of the initial gap size versus the average centreline eutectic size is shown in Figure 4-11. The plot reveals that a linear relationship exists between the initial gap size and the width of the centreline eutectic. Therefore, to achieve complete isothermal solidification, a longer time would be required for specimens with a larger gap compared to those with a smaller gap. Analytical models used in the study of TLP bonding consider the solid-liquid interface motion as being diffusion controlled [36,52,55,78,103] and this has been used to predict the time, t_f, required to produce a single phase microstructure during TLP bonding through the complete isothermal solidification of the liquated insert. Accordingly, in these models, the time t_f, can be approximated by

$$t_f^{\frac{1}{2}} = \frac{2h}{\gamma 4 D^{\frac{1}{2}}} \qquad \text{[55,71]} \qquad 4.1$$

where D is the diffusion coefficient of the MPDs in the solid base-metal, and $2h$ is the maximum width of the liquated insert upon equilibration at the solid-liquid interface, and γ is a dimensionless parameter, which is estimated by numerically solving the following equation:

$$\frac{C_\alpha - C_m}{C_\beta - C_\alpha} = \gamma\sqrt{\pi}\exp(\gamma^{\frac{1}{2}}(1 + erf\gamma)) \qquad 4.2$$

where C_α and C_β are the solute concentrations in the solid and liquid phase at the migrating interface, respectively, and C_m is the initial solute concentration in the base alloy.

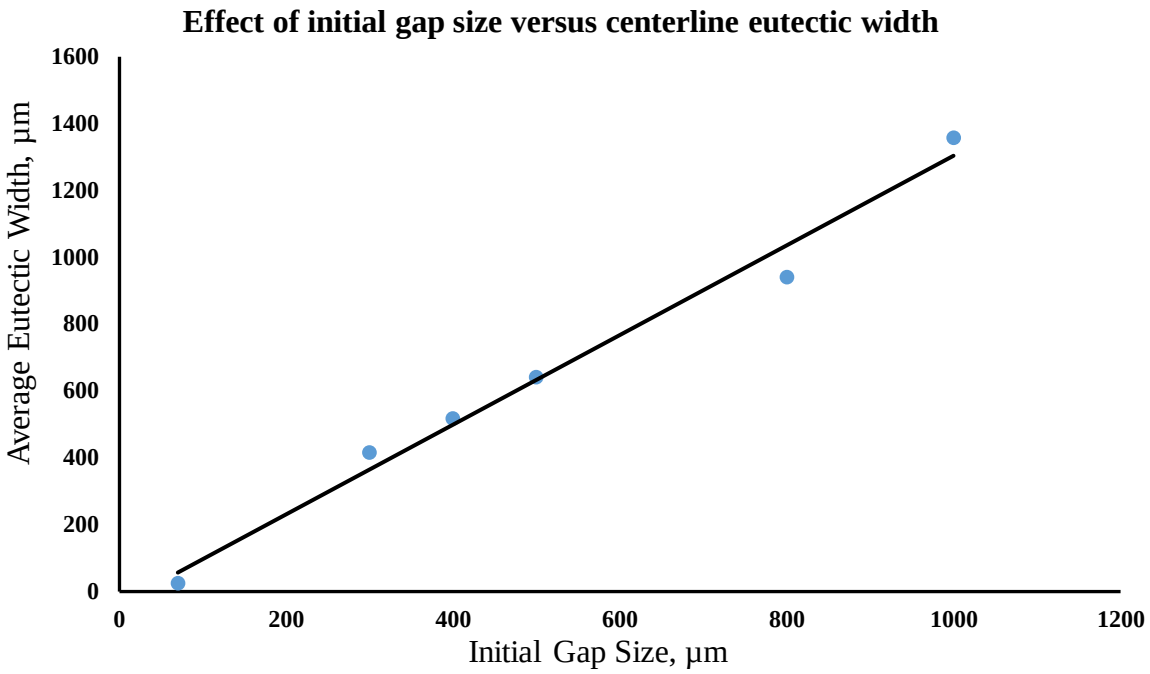

Figure 4-11 : Variation of centreline eutectic width with initial gap size.

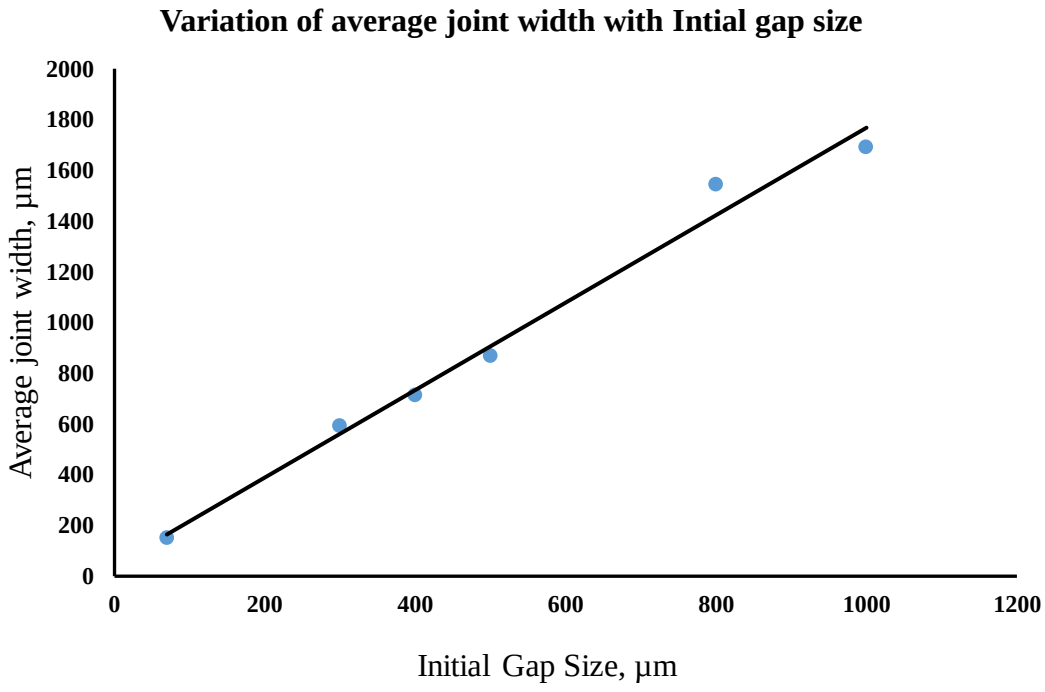

Figure 4-12: Increase in joint width with initial gap size

4.3.2 Effect of Holding Time

To study the effect of the holding time on the microstructure of TLP bonded joints, IN 738 SX specimens with an initial gap size of 300 µm were bonded with NB150 at 1150˚C for 1, 5, 10, 20, 30 and 35 hrs. The microstructures at the different holding times consist of a continuous centreline eutectic, and the average width of this centreline eutectic considerably decreased from 415 µm in the 1 hr specimen to 105 µm in the 35 hr specimen as shown in Figure 4-13. It can be seen that for a 300 µm gap, a holding time of 35 hrs is not sufficient for complete isothermal solidification of the liquid interlayer to achieve a homogeneous joint microstructure in IN 738 SX. Since the centreline eutectic represents the fraction of remaining liquid before the onset of athermal solidification at the end of each holding time, the width of the centreline eutectic was found to decrease with increase in the holding time.

For a given bonding temperature and initial gap size, the TLP bonding process depends on the holding time required to complete the isothermal solidification to prevent the formation of centreline eutectic phases. From Equation 4.1, it can be seen that the time, t_f, required to achieve complete isothermal solidification is inversely proportional to the diffusivity of the MPD solute. Hence for a constant value of diffusivity at the bonding temperature a longer holding time would be required to achieve complete isothermal solidification.

.

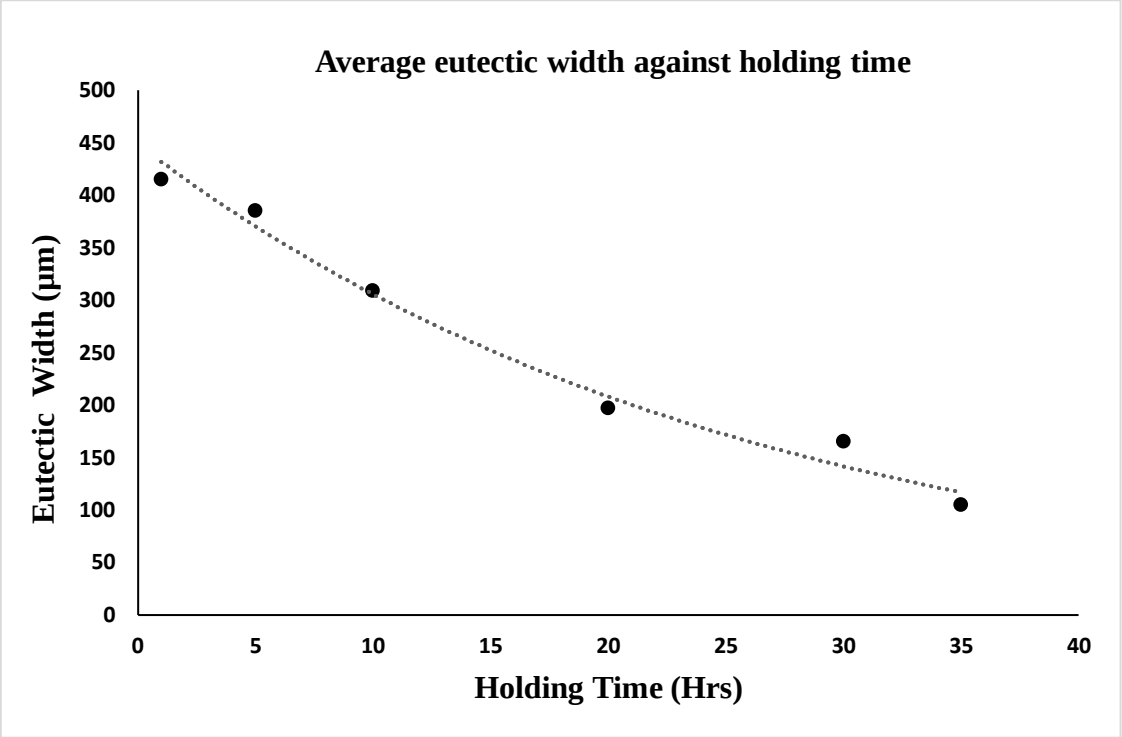

Figure 4-13: Variation of the average eutectic width with holding time.

4.3.3 Effect of Bonding Temperature

To study the effect of temperature on the final microstructure of TLP bonded joints, IN 738 SX specimens with an initial gap size of 300 µm were bonded with NB150 at bonding temperatures of 1110˚C, 1150˚C and 1150˚C for 35 hrs. The lowest bonding temperature was chosen such that it is higher than the melting point of the interlayer alloy, 1055˚C, to ensure complete melting. The microstructures of all three specimens consists of a continuous centreline eutectic, in which the average thickness across the joint varies from 214 µm in the specimen bonded at 1110˚C to 105 µm in the specimen bonded at 1150˚C, and a significant increase to 1322µm in the specimen bonded at 1190˚C specimen after a 35 hr holding time, as shown in Table 4-3. The average joint width increased with an increase in temperature from 372 µm at 1110˚C to 590 µm at 1150˚C; however, the size could not be accurately quantified in the specimen bonded at 1190˚C due to the indistinctive nature of the substrate-joint boundary.

An interesting observation in the specimen TLP bonded at 1190˚C is the absence of both the acicular and blocky Cr-rich borides/borocarbides i.e. the DAZ. The SEM micrograph of the specimen bonded at 1190˚C after a holding time of 35 hrs revealed the presence of fine γ' particles. This would have been formed by solid state precipitation during cooling, when the temperature was lower than the γ' solvus temperature, due to the increase in the concentrations of Al and Ti in the interlayer liquid. As a result of both base-metal dissolution and diffusion of Al and Ti into the joint centre, the amount of Al and Ti in the joint centre is increased

Analytical TLP models, which are generally based on binary eutectic, are hypothetical and depend on classical solutions of Fick's diffusion equations, predict that the isothermal solidification completion time decreases with increasing bonding temperature, i.e. isothermal solidification rate increases with increases in bonding temperature. This process is considered by these models to be entirely controlled by the solid state diffusion of the MPD solute out of

Table 4-3: Variation of average joint width and centreline eutectic with bonding temperature

Bonding Temperature ˚C	Average Joint width µm	Average Eutectic width µm
1110	372	214
1150	590	105
1190	-	1322

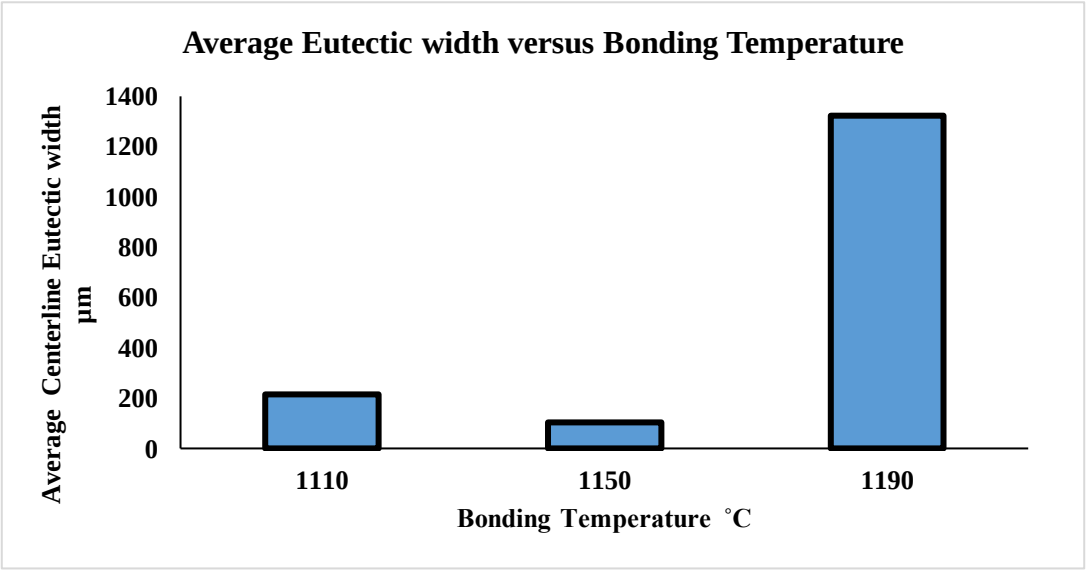

Figure 4-14: Variation of average eutectic width with increase in temperature

the liquated insert away from the joint centre and thereby establishing a linear relationship (of a parabolic nature) between the average eutectic width and the square root of time, t_f . Thus, in going from a bonding temperature of 1110˚C to 1150˚C, this assertion holds true as the average eutectic width is reduced, but does not explain the increase in the eutectic width when the bonding temperature increases to 1190˚C. This therefore allays the fact that increase in bonding temperature would increase isothermal solidification rate in and thus reduce the bonding time.

In reports by Ojo et al. [76,81,85], during the TLP bonding of IN783 with the use of an NB150 interlayer alloy, and Wikstrom et al. [104], during the bonding of IN 738 with a DF-3 interlayer alloy at higher temperatures, a deviation in the isothermal solidification rate was observed. Ojo et al. [76,80,83,105] reported that the kinetics of the isothermal solidification process do not always satisfy the parabolic relationship between the migrating solid-liquid interface and the square root of time. According to their report, the deviation from the parabolic relationship is thought to be caused as a result of the reduction of the MPD solute concentration gradient $\frac{\partial C}{\partial x}$ in the base-metal below a critical value $(\frac{\partial C}{\partial x})_c$ due to the continual diffusion of the MPD solute into the base-metal. However, studies from the Ni-B phase diagram has shown that boron has a low solubility in nickel and this solubility decreases with increase in temperature above the eutectic temperature. Hence, a decrease in the solute (B) solubility with increase in temperature would result in more pronounced deviation, by further reducing the solute concentration gradient, with a consequent increase in the isothermal solidification completion time, t_f [76]. This may explain the increase in the eutectic size when the temperature was increased from 1150˚C to 1190˚C in the present work.

4.4 TLP Bonding Using Composite Interlayer

The experimental results presented in the previous section has shown that by careful selection of the process parameters during TLP bonding of IN 738 SX, the microstructure of the joint can be controlled by limiting the size of the centreline eutectic. However, a fundamental question given the formation of more complex phases with increase in the bonding temperature is; if complete isothermal solidification can be achieved in shorter realistic times during TLP bonding of IN 738 SX. The prolonged isothermal solidification completion time has been attributed to be as a result of a reduction in the solute concentration gradient $(\frac{\partial C}{\partial x})_B$ in the base-metal [91], and therefore the use of a composite interlayer similar to wide-gap TLP bonding has been identified as having the potential to reduce the holding time required to achieve complete isothermal solidification.

4.4.1 Dissolution of Composite Interlayer

In the application of wide-gap TLP bonding, one of the main challenges has been the incomplete melting of the gap filler powder alloy, for the purpose of this work a base-metal powder was used as the gap filler alloy in conjunction with NB150 interlayer to form a composite interlayer. Three mixture ratios are investigated: $R_{13:7,}$ $R_{7:3}$ and $R_{6:4}$ which were deposited onto a sample of SX IN 738 and heated to a bonding temperature of 1150˚C, held for 1 hr and subsequently cooled to room temperature. Optical micrographs of the dissolution of these composite mixture ratios are shown in Figures 4-15 to 4-17 The results obtained are similar to those obtained by Adam [77] with composite mixture ratios of $R_{13:7}$ and $R_{6:4}$ that showed partial melting of the gap filler base-metal powder, while the composite mixture of $R_{7:3}$ showed complete melting and cooling to form eutectic microconstituents.

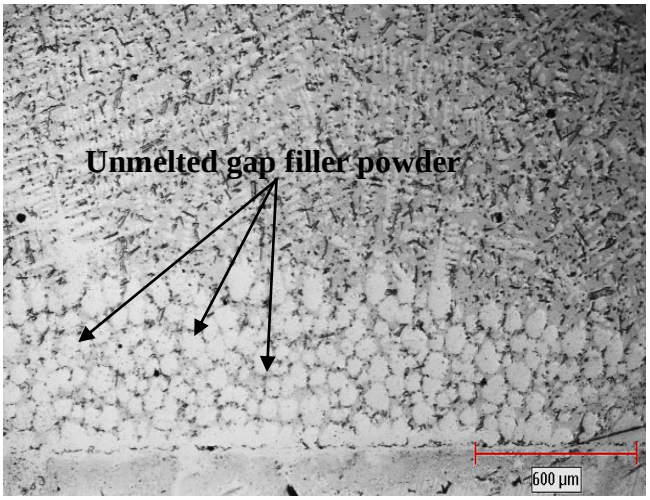

Figure 4-15: Optical micrograph of $R_{13:7}$ composite dissolution showing partial melting at 1150˚C of the gap filler alloy

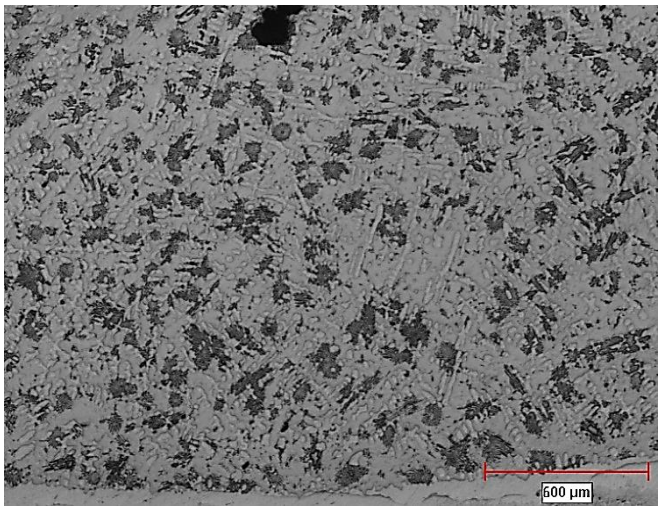

Figure 4-16: Optical micrograph of $R_{7:3}$ composite mixture dissolution showing complete melting at 1150˚C with formation eutectic microconstituents

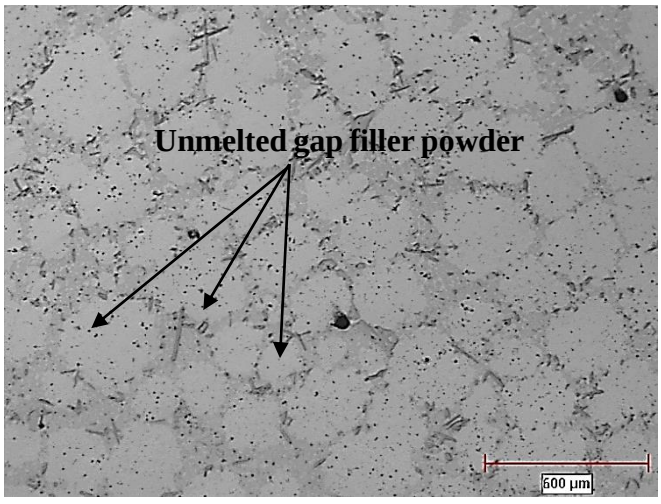

Figure 4-17: Optical micrograph of $R_{6:4}$ composite mixture dissolution showing partial melting at 1150˚C

4.4.2 Microstructure of Composite Powder Mixture TLP Bonded IN 738 SX

To study the effect of the composite powder mixture with a ratio of $R_{7:3}$ on the time to complete isothermal solidification, IN 738 SX with a gap size of 300 µm was TLP bonded in a vacuum furnace for various holding times, that ranged from 1 to 20 hrs at a temperature of 1150˚C. The TLP bonding was done in pairs, with one set containing only an NB150 interlayer and the other set of specimens, the composite powder of NB150 as the interlayer alloy and IN 738 powder as the gap filler. The microstructure at the joint centre of the TLP bonded specimens prepared with the composite mixture also comprised of three different regions; DAZ, ISZ and ASZ, as observed in the conventional TLP bonds when the holding time is not sufficient for the completion of isothermal solidification.

However, for the respective holding times, bonding temperature and constant initial gap size, the average eutectic width and average joint width in the conventionally TLP bonded specimens are larger than those in the specimens prepared with the composite powder mixture as shown in Table 4-4. A plot of the average eutectic width at the end of each holding time against the bonding time for both conventional TLP bonding and TLP bonding with use of composite powder is presented in Figure 4-18. Although both curves follow a similar trend, in that the average eutectic width with reduces with increase in holding time; TLP bonded specimens with the composite powder mixture have comparatively smaller eutectic widths. This can be attributed to the fact that the composite powder mixture contained lesser amount of boron and as a consequence, smaller amount of interlayer liquid due to reduced melt-back reaction.

From the foregoing, it can be seen that the centreline eutectic size is much smaller for the same TLP bonding process conditions when the composite interlayer is used. To evaluate extent that the use of a composite interlayer would eliminate the centreline eutectic microconstituents during TLP bonding, IN 738 SX specimens that were cut with an initial gap size of 170 µm and

300 μm were bonded at 1150˚C for various holding times. It was found that after 20 and 35 hrs respectively, for the two gap sizes, the microstructure of the TLP bonded specimen with a composite interlayer contained no centreline eutectic microconstituents while that of the conventional TLP bonds contained a significant amount of centreline eutectic microconstituents as shown in Figures 4-19(a)-(d).

Table 4-4: Variation of eutectic width with holding time for both conventional TLP bonding and composite interlayer TLP bonding

Hold Time (hrs)	Conventional TLP		Composite TLP		% Diff in AEW
	AEW	AJW	AEW	AJW	
1	415	590	298	414	28
5	385	627	201	403	48
10	309	627	148	428	52
15	263	585	109	410	59
Average Joint Width	607		413		32

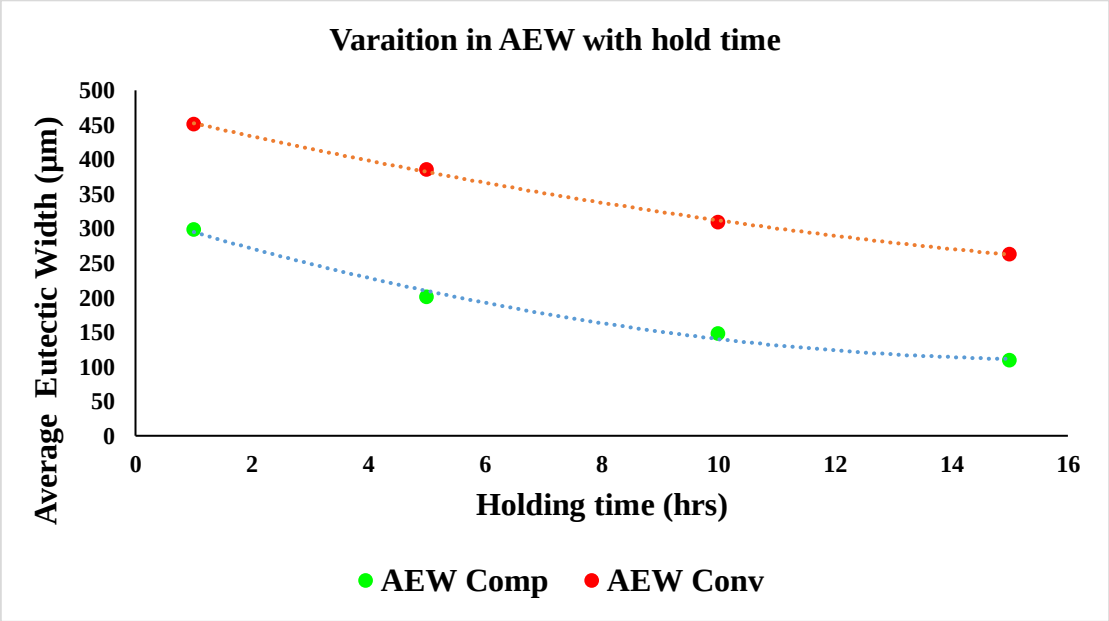

Figure 4-18: Variation of eutectic width in TLP bonded IN 738 SX using composite interlayer and conventional interlayer

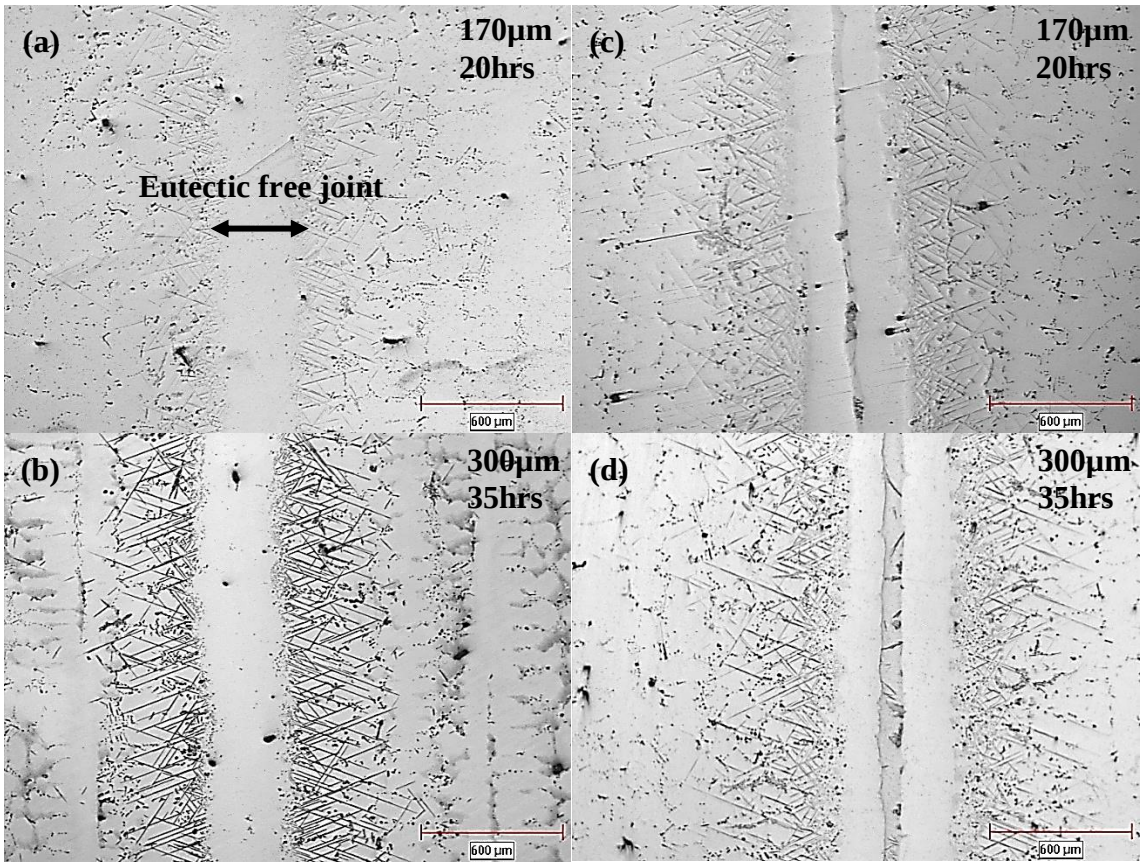

Figure 4-19: Optical micrographs of TLP bond at 1150˚C using both composite (a), (b) and conventional interlayers (c), (d) for 20 hrs and 35hrs

4.5 Electrochemical Potentiodynamic Polarization of IN 738 SX Specimens

This section of the thesis presents the results obtained from electrochemical potentiodynamic polarization in three different corrosive media. The following electrochemical corrosion measurement parameters are used to characterise the corrosion behaviour of the as-cast base metal and TLP bonded IN 738 SX under various conditions of testing: the OCP, E_{corr}, i_{corr}, i_{pass}, i_{crit} and E_{pp} as obtained from the potentiodynamic polarization in the different media. For simplicity, a representative plot will be used rather than presenting multiple plots for the same condition.

4.5.1 Corrosion Behaviour of the As-received cast IN 738 SX

The potentiodynamic polarization plot for the as-received cast IN 738 SX at room temperature in 0.6 M HNO_3 is shown in Figure 4-20. The general trend of the curve shows that once the critical anodic current density of 2.8 $\mu A/cm^2$ is reach at a passivation potential of 99.7 mV, passivation occurs. However, as the potential increases beyond the passivation potential, the anodic current density is slightly decreased to a value of 2.4 $\mu A/cm^2$. This can be attributed to the stability of the oxide film, formed upon exposure to the corrosive media. The corrosion current density measured by Tafel extrapolation is 0.8 $\mu A/cm^2$, which is expected given that IN 738 SX is designed to a have low corrosion rate and the corrosion potential is -18.4 mv. The OCP at the time of immersion was -12.5 mV, which after 1hr of exposure to the test medium, reached a more negative value of -28.5 mV due to the formation of the oxide film.

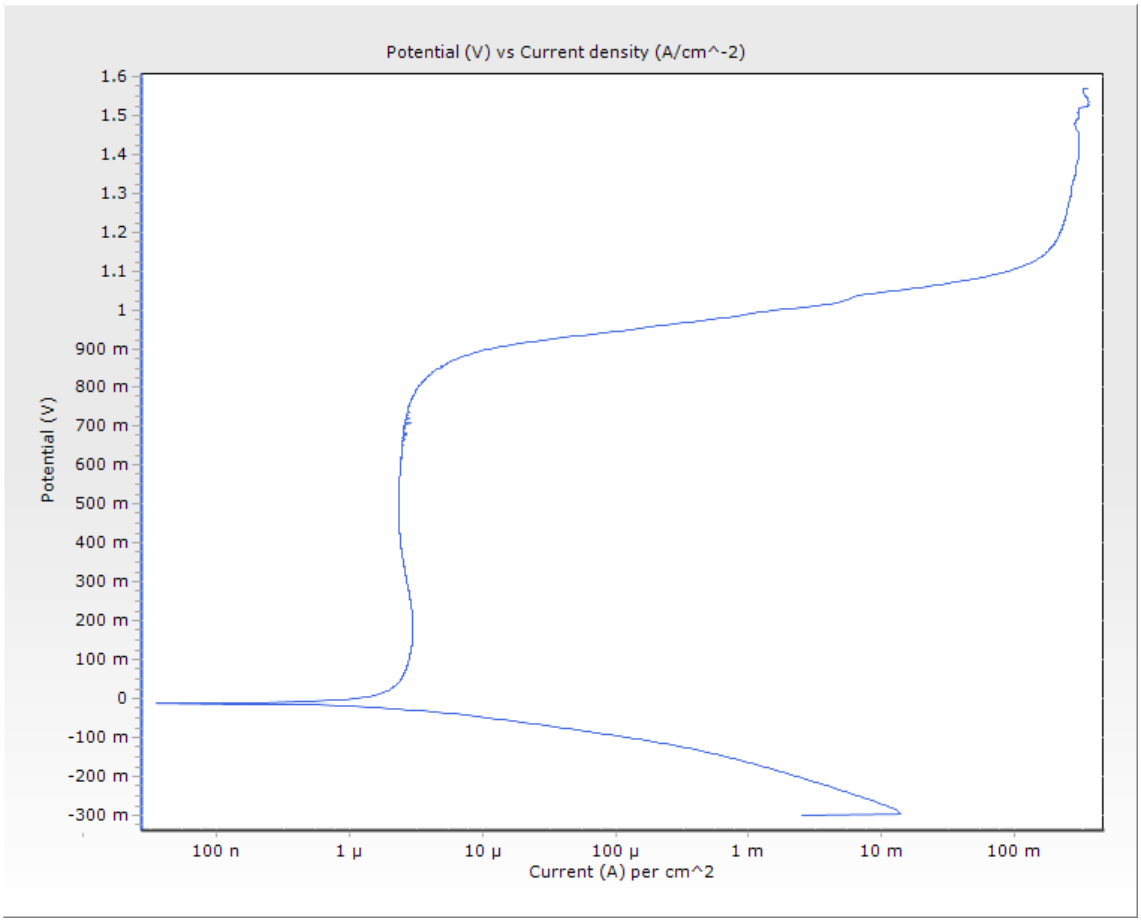

Figure 4-20: Potentiodynamic polarization of as-received cast IN 738 SX in 0.6M HNO_3

4.5.2 Corrosion Behaviour of TLP Bonded IN 738 with AMDRY 790 Interlayer

The potentiodynamic polarization plot for TLP bonded IN 738 SX specimens at room temperature with the use of an AMDRY 790 interlayer in 0.6 M HNO_3 is shown in Figure 4-21. The general behaviour follows the trend of passivating metals in transitioning from an active to a transpassive state. However, a closer observation reveals that the passivation behaviour is not well defined once the primary passivation potential, E_{pp} of 53.1 mV and critical anodic current density, i_{crit} of 48.4 µA/cm^2 were reached. As the anodic potential increases beyond the passivation potential, the current density decreases to a passivation current density, i_{pass}, of 25.9 µA/cm^2 and gradually increased throughout a potential range of 200-900 mV to a maximum value of 211.3 µA/cm^2 before sharply increasing at the onset of transpassivation.

4.5.3 Corrosion Behaviour of TLP Bonded IN 738 SX with NB150 Interlayer

The potentiodynamic polarization plot for TLP bonded IN 738 SX specimen with the use of NB150 interlayer at room temperature in 0.6 M HNO_3 is shown in Figure 4-21. The general behaviour follows the trend of passivating metals in transitioning from an active to a transpassive state. Although the specimen shows a reduction in the anodic current density to a value of 9.9 µA/cm^2 once the critical current density of 12.9 µA/cm^2 was reached, yet there is a gradual increase of the anodic current density in the anodic potential range of 100-800 mV. This behaviour is not reminiscent of active – passive metals that show relatively stable anodic current density in the passive region rather than steady increase in current density. This increase in the anodic current density could likely be as a result of changes in the composition of the passive film with increase in potential [97].

4.5.4 Corrosion Behaviour of TLP bonded IN 738 SX with AMDRY 790 versus NB150 Interlayer

The effect of the interlayer alloy used for TLP bonding is assessed by comparing the general characteristics of the potentiodynamic polarization curves for the specimens made with AMDRY 790 and NB150 interlayer alloys. The polarization plots for these two interlayer alloys obtained at room temperature in 0.6 M HNO_3 are superimposed as shown in Figure 4-21. Table 4-5 shows the values of the critical parameters obtained from each plot.

The values of the corrosion current density, i_{corr}, obtained for both specimens as shown in Table 4-5 indicate that the AMDRY 790 specimen has a higher corrosion current density than that of the NB150 specimens and thus a higher corrosion rate in the active region. This means that more corrosion is taking place in the AMDRY 790 specimen compared to that in the NB150 specimen. Also, the critical anodic current density for the AMDRY 790 specimen is approximately 4 times that of the NB150 specimen, and the passivation potential at 53.1 mV is higher than that of the NB150 specimen of 20.2 mV. Since the critical anodic current density is a measure of the ease of passivation with lower values being favourable, it thus implies that the NB150 specimen passivates much easier than the AMDRY 790 specimen as reflected in the actual values of the respective passivation current densities for both AMDRY 790 and NB150 as shown in Table 4-5. Also, a greater difference between the passive anodic current density (i_{pass}) and the critical anodic current density (i_{crit}) is required for a more effective passive film [14,93]. However, in both specimens, this difference is not significant, thus leading to less effective oxide film layer in both the AMDRY790 and NB150 specimens. The performance of IN 738 SX is dependent on its ability to maintain low corrosion rates irrespective of the conditions of use and this low corrosion rate is achieved by passivation (primary mechanism of protection) when the anodic current density is low. It thus implies that IN 738 SX TLP bonded with NB150 as the interlayer alloy has better CR than that bonded with AMDRY 790 as the interlayer.

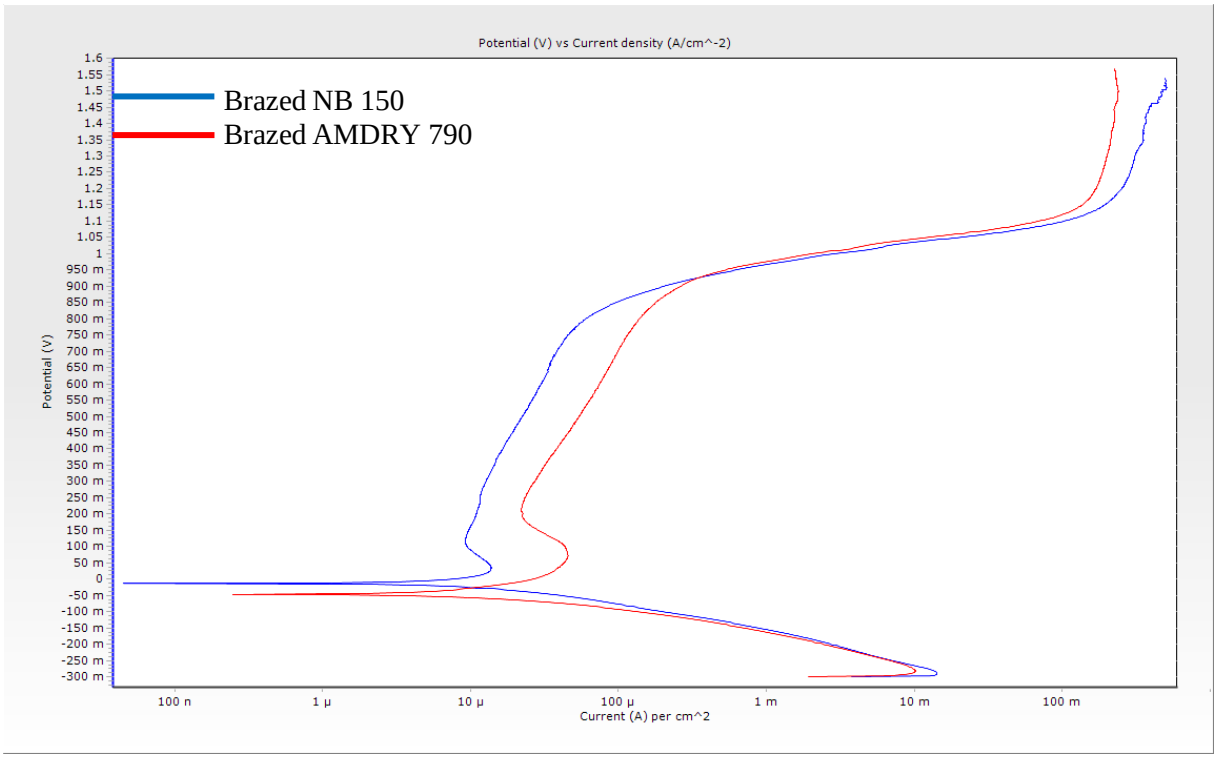

Figure 4-21: Superimposed polarization plots for AMDRY 790 and NB150 IN 738 SX TLP bonded specimens

Table 4-5: Corrosion parameters for AMDRY 790 and NB150 TLP bonded specimen in 0.6M HNO_3 at room temperature

Interlayer Type	**OCP Start (mV)**	**Rest Potential (mV)**	E_{corr} **Tafel (mV)**	i_{corr} **(µA/cm2)**	i_{crit} **(µA/cm2)**	i_{pass} **(µA/cm^2)**	E_{pp} **(mV)**
Amdry790	-30.0	-49.1	-46.3	8.8	48.4	25.9	53.1
NB150	-9.0	-19.3	-18.9	3.7	12.9	9.9	20.2

To understand this behaviour, the microstructure at the joint centre of the TLP bonded specimens which use both AMDRY 790 and NB150 as interlayers was examined. The EDS compositional analysis carried out on the SEM, by taking an area compositional analysis across the joint in both of the TLP bonded specimens is shown in Table 4-6. Taking into account the relative proportions of oxide formers at low temperatures in aqueous solutions, (Al, Co, Cr and Ni) in both the AMDRY 790 and NB 150 specimens, it was observed that the relative difference in proportions for Al and Co are very marginal while those of Cr and Ni are considerably significant. This is expected given the composition of each interlayer alloy, in that AMDRY 790 contains Ni-Si-B while NB150 contains Ni-Cr-B. In Ni alloys that contain Cr, the CR increases approximately in proportion to the Cr content provided that it is more than 10 wt% [100,106]. Hence, TLP bonding carried out with an AMDRY 790 interlayer for IN 738 SX deprives the joint region of much needed Cr required to achieve low corrosion rates.

Table 4-6: EDS compositional analysis across joint section in TLP bonded IN 738 SX using different interlayers, wt%.

Filler Type	Al	Ti	Cr	Co	Ni	Mo	Ta	W
AMDRY790	2.7	1.8	8.1	3.4	78.8	0.6	3.0	1.6
NB150	2.1	2.2	18.0	4.8	67.2	1.2	2.1	2.4

4.5.5 Corrosion Behaviour of TLP Bonded IN 738 SX with NB150 Interlayer versus As-received cast Base-metal Alloy

Having established that TLP bonding which uses NB150 as the interlayer alloy has a better CR than TLP bonding with the use of AMDRY 790, a comparison of the performance of the bonded specimen with NB150 with the as-received cast base-metal alloy was done. Figure 4-22 shows the superimposed plot for both the as-received cast base-metal alloy and TLP bonded specimen with NB150 interlayer. Through a visual inspection, it can be seen that the base-metal alloy has a constant anodic current density in the potential range from 100-800 mV and the location of the curve for the bonded specimen with NB150 is to the far right in the direction of the increasing current density. A detailed inspection carried out by comparing the corrosion indicating parameters obtained from both plots as shown in Table 4-7, reveals that the specimen bonded with NB150 has a higher corrosion rate in the active region with an anodic current density of 3.7 $\mu A/cm^2$ compared to 0.8 $\mu A/cm^2$ for the as-received cast base-metal alloy, which is approximately a 4 times increase.

Consideration of the OCPs show that the as-received cast base-metal alloy has a more negative potential both at the time of immersion and after one hour of exposure time in the testing solution, thus indicating that it is more active than the bonded specimen with NB150. In terms of the effectiveness of the passive film formed, the as-received cast base-metal alloy has more stability in the passive region than the bonded specimen with NB150 while also achieving this passivity at a much lower passivation anodic current density. The critical anodic current density for the bonded specimen with NB150 is approximately 5 times higher than that of the as-received cast base-metal alloy thus indicating that it is much harder to achieve passivation in the former. This thus indicate that the TLP bonded specimen with NB150 has an inferior CR compared to that of the base metal alloy.

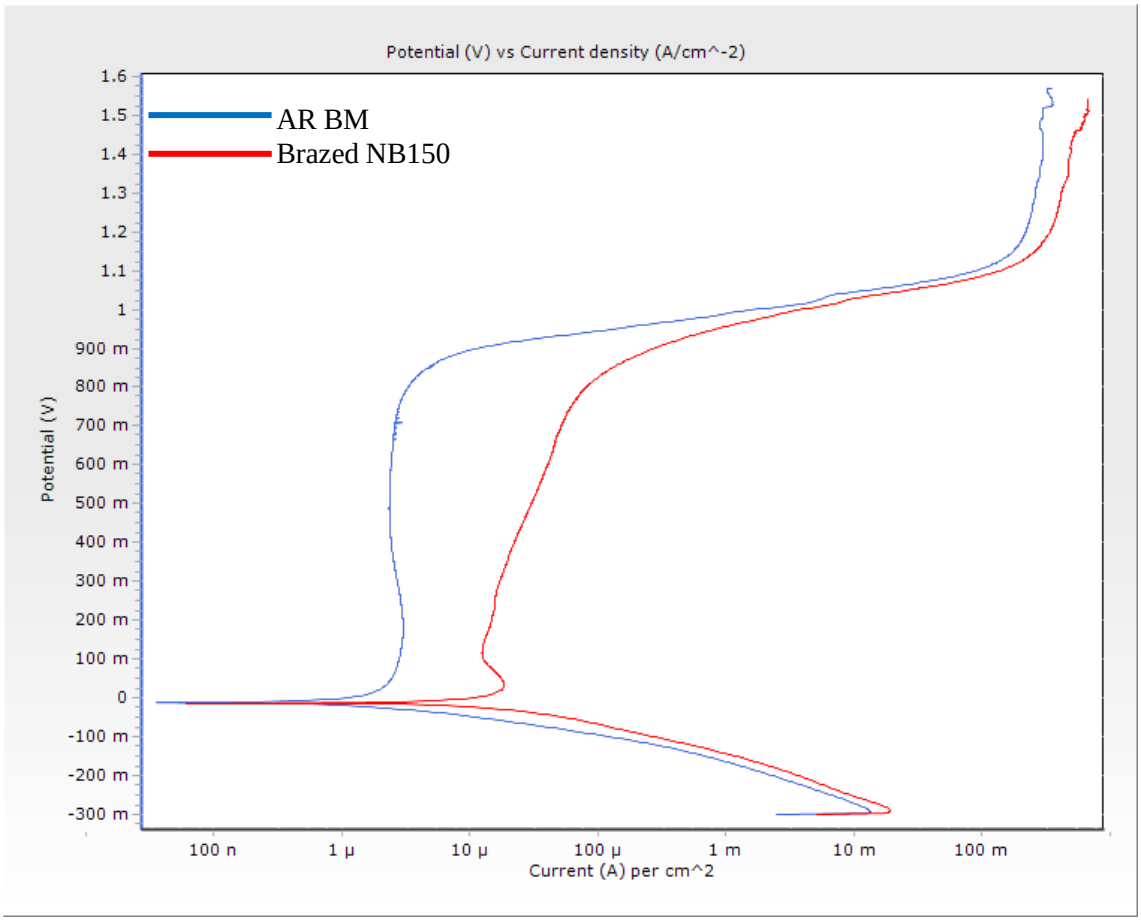

Figure 4-22: Superimposed potentiodynamic polarization plot of as received cast IN 738 SX and TLP bonded IN 738 SX using NB150 interlayer

Table 4-7: Corrosion measurement parameters for as-received cast base-metal and TLP bonded using NB150 interlayer in 0.6M HNO_3

Condition	**OCP Start (mV)**	**Rest Potential (mV)**	***E*$_{corr}$ Tafel (mV)**	***i*$_{corr}$ (µA/cm^2)**	***i*$_{crit}$ (µA/cm^2)**	***i*$_{pass}$ (µA/cm^2)**	***E*$_{pp}$ (mV)**
BM AR	-12.5	-28.5	-18.4	0.8	2.8	2.4*	99.7
NB 150	-9.1	-19.3	-18.9	3.7	12.9	9.9	20.2

* minimum passivation current density in the passive region

To further establish this, the corrosion performance of the TLP bonded IN 738 SX was tested in a reducing medium of 0.6 M H_2SO_4 and at room temperature. The superimposed plot for both the as-received cast base-metal alloy and the TLP bonded specimen with NB150 is shown in Figure 4-23, while the corrosion measuring parameters are shown in Table 4-8.

Although the critical current density is high for both the as-received cast base-metal alloy and the specimen bonded with NB150, which is characteristic of Cr and alloys that contain Cr in dilute sulfuric acids, the values of the various current densities are larger for the TLP bonded specimen with NB150. The passive current density for the TLP bonded specimen is 6 times that of the as-received base-metal alloy. For metallic materials of which the primary defence mechanism from corrosion is passivation, three key factors are of paramount importance: ease of passivation, effectiveness of passivation and stability of the passive film in the passive region. For the potentiodynamic polarization in both an oxidizing medium, HNO_3, and a reducing medium, H_2SO_4, it can be seen that the TLP bonded specimen with NB150 does not show these key features as compared to the as-received cast base-metal alloy.

Hence it can be observed that the TLP bonding of IN 738 SX causes a reduction in the CR even when the TLP bonding is done with a Cr bearing filler. However, it was shown earlier in this chapter that the microstructure at the centre of the joint is influenced by the process parameters used in the TLP bonding process, in that it controls the presence or absence of a centreline eutectic and the width of this eutectic. Hence in the next section, the effect of the size of the centreline eutectic on CR is considered.

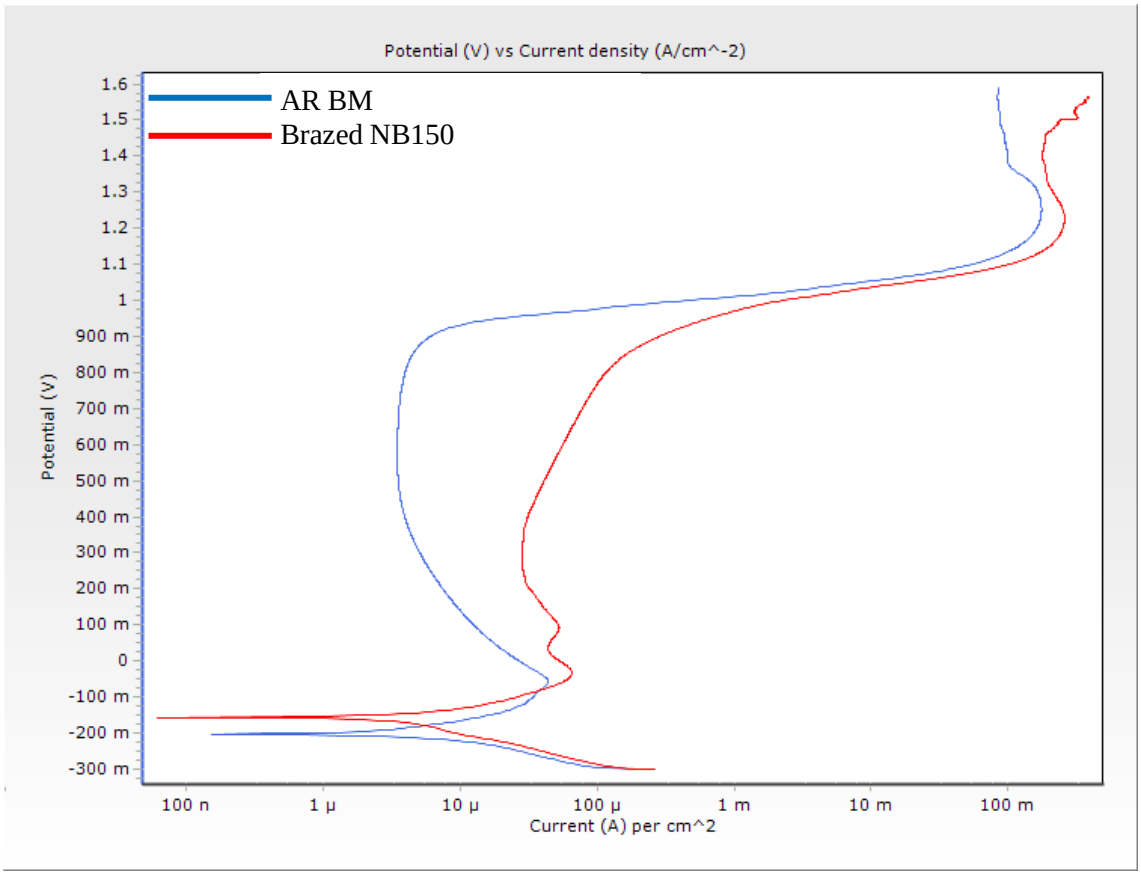

Figure 4-23: Potentiodynamic polarization plot for as-received cast base-metal and TLP bonded using NB150 interlayer in 0.6M H_2SO_4 at room temperature.

Table 4-8: Corrosion measurement parameters for potentiodynamic polarization in 0.6M H_2SO_4 at room temperature

Specimen	**OCP Start (mV)**	**Rest Potential (mV)**	E_{corr} **Tafel (mV)**	i_{corr} **(µA/cm^2)**	i_{crit} **(µA/cm^2)**	i_{pass} **(µA/cm^2)**	E_{pp} **(mV)**
BM AR	-88.6	-115.0	-202.5	2.8	41.7	3.6	-71.5
NB150	-82.5	-116.2	-156.5	6.0	46.0	21.1	-48.1

4.5.6 Influence of Centreline Eutectic Size on Corrosion Resistance

The outcome of the microstructure during TLP bonding process can be engineered through the careful design and selection of the process parameters. Therefore, for a given set of parameters as used in the experimental work for this research, the effect of the various width of the centreline eutectic obtained by conventional TLP bonding on the CR is assessed. For this purpose, the following average eutectic sizes are categorized as AEW<50 µm, 50 µm <AEW<150 µm and AEW> 150µm. Figures 4-24 and 4-25 show the potentiodynamic polarization plots of TLP bonded IN 738 SX specimens with various centreline eutectic width as measured in 0.6 M HNO_3 and 0.6 M H_2SO_4 solutions, respectively, at room temperature. Tables 4-9 and 4-10 present the respective values of the corrosion performance metrics. The general trend in both of these testing conditions indicates that as the eutectic width decreases, the corrosion performance of the TLP bonded IN 738 SX specimen approaches that of the as-received cast base-metal alloy. This is also reflected in the respective values for the current densities, as shown in Tables 4-9 and 4-10. In the conventional TLP bonded specimens with the smallest size eutectic width, the values for the corrosion, critical and passivation current densities are approximately double that of the as-received cast base-metal alloy.

In correlating the results obtained from the microstructural analysis of the TLP bonded specimens and the potentiodynamic polarization results, it can be observed that reducing the size of the centreline eutectic in TLP bonded joint produced a better corrosion performance. Previous work shows that the use of a composite interlayer can reduce the isothermal solidification completion time during TLP bonding. As such, for the same initial gap size, bonding temperature and holding time, the size of the centreline eutectic in the TLP bonded specimen with composite interlayer is much smaller than that in the conventional TLP bonded specimen. Thus the CR of the TLP bonded specimen with a composite interlayer may be superior to that with the conventional interlayer.

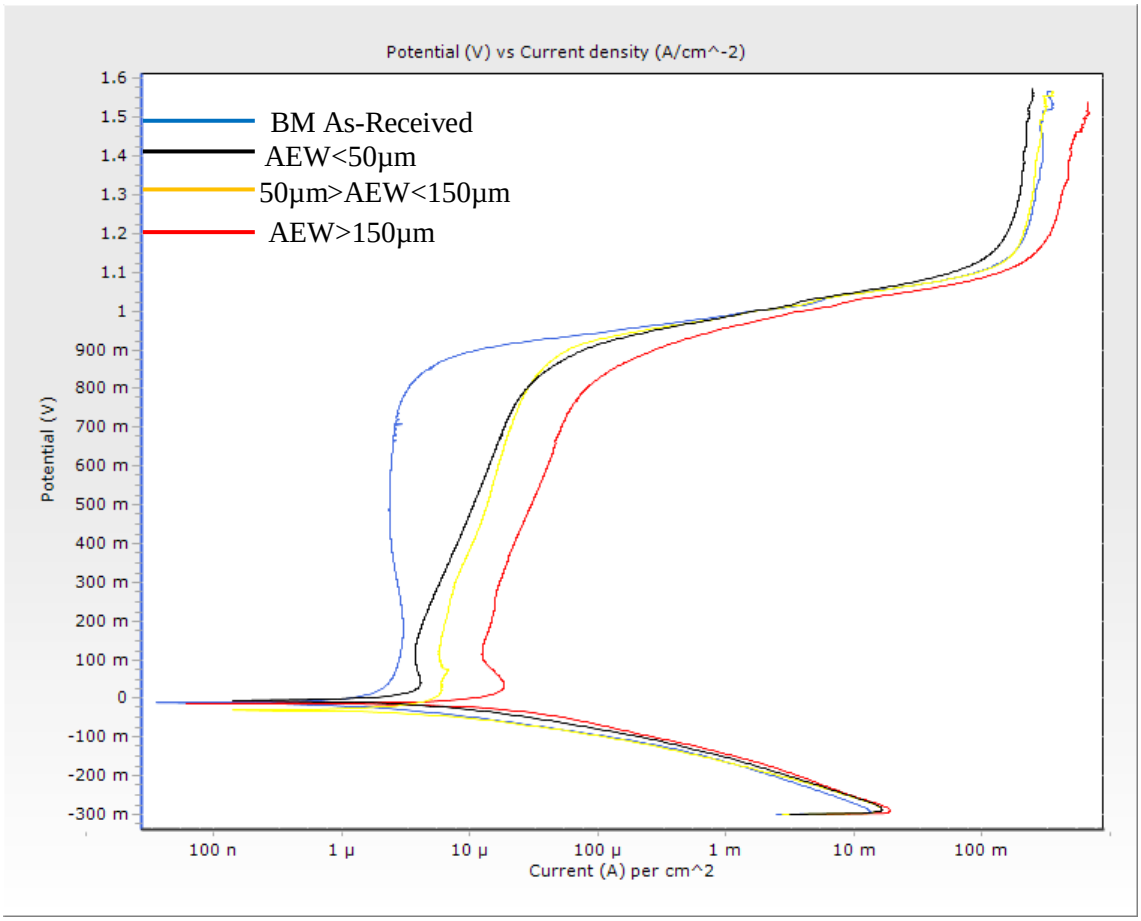

Figure 4-24: Potentiodynamic polarization of TLP bonded IN 738 SX using NB150 interlayer with variation in the width of the centreline eutectic in 0.6M HNO_3

Table 4-9: Variation of corrosion measurement parameters in 0.6M HNO_3 with average eutectic width in TLP bonded IN 738 SX with NB150 as interlayer alloy

Condition/ Average Eutectic Width	**OCP Start (mV)**	**Rest Potential (mV)**	**E_{corr} Tafel (mV)**	**i_{corr} (µA/cm^2)**	**i_{crit} (µA/cm^2)**	**i_{pass} (µA/cm^2)**	**E_{pp} (mV)**
BM AR	-12.5	-28.5	-18.4	0.8	2.8	2.4	99.7
AEW<50µm	-7.3	-13.2	1.5	1.9	4.7	4.7	26.7
50µm>AEW<150µm	2.8	-38.0	-38.3	2.7	5.6	5.9	6.4
AEW>150µm	-9.0	-19.3	-18.9	3.7	12.9	9.9	20.2

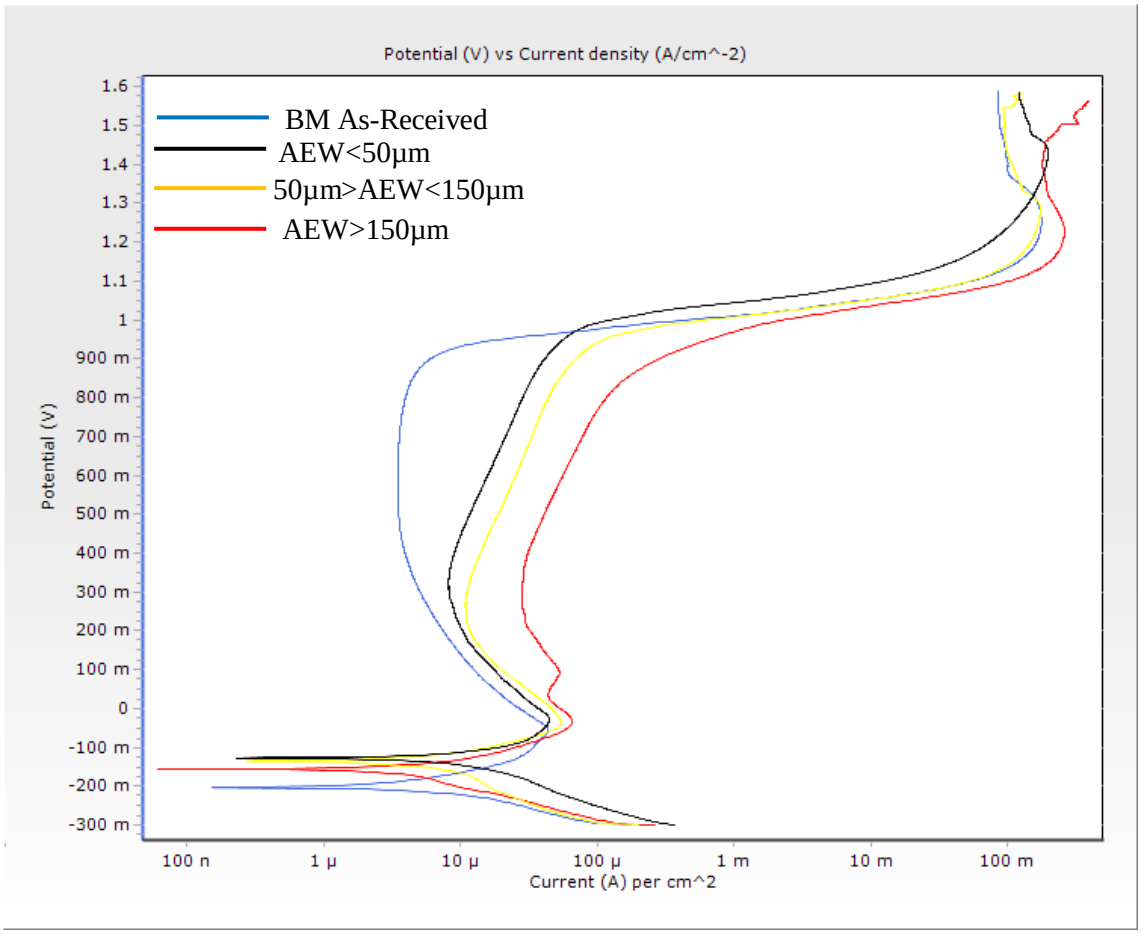

Figure 4-25: Potentiodynamic polarization of TLP bonded IN 738 SX using NB150 interlayer with variation in the width of the centreline eutectic in 0.6M H_2SO_4

Table 4-10: Variation of corrosion measurement parameters in 0.6M H_2SO_4 with average eutectic width in TLP bonded IN 738 SX with NB150 as interlayer alloy

Condition/ Average Eutectic Width	**OCP Start (mV)**	**Rest Potential (mV)**	**E_{corr} Tafel (mV)**	**i_{corr} (µA/cm^2)**	**i_{crit} (µA/cm^2)**	**i_{pass} (µA/cm^2)**	**E_{pp} (mV)**
BM AR	-88.9	-115.0	-202.5	2.8	41.7	3.61	-71.5
AEW<50µm	-58.7	-72.7	-127.4	5.1	43.2	6.8	-43.2
50µm>AEW<150µm	-73.6	-122.7	-135.7	5.5	46.4	11.7	-51.2
AEW>150µm	-82.5	-116.2	-156.5	6.0	47.2	21.1	-48.1

Figures 4-26 and 4-27 show a superimposed polarization plots for these two TLP bonding variants for holding times of 1 hr and 20 hrs respectively. As expected, the corrosion performance for the TLP bonded specimen with a composite interlayer is better than that of the conventional TLP bonded specimen. This is indicated by the position of the curve for the conventional TLP bonded specimen in the direction of increasing anodic current density as well as the respective values of the various corrosion metrics which are higher, i.e. i_{crit}, i_{corr} *and* i_{pass} as shown in Table 4-11. It can be seen that given the same process conditions during TLP bonding the use of a composite interlayer not only reduces the eutectic size but also produces a joint with a much better corrosion resistance than use of a conventional interlayer.

Although it can be argued that the composite mixture contains the base-metal alloy powder and hence enriches the joint centre [63,69,70]. The dissolution of the base-metal during TLP bonding, which enriches the joint centre, is dependent on the amount of MPD solute present in the interlayer, composition of the MPD solute in the interlayer and the bonding temperature [8,10,52]. In both types of TLP bonding the liquid insert must attain local equilibrium (i.e. equilibration of the liquid insert occurs) before isothermal solidification can begin, hence the compositions of the joint centre in both cases should be similar. The EDS compositional analysis of all of the joint centres of the different specimens in both cases shown in Table 4-12, indicates relatively marginal differences between the constituent elements. Therefore, the difference in the corrosion behaviour between the composite TLP bonded specimen and the conventional TLP bonded specimen cannot be attributed to difference in the initial composition of the interlayers but rather to the difference in the size of the eutectic which had been found to degrade corrosion resistance.

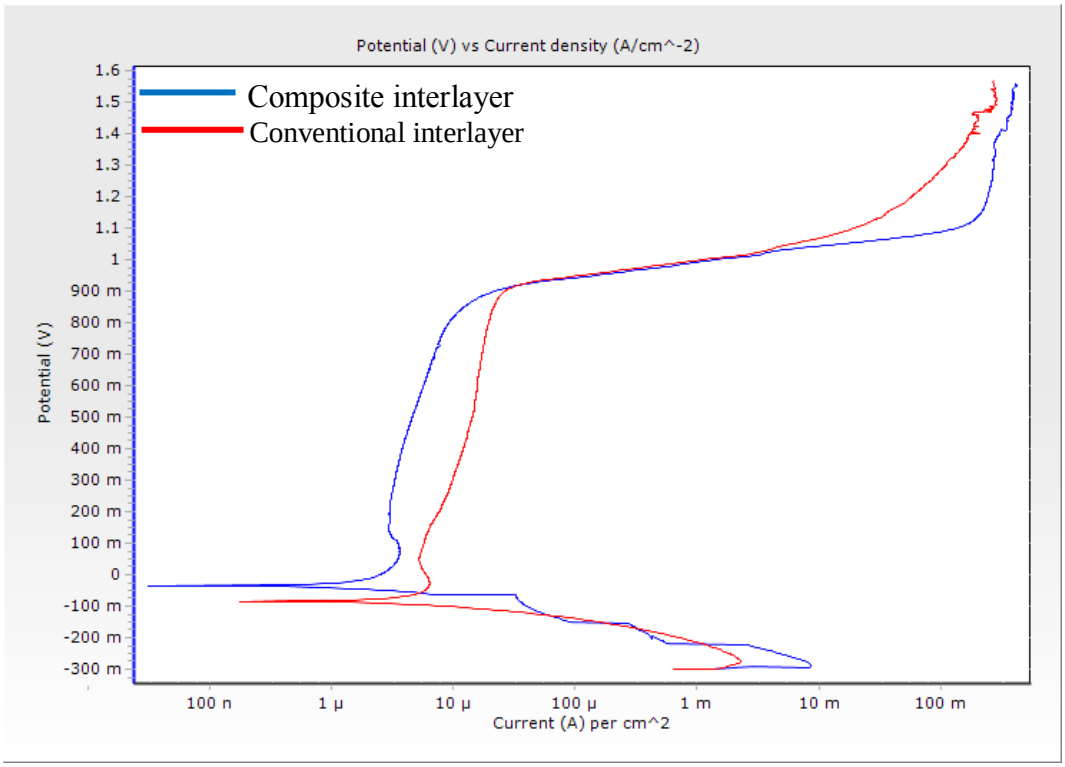

Figure 4-26: Potentiodynamic polarization in 0.6M HNO_3 at room temperature for TLP bonded specimen for the same holding time (1hr) in both conventional and composite mixture interlayer

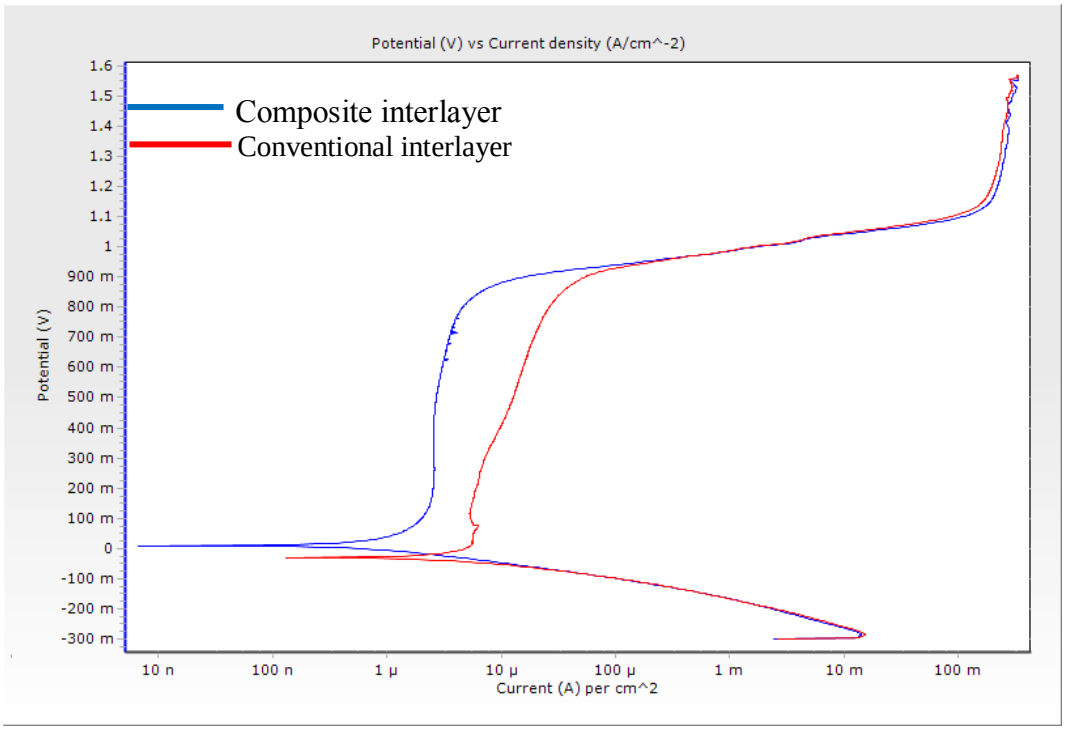

Figure 4-27: Potentiodynamic polarization in 0.6M HNO_3 at room temperature for TLP bonded specimen for the same holding time (20hrs) in both conventional and composite mixture interlayer

Table 4-11: Corrosion parameters for TLP bonded specimen of similar process conditions in 0.6M HNO_3 at room temperature

Condition	**OCP Start (mV)**	**Rest Potential (mV)**	E_{corr} **Tafel (mV)**	i_{corr} **(µA/cm²)**	i_{crit} **(µA/cm²)**	i_{pass} **(µA/cm²)**	E_{pp} **(mV)**
1Hr							
Conv.	-16.1	-31.6	-18.7	6.5	7.6	7.2	46.6
Comp.	-21.7	-43.2	-34.7	3.2	3.4	2.7	106.4
20hrs							
Conv.	-7.3	-38.0	-39.3	5.7	7.7	5.5	5.2
Comp.	2.8	-25.5	19.0	0.8	2.4	2.5	163.2

Table 4-12: EDS compositional analysis of entire joint centre in TLP bonded joints with centreline eutectic

TLP Bonding	**Element**	**Al**	**Ti**	**Cr**	**Co**	**Ni**	**Mo**	**Ta**	**W**
Conventional	Avg. Weight%	2.1	2.2	18.0	4.8	67.2	1.2	2.1	2.4
Composite	Avg. Weight%	2.3	2.5	16.4	5.4	67.9	1.2	1.8	2.5

An assessment of how much an improvement that is obtainable when the centreline eutectic in the TLP bonded specimen is eliminated by using a composite interlayer was performed in both HNO_3 and $H2SO_4$. Shown in Figures 4-28 and 4-29 are superimposed plots of: a conventional interlayer TLP bonded specimen with centreline eutectic, a composite interlayer TLP bonded specimen with no centreline eutectic and the as-received cast base-metal. Both of these plots reveal that the TLP bonded specimen with no centreline eutectic has a much better CR than the TLP bonded specimen with a centreline eutectic and this CR is comparable to that of the as-received cast base-metal. Table 4.13 shows the corrosion current densities and potentials with the no eutectic TLP bonded specimen having approximate values to the as-received cast base metal.

The similarity of the CR in the composite mixture TLP bonded specimen with no centreline eutectic to that of the as-received cast base-metal can further be assessed with the presence of a more aggressive species, such as halides. Figure 4-30 shows the potentiodynamic polarization plot of all three specimens in 0.6 M HCl, while Table 4-13 shows the respective values of the corrosion current densities and potentials. The trend of the plot for all three specimens is similar to that of most passivating metals in chloride containing environments. For all three specimens, the rate of corrosion in the active region is high, with a critical current density that reaches 200.4 µA/cm2 for the as-received cast base-metal, 199.1 µA/cm2 for the TLP bonded specimen that has no centreline eutectic and a very high value of 2473.4 µA/cm2 for the TLP bonded specimen with centreline eutectic. These values are high due to the difficulty of passivation in the presence of Cl- ions, which are known to easily break down passivation films, due to the ease with which they are absorbed on the specimen surface, and results in subsequent weakening and thinning of the passive film.

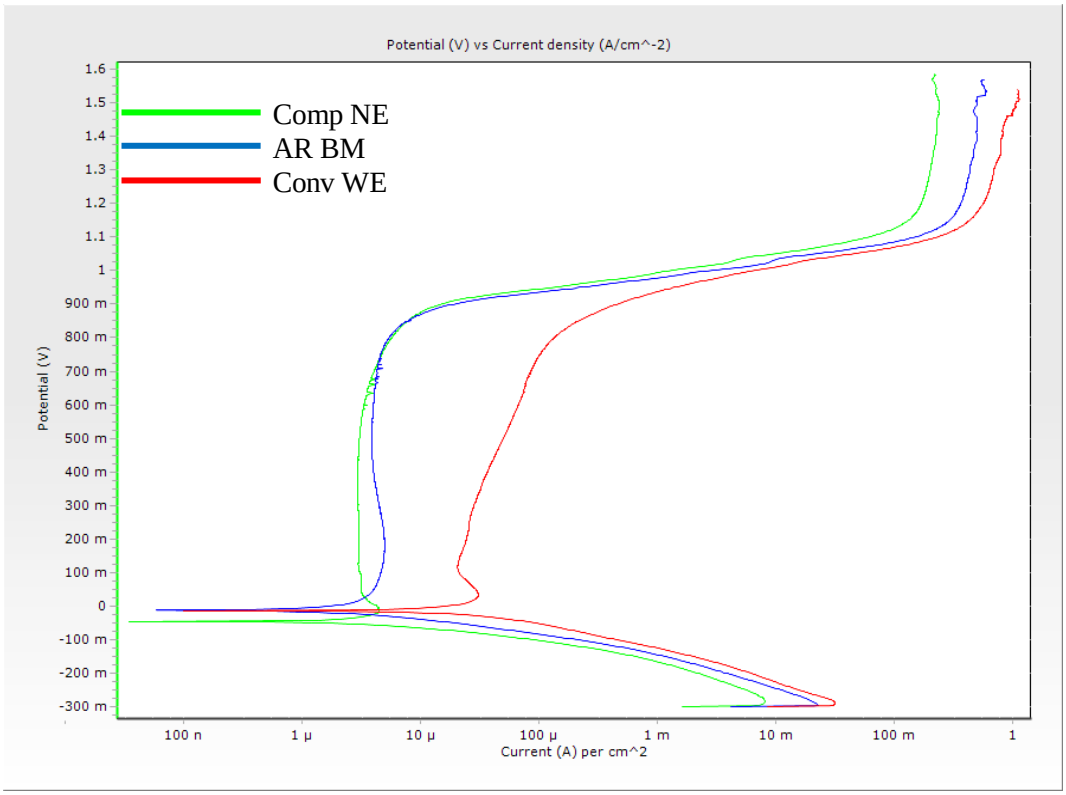

Figure 4-28: Potentiodynamic polarization of TLP bonded IN 738 SX with and without centreline eutectic in 0.6M HNO_3 at room temperature

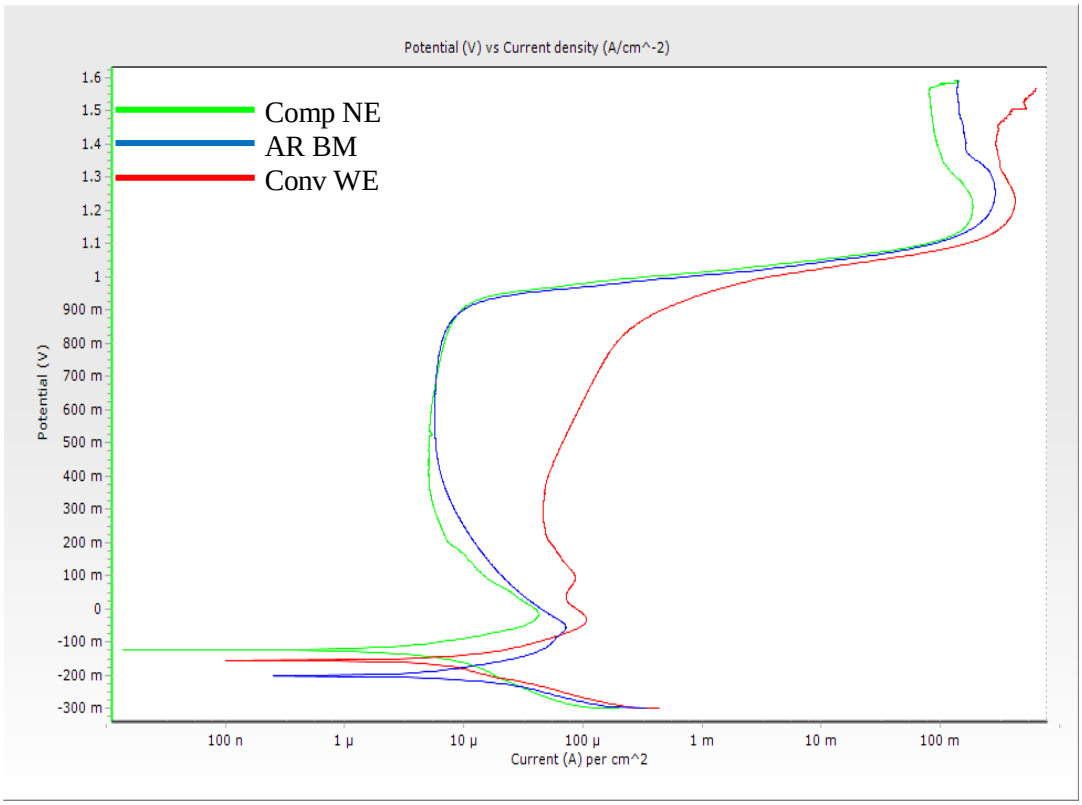

Figure 4-29: Potentiodynamic polarization of TLP bonded IN 738 SX with and without centreline eutectic in 0.6M H_2SO_4 at room temperature

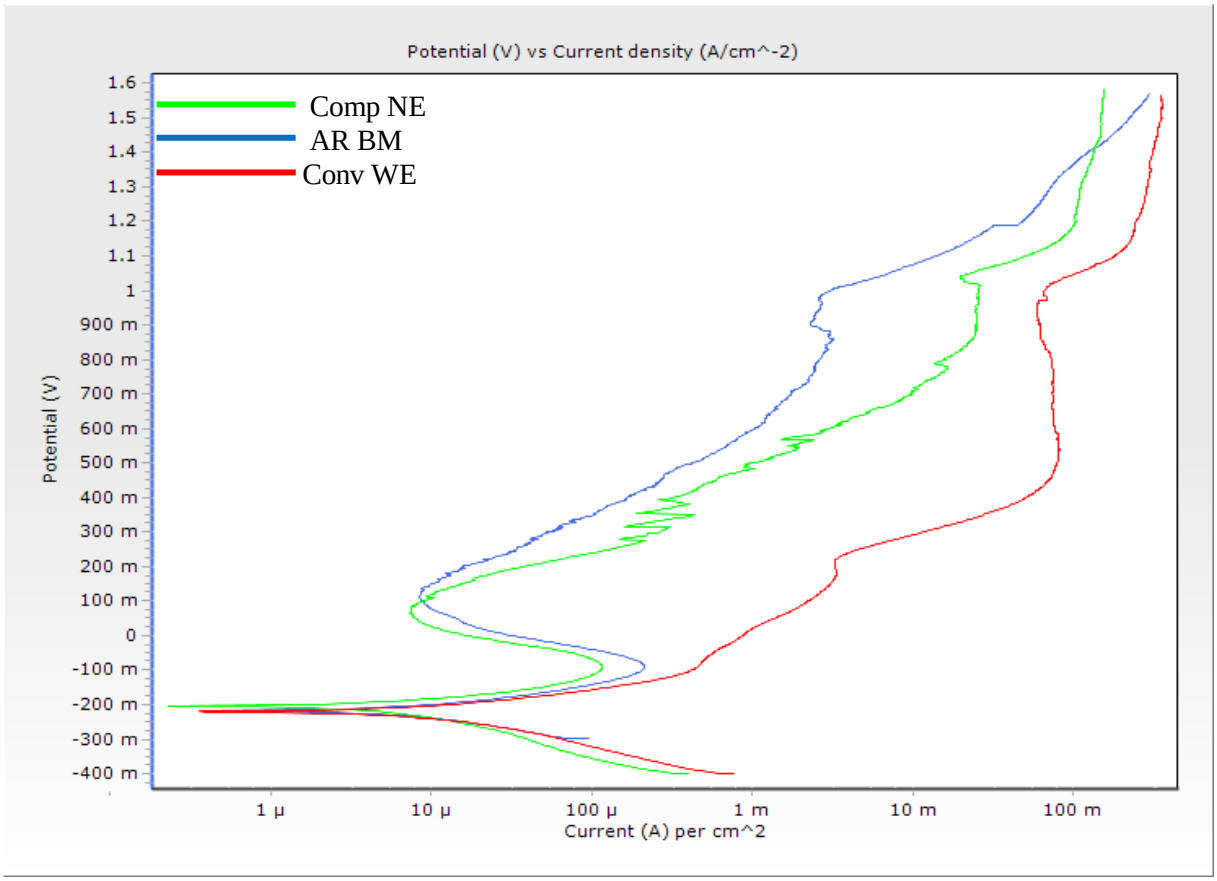

Figure 4-30: Potentiodynamic polarization of TLP bonded IN 738 SX using composite interlayer with no eutectic in 0.6M HCl at room temperature

Table 4-13: Corrosion parameters for potentiodynamic polarization of as-received case base-metal and TLP bonded specimens in 0.6M HNO_3, H_2SO_4, HCl at room temperature

0.6M HNO_3							
Condition	**OCP Start (mV)**	**Rest Potential (mV)**	**E_{corr} Tafel (mV)**	**i_{corr} (µA/cm^2)**	**i_{crit} (µA/cm^2)**	**i_{pass} (µA/cm^2)**	**E_{pp} (mV)**
AR BM	-12.5	-28.5	-18.4	0.8	2.8	2.4*	99.9
Comp NE	-16.9	-61.3	-48.2	0.8	2.7	2.3*	-23.3
Conv WE	-9.0	-19.3	-18.9	3.7	12.9	9.8	20.2
0.6M H_2SO_4							
AR BM	-88.6	-115.0	-202.5	2.8	41.2	3.6	-71.5
Comp NE	-81.5	-118.7	-124.9	2.6	39.9	3.6	-33.4
Conv WE	-82.5	-116.2	-156.5	6.0	46.0	21.1	-48.1
0.6M HCl							
AR BM	-138.0	-216.2	-217.4	6.0	200.4	9.9	-103.0
Comp NE	-127.3	-207.6	-203.5	6.0	199.1	15.7	-108.0
Conv WE	-142.3	-209.3	-220.2	7.1	2473.4	2398.7	165.1

This film eventually breaks down with increasing anodic potential [109,110]. The presence of Cl- ions results in continuous active dissolutioning as the anodic potential is increased, however, this effect is more significant in the conventional interlayer TLP bonded specimen with centreline eutectic.

EDS composition analysis of the joint centre in both of the TLP bonded specimens and the as received cast base-metal is shown in Table 4-14, it can be seen that the relative proportions of constituent elements in both TLP bonded specimens are of very marginal differences. EDS line-scan analysis for Cr across the joint section in both TLP bonded specimens and the as-received cast base-metal is shown in Figure 4-31. It is observed that in both the composite interlayer TLP bonded specimen with no centreline eutectic and the as-received cast base-metal the Cr profile is dense and uniformly distributed while the conventional interlayer TLP bonded specimen with centreline eutectic has randomly distributed high Cr peaks across the joint section. This thus accounts for the similarity in the CR of the TLP bonded specimens with a composite interlayer that have no centreline eutectic with the as-received cast base-metal.

Hence, in the severe service conditions when IN 738 SX is used, a centreline eutectic in the joint microstructure during TLP bonding poses a challenge to this normally corrosion resistant alloy by reducing its CR. It has been reported [33,107-110] that when present, the centreline eutectic is deleterious to the mechanical properties of the TLP bonded joint. The key challenge in the TLP bonding process is achieving complete isothermal solidification in the joint, which as discussed in previous section requires significant hold time at moderately high temperatures, therefore reducing the time, t_f, required to eliminate the deleterious centreline eutectic would enhance the commercial applicability of the process.

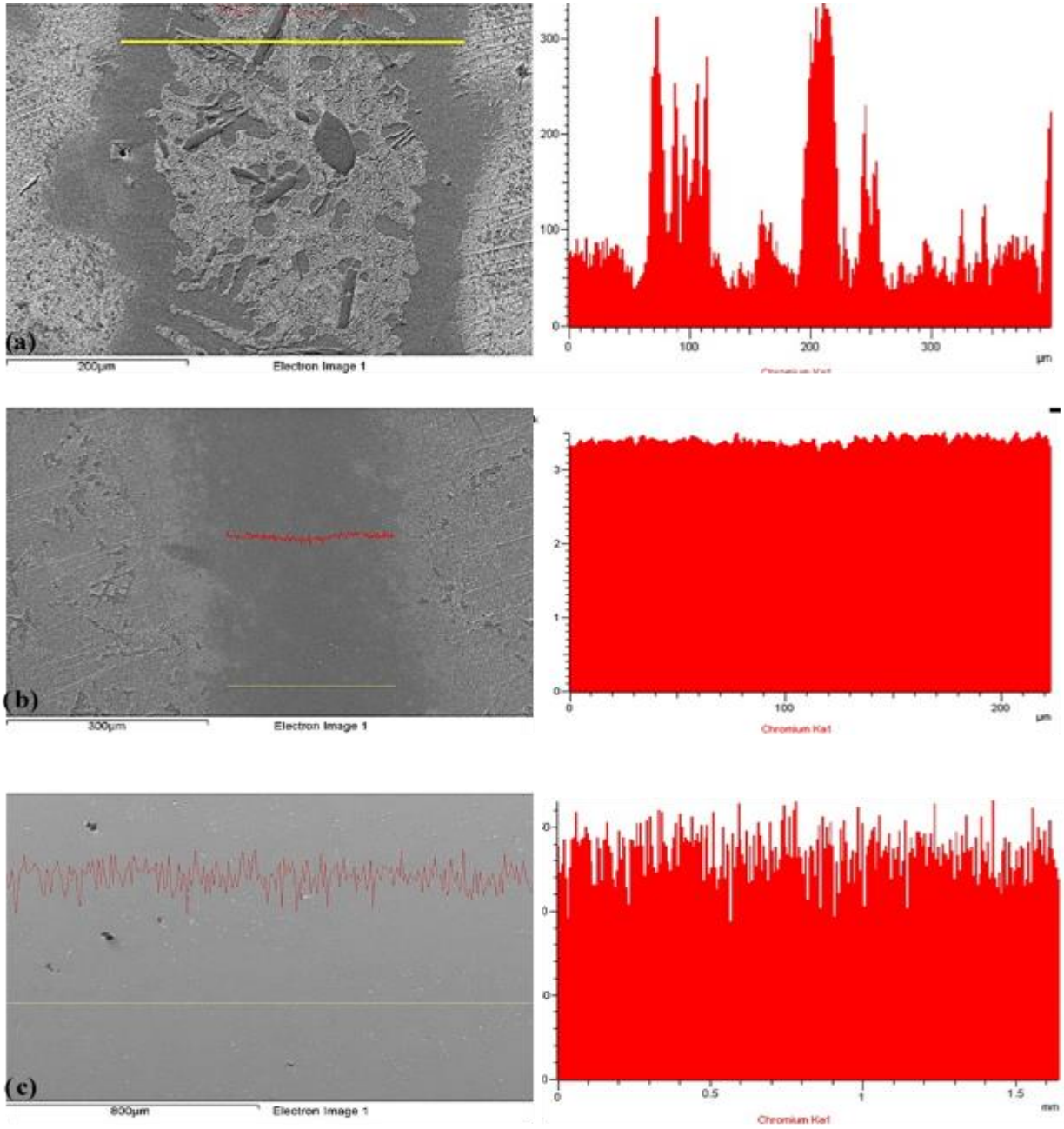

Figure 4-31: EDS linescan profile for Cr across joint centre in (a) TLP bond with eutectic (b) TLP bond with no eutectic (c) as-received base-metal

Table 4-14: EDS compositional analysis of the as-received base-metal, TLP bonded joints with no eutectic and with eutectic

Condition	Element	Al	Ti	Cr	Co	Ni	Mo	Ta	W
AR BM	Avg. Wgt%	3.4	3.5	16.7	8.8	59.8	1.8	2.2	3.8
Comp NE	Avg. Wgt%	2.7	2.2	16.3	5.3	68.3	1.0	1.5	2.6
Conv WE	Avg. Wgt%	2.1	2.2	18.0	4.8	67.2	1.2	2.1	2.4

4.5.7 Effect of Concentration and Temperature

The influence of the changes in the concentration of active ions in an oxidizing medium such as HNO_3, on the corrosion performance of IN 738SX in the bonded state was evaluated by varying the concentration from 0.1 M to 3.0 M at room temperature. Figures 4-32 to 4-35 show the different potentiodynamic polarization plots of solutions with 0.1, 0.3, 1.2 and 3.0 M solutions while Table 4-15 presents the values obtained from the plots. Both the conventional TLP bonded specimen with eutectic and TLP bonded specimen with the composite interlayer and no eutectic demonstrate that increases in the concentration up to 1.2 M have no practical effect on the corrosion potential, E_{corr}, which is within the ±50 mv range, while the primary passivation potential, E_{pp}, shifts in the noble direction. However, at a concentration of 3.0 M, passivation instantly occurs in all of the specimens with a shift in the corrosion potential, E_{corr}, towards more noble values.

The critical anodic current density increases with increasing concentration of HNO_3 for both conventional and composite TLP bonded specimens. However, the conventional TLP bonded specimen, which contained centreline eutectic, showed greater increases in the critical current density values with changes in the concentration compared to the composite TLP bonded specimen with no centreline eutectic; that is over a 100% increase between each increase in concentration. This implies that, the benefit of using the composite powder mixture to eliminate the centreline eutectic is even more pronounced as the severity of the environment increases.

Changes in temperature can influence both the thermodynamics and kinetics of a process, such as metallic corrosion in an aqueous media, either by overcoming the activation complex to favour one reaction or changing the nature of a possible reaction when certain ions (or reactions) are activated at higher temperatures. The effect of temperature increases on the corrosion resistance of TLP bonded specimens is examined with 0.6 M HNO_3 at 85˚C. The

potentiodynamic polarization plot is shown in Figure 4-36, while Table 4-16 presents the respective values of the parameters obtained from the plot. During electrochemical corrosion in an aqueous medium, an increase in temperature reduces the polarization and enhances the dissolution kinetics thereby decreasing the passive range while increasing the critical current density [111]. This phenomenon is demonstrated by all three specimens as shown in Figure 4-36. For both the as-received cast base-metal and the TLP bonded specimen with a composite interlayer the current density exceeds the critical current density at E_{corr} and thus passivation occurs, and results in a short passive potential range. A direct comparison of the two TLP bonding conditions is shown in Figure 4-37. The conventional TLP bonded specimen shows a marked increase in the corrosion rate with a shift of the polarization curve further in the direction of increasing anodic current density when the temperature is increased from 25˚C to 85˚C compared to that of the TLP bonded specimen with a composite layer that has no eutectic. A comparison of the values of the actual corrosion current density, $i_{corr,}$ show that with increase in temperature from 25˚C to 85˚C, i_{corr} in both the as-received cast base-metal and the TLP bonded specimen with a composite layer which has no eutectic increases by an approximate factor of 2, while i_{corr} in the conventional TLP bonded specimen increases by an approximate factor of 64. This again shows that use of a composite powder interlayer is beneficial to the TLP joint than use of a conventional interlayer and this benefit becomes more significant at higher temperatures.

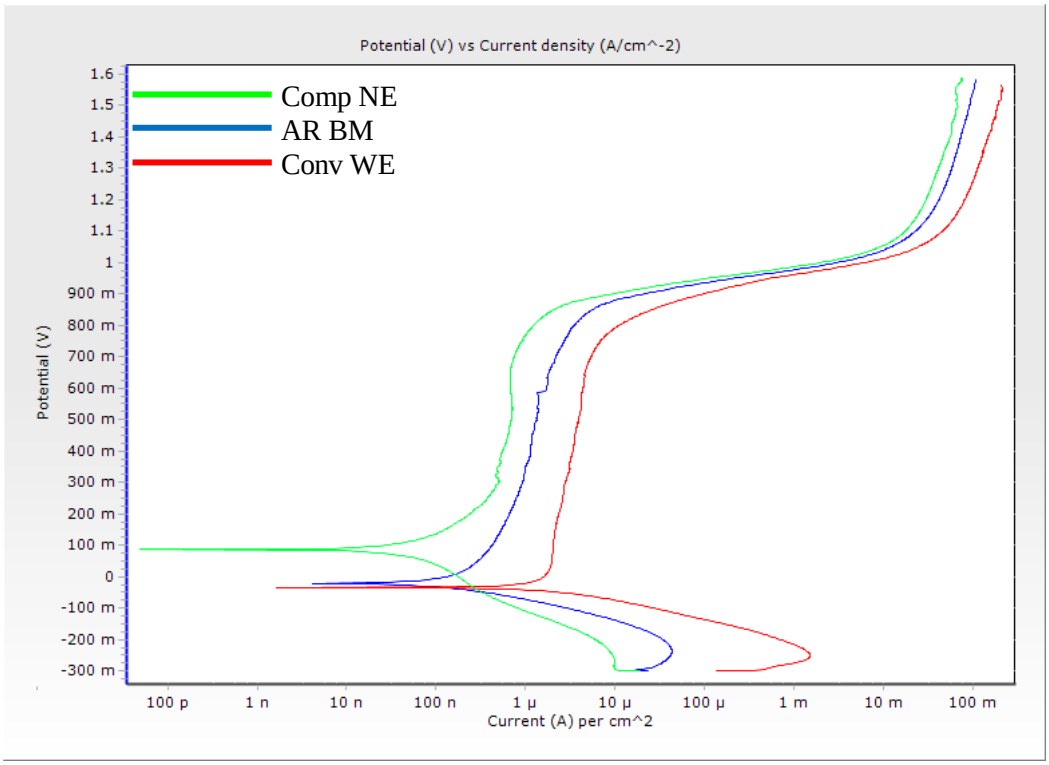

Figure 4-32: Potentiodynamic polarization of TLP bonded IN 738 SX using composite interlayer eutectic in 0.1M HNO_3 at room temperature

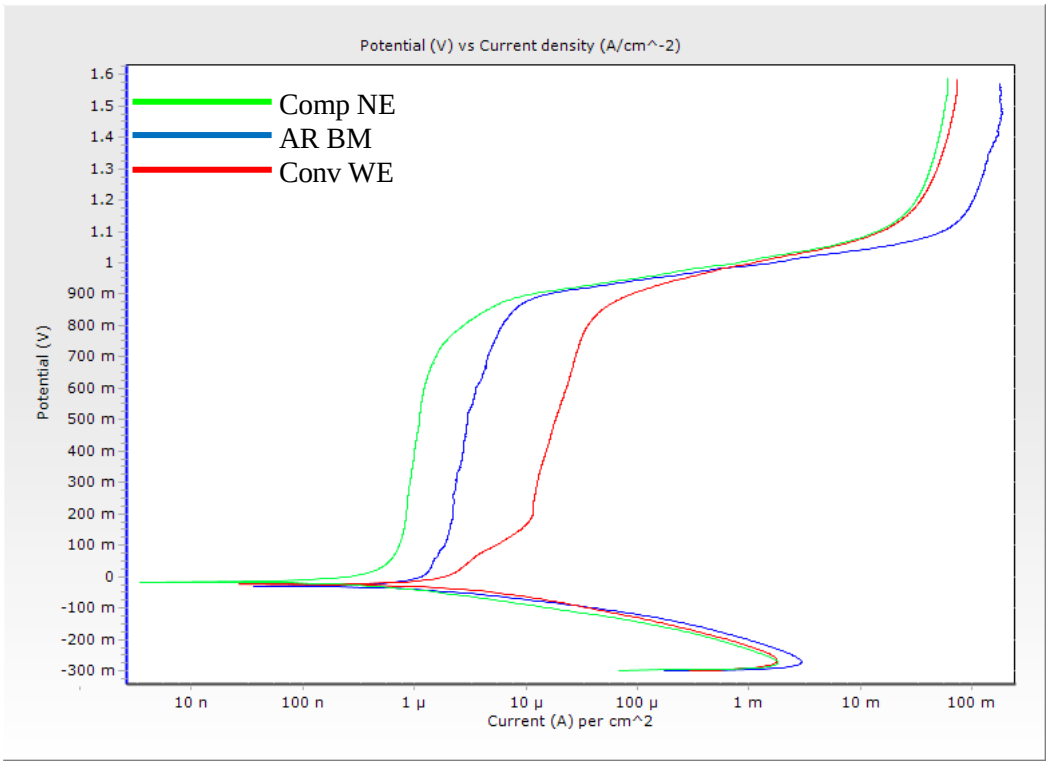

Figure 4-33: Potentiodynamic polarization of TLP bonded IN 738 SX using composite interlayer eutectic in 0.3M HNO_3 at room temperature

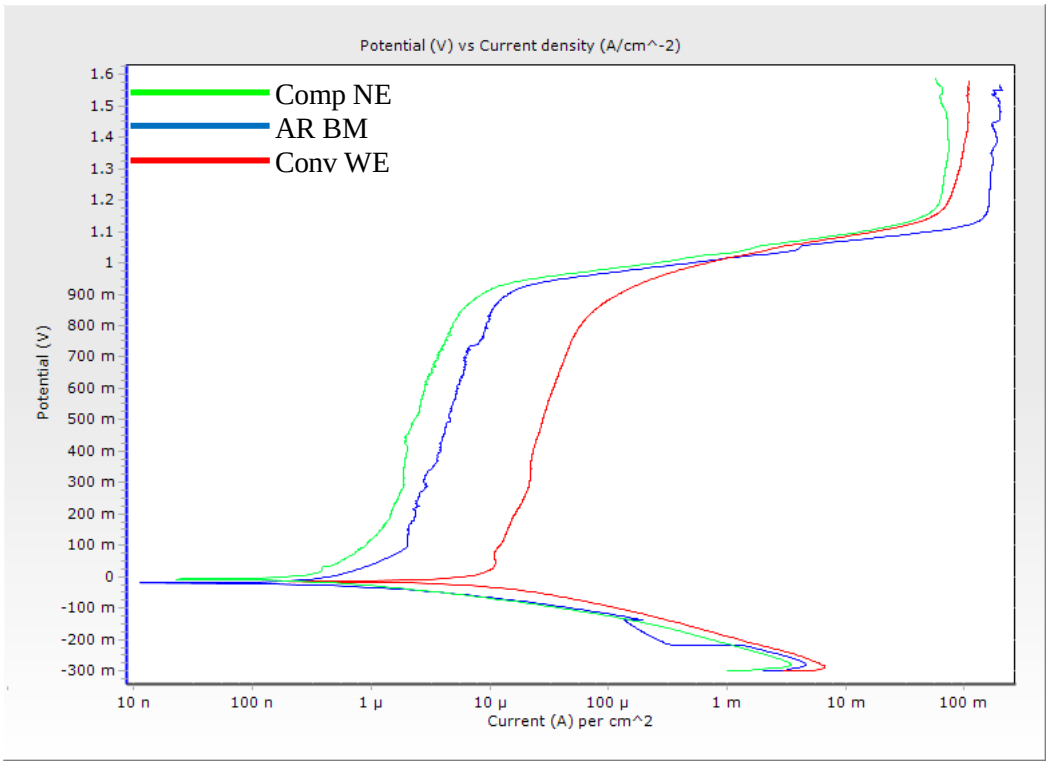

Figure 4-34: Potentiodynamic polarization of TLP bonded IN 738 SX using composite interlayer eutectic in 1.2M HNO_3 at room temperature

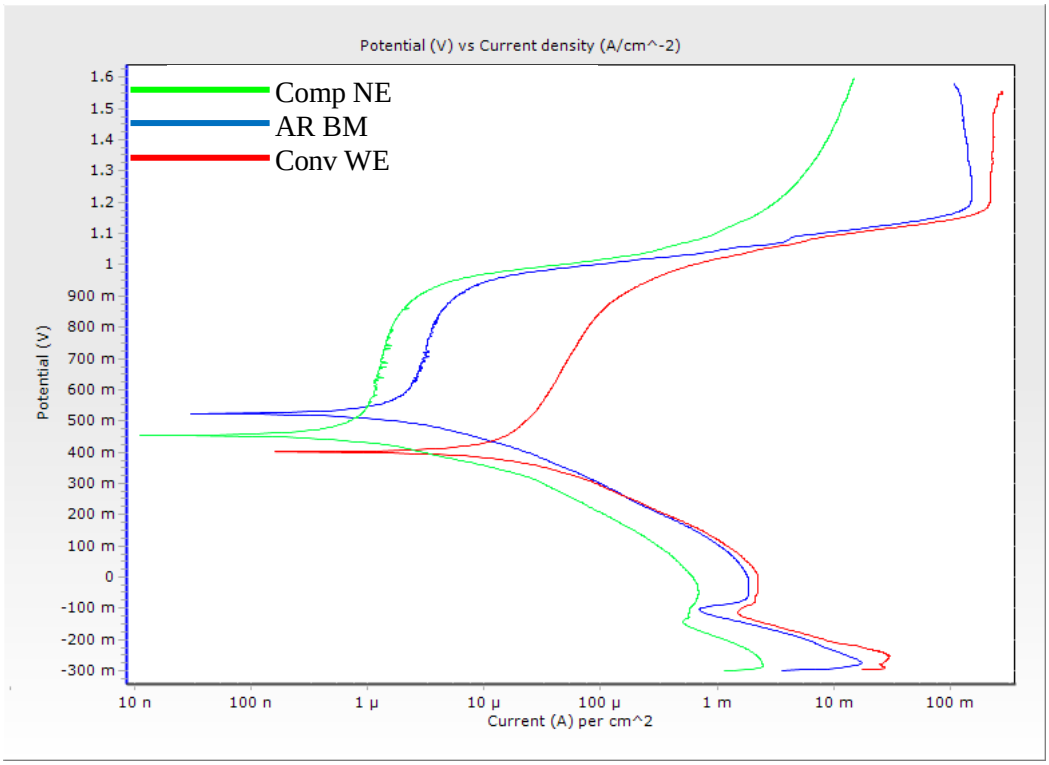

Figure 4-35: Potentiodynamic polarization of TLP bonded IN 738 SX using composite interlayer eutectic in 3M HNO_3 at room temperature

Table 4-15: Variation of corrosion resistance with increase in concentration at 25ºC in HNO_3

Condition	OCP Start (mV)	Rest Potential (mV)	E_{corr} Tafel (mV)	i_{corr} (µA/cm^2)	i_{crit} (µA/cm^2)	i_{pass} (µA/cm^2)	E_{pp} (mV)
0.1M HNO_3							
AR BM	-8.0	138.9	-22.0	0.2	1.2	-	46.5
Conv WE	-9.3	-42.6	-41.4	1.1	2.3	2.6	12.9
Comp NE	17.9	175.4	86.1	0.2	1.6	1.6	274.5
0.3M HNO_3							
AR BM	-4.6	-38.0	-36.5	0.5	1.5	1.2-8.1	0.3
Conv WE	15.1	-10.1	-32.8	3.9	6.3	-	3.4
Comp NE	-3.8	-31.9	-28.8	0.7	1.7	2.3-9.3	28.5
0.6M HNO_3							
AR BM	-12.5	-28.2	-18.4	0.8	2.8	2.4*	99.9
Conv WE	-9.0	-19.3	-18.9	3.7	12.9	9.9	20.2
Comp NE	-16.9	-61.3	-48.2	0.8	2.7	2.3*	-23.3
1.2M HNO_3							
AR BM	-12.0	-75.8	-19.5	1.4	2.9	1.9*	89.9
Conv WE	4.5	-22.4	-26.4	12.9	33.4	32.7	24.8
Comp NE	3.8	-50.6	-7.3	1.4	3.1	6.0-27.1	93.2
3.0M HNO_3							
AR BM	-44.1	20.5	523.7	1.9	3.8	-	589.5
Conv WE	14.8	28.5	401.6	16.0	31.4	-	507.9
Comp NE	19.8	15.9	454.2	1.6	3.2	3.2-8.3	530.9

*minimum passivation current density in the passive range

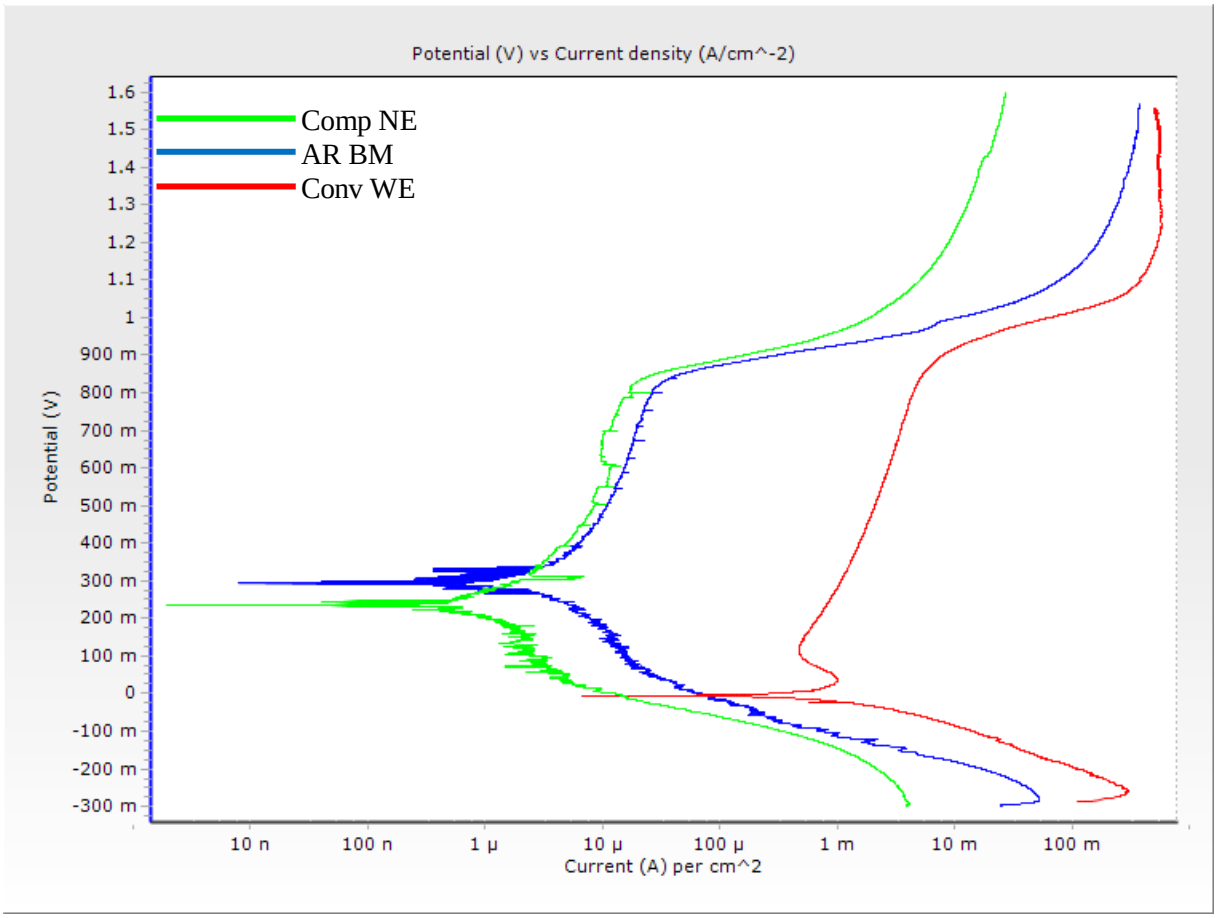

Figure 4-36: Potentiodynamic polarization of in 0.6M HNO_3 at 85˚C

Table 4-16: Corrosion parameters for potentiodynamic polarization in HNO3 at 85˚C

Condition	**OCP Start (mV)**	**Rest Potential (mV)**	E_{corr} **Tafel (mV)**	i_{corr} **(µA/cm²)**	i_{crit} **(µA/cm²)**	i_{pass} **(µA/cm²)**	E_{pp} **(mV)**
BM AR	-16.2	53.4	294.2	1.5	-	-	-
Comp NE	-20.9	25.1	236.5	1.3	-	-	-
Conv WE	-16.8	4.0	-11.3	233.5	699.0	381.9	30.0

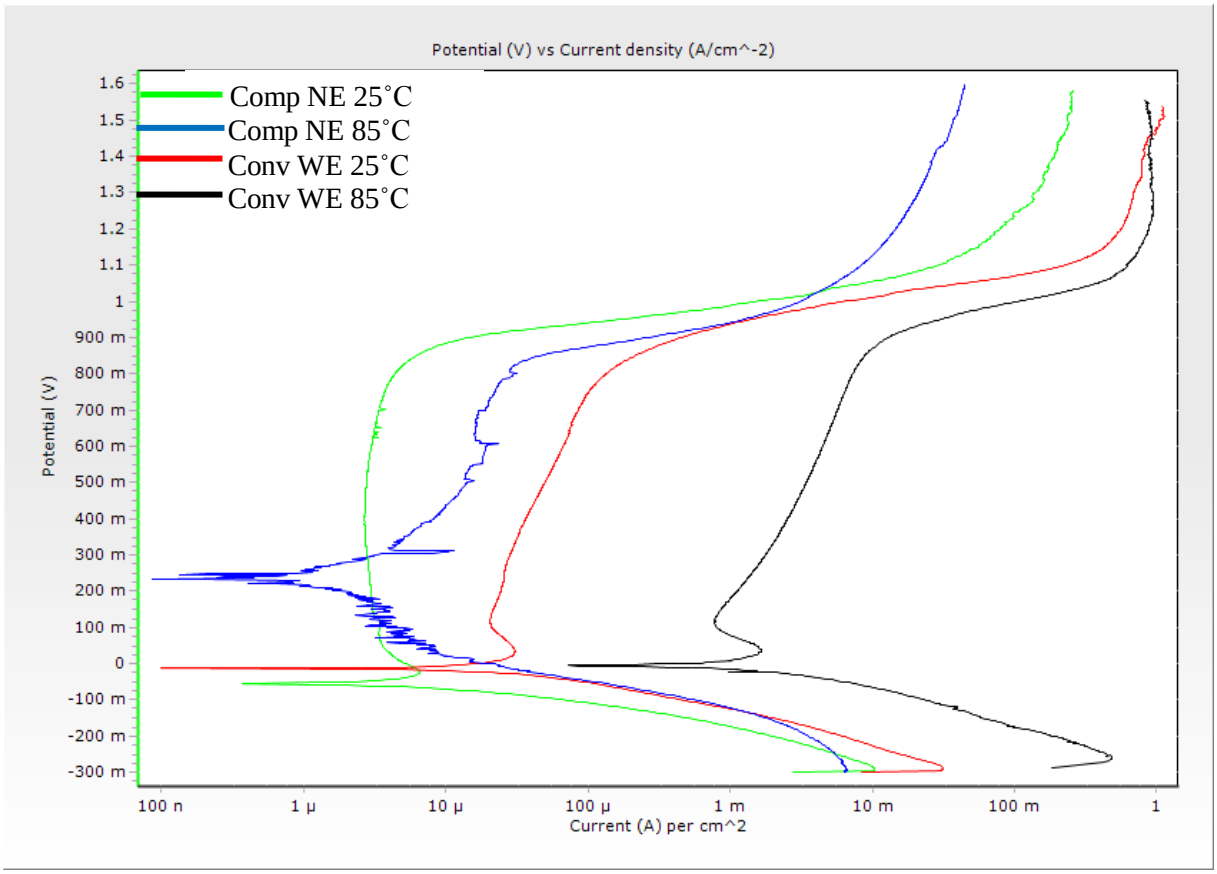

Figure 4-37: Effect of increase in temperature from 25˚C to 85˚C in 0.6M HNO_3

CHAPTER 5. Conclusions & Suggestions for Future Work

The influence of TLP bonding on the corrosion resistance examined through the electrochemical potentiodynamic polarization of IN 738 SX has been investigated. The investigation was actualized by varying the process parameters during the TLP bonding process, such as the type of interlayer alloy, (by using commercially available interlayer alloys AMDRY 790, NB150 and a composite powder mixture), initial gap size, diffusion time and bonding temperature. These parameters are known to greatly influence the nature of the final microstructure of the joint. The key results and conclusions for both the TLP bonding of IN 738 SX and the evaluation of the corrosion resistance examined by using potentiodynamic polarization are presented below.

5.1 TLP Bonding of IN 738 SX

1. The formation of deleterious centreline eutectic through the non-equilibrium transformation of the residual liquid occurs during the TLP bonding of IN 738 SX due to incomplete isothermal solidification of the liquated interlayer alloy in the joint centre.
2. The width of the deleterious eutectic microconstituents under non equilibrium solidification increases with increases in the initial gap size and decreases as the holding/diffusion time is increased.
3. A dual response to increase in bonding temperature by the width of the deleterious eutectic microconstituents occurs. Initially, as the bonding temperature increases the eutectic width reduces and afterwards the eutectic width increases with increase in temperature.
4. The use of a composite mixture that incorporates an interlayer alloy and base-metal powder with a ratio of 7:3 in lieu of a single interlayer alloy as commonly found in

conventional TLP bonding can be used to reduce the width of the deleterious centreline eutectic microconstituents and consequently the isothermal solidification completion time, t_f.

5.2 Corrosion Resistance of TLP Bonded IN 738 SX

1. The degree of reduction in the corrosion resistance is greatly influenced by the type of interlayer alloy used in the conventional TLP bonding process. A chromium bearing interlayer, such as NB150, has a better corrosion performance than the interlayer alloy free of chromium. Therefore, chromium is essential in the interlayer alloy to enhance the corrosion resistance of the joint
2. The presence of a deleterious centreline eutectic in the joint centre produced as a result of incomplete isothermal solidification of the liquated interlayer alloy during conventional TLP bonding reduces the corrosion resistance of IN 738 SX in the bonded state.
3. The corrosion resistance of conventional TLP bonds increases as the width of the centreline eutectic is reduced.
4. TLP bonds produced by the use of a composite interlayer to eliminate the centreline eutectic at shorter isothermal solidification completion time produced corrosion resistance comparable to the as-received cast base alloy.
5. In contrast to what has been generally reported, aside from the mere presence of Cr, the enhanced corrosion resistance obtained with complete isothermal solidification is attributable to uniform Cr distribution within the TLP joint region.
6. The benefit of using a composite powder mixture to produce TLP joints devoid of the deleterious centreline eutectic is more pronounced in aggressive environments with high concentrations of corrosive species and high temperatures.

5.3 Suggestions for Future Work

1. The influence of post bond heat treatment, normally used for the formation of secondary strengthening phases within the TLP joint, on corrosion performance needs to be systematically studied.
2. The effect of using a composite interlayer on the mechanical properties of TLP bonded SX IN 738 should be investigated.
3. The benefit of the composite interlayer on corrosion and mechanical properties of TLP bonds of other superalloys should be studied.

CHAPTER 6. References

[1] M. Durand-Charre, The Microstructure of Superalloys, CRC press, 1998.

[2] R.C. Reed, The Superalloys: Fundamentals and Applications, Cambridge university press, 2006.

[3] T.M. Pollock, S. Tin, Nickel-based superalloys for advanced turbine engines: chemistry, microstructure and properties, J. Propul. Power. 22 (2006) 361-374.

[4] H. Penkalla, J. Wosik, A. Czyrska-Filemonowicz, Quantitative microstructural characterisation of Ni-base superalloys, Mater. Chem. Phys. 81 (2003) 417-423.

[5] D. Duvall, W. Owczarski, Further heat-affected-zone studies in heat- resistant nickel alloys (Hot-cracking and microstructure characteristics in weld heat resistant Ni alloys evaluated by synthetic specimen technique), WELDING JOURNAL, RESEARCH SUPPLEMENT. 46 (1967).

[6] D. DUVALL, TLP^* Bonding: a New Method for Joining Heat Resistant Alloys, Welding Journal. (1974).

[7] M. Kuntz, B. Panton, S. Wasiur-Rahman, Y. Zhou, S. Corbin, An Experimental Study of Transient Liquid Phase Bonding of the Ternary Ag-Au-Cu System Using Differential Scanning Calorimetry, Metallurgical and Materials Transactions A. 44 (2013) 3708-3720.

[8] G.O. Cook III, C.D. Sorensen, Overview of transient liquid phase and partial transient liquid phase bonding, J. Mater. Sci. 46 (2011) 5305-5323.

[9] R. Aluru, W. Gale, S. Chitti, N. Sofyan, R. Love, J. Fergus, Transient liquid phase bonding of dissimilar nickel base superalloys—wettability, microstructure and mechanical properties, Materials Science and Technology. 24 (2008) 517-528.

[10] W. Gale, D. Butts, Transient liquid phase bonding, Science and Technology of Welding & Joining. 9 (2004) 283-300.

[11] W. Gale, E. Wallach, Microstructural development in transient liquid-phase bonding, Metallurgical Transactions A. 22 (1991) 2451-2457.

[12] E. Storchai, Examination of the corrosion resistance of brazed joints, Welding International. 1 (1987) 345-346.

[13] D.A. Jones, Principles and Prevention of Corrosion: Pearson New International Edition, Pearson Education, Limited, 2013.

[14] M.G. Fontana, Corrosion Principles, Corrosion Engineering., Third ed., McGraw-Hill, New York, 1886, pp. 16-17.

[15] R. Javaherdashti, C. Nwaoha, H. Tan, Corrosion and Materials in the Oil and Gas Industries, CRC PressI Llc, 2013.

[16] M.J. Donachie, S.J. Donachie, Superalloys: A Technical Guide, ASM international, 2002.

[17] C.T. Sims, N.S. Stoloff, W.C. Hagel, superalloys II, (1987).

[18] A. Jena, M. Chaturvedi, The role of alloying elements in the design of nickel-base superalloys, J. Mater. Sci. 19 (1984) 3121-3139.

[19] R.F. Decker, Strengthening Mechanisms in Nickel-Base superalloys, (May 1969) 5-6.

[20] I. Alloy, 738: Technical Data, INCO, New York, NY. 1-11.

[21] J. Larson, Carbide morphology in p/m IN-792, Metallurgical Transactions A. 7 (1976) 1497-1502.

[22] H. Zhang, O. Ojo, M. Chaturvedi, Nanosize boride particles in heat-treated nickel base superalloys, Scr. Mater. 58 (2008) 167-170.

[23] R. Reed, M. Jackson, Y. Na, Characterization and Modeling of the Precipitation of the Sigma Phase in UDIMET 720 and UDIMET 720LI, Metallurgical and Materials Transactions A. 30 (1999) 521-533.

[24] G. Erickson, Superalloy developments for aero and industrial gas turbines, Advanced materials and coatings for combustion turbines. (1994) 29-41.

[25] D.G. Brandon, W.D. Kaplan, Joining processes: an introduction, Joining Processes: An Introduction, by David G.Brandon, Wayne D.Kaplan, pp.378.ISBN 0-471-96488-3.Wiley-VCH, May 1997. 1 (1997).

[26] M.G. Nicholas, Joining Processes: Introduction to Brazing and Diffusion Bonding, Dordrecht; Boston: Kluwer Academic Publishers, 1998.

[27] S. Kou, Welding Metallurgy, Cambridge Univ Press, 1987.

[28] J.A. Schey, Introduction to Manufacturing Processes, McGraw-Hill New York etc., 1987.

[29] M. Haafkens, J. Matthey, A new approach to the weldability of nickel-base As-cast and power metallurgy superalloys, Weld.J.(Miami);(United States). 61 (1982).

[30] O. Ojo, N. Richards, M. Chaturvedi, Contribution of constitutional liquation of gamma prime precipitate to weld HAZ cracking of cast Inconel 738 superalloy, Scr. Mater. 50 (2004) 641-646.

[31] M.M. Schwartz, Brazing, ASM international, 2003.

[32] M.P. Groover, Fundamentals of Modern Manufacturing: Materials Processes, and Systems, John Wiley & Sons, 2007.

[33] O.A. Ojo, The Effects of Brazing Parameters on Microstructure and Properties of Diffusion Brazed Joint of IN-738 Superalloy, (2002).

[34] D.M. Jacobson, G. Humpston, Principles of Brazing, (2005).

[35] D.D. Scott, O.W. A, P.D. F, Diffusion bonding utilizing transient liquid phase, (1972).

[36] W. MacDonald, T. Eagar, Transient liquid phase bonding, Annual review of materials science. 22 (1992) 23-46.

[37] Y. Zhou, W. Gale, T. North, Modelling of transient liquid phase bonding, International Materials Reviews. 40 (1995) 181-196.

[38] T. Illingworth, I. Golosnoy, T. Clyne, Modelling of transient liquid phase bonding in binary systems—A new parametric study, Materials Science and Engineering: A. 445 (2007) 493-500.

[39] Y. NAKAO, K. Nishimoto, K. Shinozaki, C. Kang, Theoretical research on transient liquid insert metal diffusion bonding of nickel base alloys, Transactions of the Japan Welding Society. 20 (1989) 60-65.

[40] C. Sinclair, G. Purdy, J. Morral, Transient liquid-phase bonding in two-phase ternary systems, Metallurgical and Materials Transactions A. 31 (2000) 1187-1192.

[41] I. Tuah-Poku, M. Dollar, T. Massalski, A study of the transient liquid phase bonding process applied to a Ag/Cu/Ag sandwich joint, Metallurgical Transactions A. 19 (1988) 675-686.

[42] Y. Nakao, K. Nishimoto, K. Shinozaki, C. Kang, Transient Insert Metal Diffusion Bonding of Ni-Base Cast Superalloy MM007, International Institute for Welding, Abingdon, United Kingdom, Document No. IA-334-86-OE. (1986).

[43] T. Illingworth, I. Golosnoy, V. Gergely, T. Clyne, Numerical modelling of transient liquid phase bonding and other diffusion controlled phase changes, J. Mater. Sci. 40 (2005) 2505-2511.

[44] K. Ohsasa, T. Narita, T. Shinmura, Numerical modeling of the transient liquid phase bonding process of Ni using Ni-B-Cr ternary filler metal, Journal of phase equilibria. 20 (1999) 199-206.

[45] Y. Natsume, K. Ohsasa, T. Narita, Phase-field simulation of transient liquid phase bonding process of Ni using Ni-P binary filler metal, Materials Transactions. 44 (2003) 819-823.

[46] C. Campbell, W. Boettinger, Transient liquid-phase bonding in the Ni-Al-B system, Metallurgical and Materials Transactions A. 31 (2000) 2835-2847.

[47] J. Niemann, R. Garrett, Transient Liquid Phase Bonding, Welding J. 53 (1974) 175-184.

[48] K. Saida, Y. Zhou, T. North, The influence of base metal grain size on isothermal solidification during transient liquid-phase brazing of nickel, J. Mater. Sci. 28 (1993) 6427-6432.

[49] P. Kotval, J. Venables, R. Calder, The role of hafnium in modifying the microstructure of cast nickel-base superalloys, Metallurgical transactions. 3 (1972) 457-462.

[50] J. Ambrose, M. Nicholas, A. Stoneham, Dynamics of braze spreading, Acta metallurgica et materialia. 40 (1992) 2483-2488.

[51] D. Manente, Brazing of Heat-Resistant Alloys, Low-Alloy Steels, and Tool Steels, ASM International, ASM Handbook. 6 (1993) 924-930.

[52] N. Bosco, F. Zok, Critical interlayer thickness for transient liquid phase bonding in the Cu–Sn system, Acta Materialia. 52 (2004) 2965-2972.

[53] O. Ojo, N. Richards, M. Charturvedi, Effect of gap size and process parameters on diffusion brazing of Inconel 738, Science and Technology of Welding & Joining. 9 (2004) 209-220.

[54] A. Sakamoto, Optimizing Processing Variables in High-Temperaure Brazing with Nickel-Based Filler Metals, Weld.J. 69 (1989) 63-71.

[55] O. Ojo, N. Richards, M. Chaturvedi, Isothermal solidification during transient liquid phase bonding of Inconel 738 superalloy, Science and Technology of Welding & Joining. 9 (2004) 532-540.

[56] K. Nishimoto, K. Saida, D. Kim, t.l.Y. Nakao, Transient liquid phase bonding of Ni-base single crystal superalloy, CMSX-2, ISIJ Int. 35 (1995) 1298-1306.

[57] X. Zhang, Y. Shi, A dissolution model of base metal in liquid brazing filler metal during high temperature brazing, Scr. Mater. 50 (2004) 1003-1006.

[58] E.P. DeGarmo, J.T. Black, R.A. Kohser, DeGarmo's Materials and Processes in Manufacturing, John Wiley & Sons, 2011.

[59] B. Rhee, S. Roh, D. Kim, Transient Liquid Phase Bonding of Nitrogen Containing Duplex Stainless Steel UNS S31803 Using Ni-Cr-Fe-Si-B Insert Metal, Materials Transactions. 44 (2003) 1014-1023.

[60] R. Shiue, S. Wu, C. Hung, Infrared repair brazing of 403 stainless steel with a nickel-based braze alloy, Metallurgical and Materials Transactions A. 33 (2002) 1765-1773.

[61] X. Wu, R. Chandel, H. Li, Evaluation of transient liquid phase bonding between nickel-based superalloys, J. Mater. Sci. 36 (2001) 1539-1546.

[62] E. Lugscheider, T. Schittny, E. Halmoy, Metallurgical aspects of additive-aided wide-clearance brazing with nickel-based filler metals, Welding Res.Suppl., Jan. (1989) 9s-13s.

[63] W. Gale, D. Butts, T. Zhou, M. Di Ruscio, Microstructure and mechanical properties of titanium aluminide wide-gap, transient liquid-phase bonds prepared using a slurry-deposited composite interlayer, Metallurgical and Materials Transactions A. 33 (2002) 3205-3214.

[64] N. Sheng, J. Liu, T. Jin, X. Sun, Z. Hu, Wide gap TLP bonding a single-crystal superalloy: evolution of the L/S interface morphology and formation of the isolated grain boundaries, Metallurgical and Materials Transactions A. 44 (2013) 1793-1804.

[65] E. Lugscheider, V. Dietrich, J. Mittendorff, Wide joint clearance brazing with nickel-base filler metals, Welding journal. 67 (1988).

[66] W. Gale, Y. Xu, X. Wen, Z.A. Abdo, Wide-gap transient liquid-phase bonding of Ti-48 at. pct Al-2 at. pct Cr-2 at. pct Nb, Metallurgical and Materials Transactions A. 30 (1999) 2723-2726.

[67] Y. Nakao, C. Kang, Advanced Transient Liquid Insert Metal Diffusion Bonding Using Alloying Powder, (1990) 139-144.

[68] Y. NAKAO, K. NISHIMOTO, K. SHINOZAKI, C.Y. KANG, H. SHIGETA, Analysis of Homogenizing Process of Alloying Elements on Transient Liquid Insert Metal Diffusion Bonding, Transactions of the Japan Welding Society. 23 (1992) 26-32.

[69] W. Zhuang, T. Eagar, Transient liquid-phase bonding using coated metal powders, Welding Journal-Including Welding Research Supplement. 76 (1997) 157s.

[70] Y. Kwon, J. Kim, J. Moon, M. Suk, Transient liquid phase bonding process using liquid phase sintered alloy as an interlayer material, J. Mater. Sci. 35 (2000) 1917-1924.

[71] M. Arafin, M. Medraj, D. Turner, P. Bocher, Transient liquid phase bonding of Inconel 718 and Inconel 625 with BNi-2: Modeling and experimental investigations, Materials Science and Engineering: A. 447 (2007) 125-133.

[72] W. MacDonald, T. Eagar, Isothermal solidification kinetics of diffusion brazing, Metallurgical and materials Transactions A. 29 (1998) 315-325.

[73] Y. Zhou, T. North, Kinetic modelling of diffusion-controlled, two-phase moving interface problems, Modell Simul Mater Sci Eng. 1 (1993) 505.

[74] C. Sinclair, Modeling transient liquid phase bonding in multicomponent systems, Journal of phase equilibria. 20 (1999) 361-369.

[75] N. Sheng, X. Hu, J. Liu, T. Jin, X. Sun, Z. Hu, M3B2 and M5B3 Formation in Diffusion-Affected Zone During Transient Liquid Phase Bonding Single-Crystal Superalloys, Metallurgical and Materials Transactions A. 46 (2015) 1670-1677.

[76] A. Ghoneim, O. Ojo, Understanding reversed temperature dependence of diffusional solidification time in single crystal superalloy brazement, Philosophical Magazine. 91 (2011) 3649-3666.

[77] A. Ghoneim, Numerical Simulation and Experimental Study of Transient Liquid Phase Bonding of Single Crystal Superalloys, Numerical Simulation and Experimental Study of Transient Liquid Phase Bonding of Single Crystal Superalloys. (2011).

[78] J. Ramirez, S. Liu, Diffusion brazing in the nickel-boron system, WELDING JOURNAL-NEW YORK-. 71 (1992) 365-s.

[79] G. Adam, A.O. Olanrewaju, Cellular Automata Simulation of Gap-Filler Dissolution during Transient Liquid Phase Bonding of Single Crystal Materials, Modeling and Numerical Simulation of Material Science. 2012 (2012).

[80] O. Ojo, M. Abdelfatah, On deviation from parabolic behaviour during transient liquid phase bonding, Materials Science and Technology. 24 (2008) 739-743.

[81] M.N. Wikstrom, M.O. Idowu, O. Ojo, M.C. Chaturvedi, Deviation from Conventional Transient Liquid Phase Bonding Models During Diffusion Brazing of Nickel-Base Superalloys, (2006) 6.

[82] O.A. Ojo, A. Ghoneim, J. Hunedy, Transient Liquid Phase Bonding of Single Crystal Ni3Al-Based Intermetallic Alloy, (2012).

[83] M. Abdelfatah, O. Ojo, On the extension of processing time with increase in temperature during transient-liquid phase bonding, Metallurgical and Materials Transactions A. 40 (2009) 377-385.

[84] M. Abdelfattah, An experimental and theoretical study of transient liquid phase bonding of nickel based materials, (2008).

[85] O. Idowu, N. Richards, M. Chaturvedi, Effect of bonding temperature on isothermal solidification rate during transient liquid phase bonding of Inconel 738LC superalloy, Materials Science and Engineering: A. 397 (2005) 98-112.

[86] M. Pouranvari, A. Ekrami, A. Kokabi, Effect of bonding temperature on microstructure development during TLP bonding of a nickel base superalloy, J. Alloys Compounds. 469 (2009) 270-275.

[87] R. Saha, T. Khan, Effect of bonding temperature on transient liquid phase bonding behavior of a Ni-based oxide dispersion-strengthened superalloy, Journal of materials engineering and performance. 15 (2006) 722-728.

[88] B.K. Lee, W.Y. Song, D.U. Kim, I.S. Woo, C.Y. Kang, Effect of bonding temperatures on the transient liquid phase bonding of a directionally solidified Ni-based superalloy, GTD-111, Metals and Materials International. 13 (2007) 59-65.

[89] A. Ghoneim, O. Ojo, Microstructure and mechanical response of transient liquid phase joint in Haynes 282 superalloy, Mater Charact. 62 (2011) 1-7.

[90] A. Ghoneim, O. Ojo, Asymmetric diffusional solidification during transient liquid phase bonding of dissimilar materials, Metallurgical and Materials Transactions A. 43 (2012) 900-911.

[91] O. Ojo, On an effective approach for reducing TLP bonding time in single crystal superalloys, J. Mater. Sci. 47 (2012) 1598-1602.

[92] D.A. Jones, Thermodynamics and Electrode Potential, Principles and Prevention of Corrosion, Second ed., PEARSON, England, 2014, pp. 50-51,52.

[93] D.A. Jones, Principles and Prevention of Corrosion, Second ed., Pearson Education Limited, England, 2014.

[94] L. Shreir, R. Jarman, G. Burstein, Corrosion, vol. 1, Newnes-Butterworths, London, Boston. (1976) 4.

[95] M. Pourbaix, Atlas of electrochemical equilibria in aqueous solutions, (1974).

[96] G. Burstein, Passivity and localized corrosion, Shreir's Corros. 2 (2010) 731-752.

[97] P. Marcus, Corrosion Mechanisms in Theory and Practice, CRC Press, 2011.

[98] D.G. Nair, K. Hansdah, B. Dhal, K. Mehta, B. Pandey, Bioremoval of Chromium (Iii) from model tanning effluent by novel microbial isolate, International Journal of Metallurgical Engineering. 1 (2012) 12-16.

[99] M. Abdallah, A. El-Etre, Corrosion inhibition of nickel in sulfuric acid using tween surfactants, Portugaliae Electrochimica Acta. 21 (2003) 315-326.

[100] T.J. Richardson, Aqueous Corrosion of Nickel and its Alloys, Shreir's Corrosion, Volume 3, Elsevier, 2009, pp. 1879-1915.

[101] R. Cottis, R. Cottis, M. Graham, R. Lindsay, S. Lyon, J. Richardson, J. Scantlebury, H. Stott, Electrochemical Methods, Shreir's Corrosion, Elsevier BV Amsterdam, 2010, pp. 1341-1373.

[102] M.G. Fontana, Corrosion Engineering, Tata McGraw-Hill Education, 2005.

[103] Y. Zhou, Analytical modeling of isothermal solidification during transient liquid phase (TLP) bonding, J. Mater. Sci. Lett. 20 (2001) 841-844.

[104] N. Wikstrom, O. Ojo, M. Chaturvedi, Influence of process parameters on microstructure of transient liquid phase bonded Inconel 738LC superalloy with Amdry DF-3 interlayer, Materials Science and Engineering: A. 417 (2006) 299-306.

[105] N.P. Wikstrom, The effect of process parameters on microstructure of transient liquid phase bonded superalloys inconel 738 and waspaloy, (2007).

[106] J.R. Hayes, J.J. Gray, A.W. Szmodis, C.A. Orme, Influence of Chromium and Molybdenum on the Corrosion of Nickel-Based Alloys, Corrosion. 62 (2006) 491-500.

[107] M. Abdelfatah, O. Ojo, Formation of eutectic-type microconstituent during transient liquid phase bonding of nickel: influence of process parameters, Materials Science and Technology. 25 (2009) 61-67.

[108] T. LIN, H. LI, P. HE, X. YANG, Y. HUANG, L. LI, L. HAN, Effect of bonding parameters on microstructures and properties during TLP bonding of Ni-based super alloy, Transactions of Nonferrous Metals Society of China. 22 (2012) 2112-2117.

[109] M. Pouranvari, Diffusion brazing of a nickel based superalloy part 2–effect of solidification mode on the mechancial properties, Acta facultatis medicae Naissensis. 27 (2010).

[110] P. Majid, E. Ali, K. Hossien, Effect of The Bonding Time On the Microstructure and Mechanical Properties of a Transient-Liquid-Phase Bonded In718 Using A Ni-Cr-B Filler Alloy, Materiali in tehnologije. 47 (2013) 593-599.

[111] Z. Ahmad, Principles of Corrosion Engineering and Corrosion Control, Butterworth-Heinemann, 2006.